A Prokaryotic Perspective on Pentameric Ligand-Gated Ion Channels

Dissertation
zur Erlangung der naturwissenschafltichen Doktorwürde
(Dr. sc. nat.)

vorgelegt der

Mathematisch-naturwissenschaftlichen Fakultät der
Universität Zürich

von
Ricarda J. C. Hilf
aus Deutschland

Promotionskomitee
Prof. Dr. Raimund Dutzler (Leitung und Vorsitz)
Prof. Dr. Bernd Fakler
Prof. Dr. Ben Schuler

Zürich 2009

ACKNOWLEDGEMENTS

A lot of people have contributed directly or indirectly to the completion of this work and I would like to express my gratitude here.

First and overall I would like to thank my thesis supervisor Raimund Dutzler for giving me the opportunity to carry out my PhD thesis in his lab on this fascinating project. Additionally I want to thank him for providing support at any stage of my time here.

I would like to thank Bernd Fakler, Julia Fritz-Steuber and Ben Schuler for being on my thesis committee.

I wish to thank all the members of the Dutzler lab for help, suggestions, chats and a nice atmosphere.

Many thanks to the staff of the Institute of Biochemistry, the IT-service and the workshop for keeping everything up and running. Especially Margrit Mathys for coping with all the bureaucratic obstacles and for proof-reading of the papers and the thesis, and Sascha Weidner for fast and creative solutions in building new equipment.

Meinen Eltern für ihre Unterstützung während meines Studiums möchte ich herzlich danken.

Meinen Mitbewohnern in der Regensbergstr. 89 – Sonja, Laui, Roland, Pasci, Pasci, Silvia, Francois und Tijana – danke ich für lange Diskussionen, gemeinsame Essen und viel Spass am Leben drumherum.

My thanks also go to all the people who joined me in the mountains, lakes and short trips around (and long trips away from) Zurich – helping to regenerate from long hours in the lab. Barbara und Karin danke ich besonders für viele gemeinsame Abende und kreative Essenszubereitungen.

CONTENTS

LIST OF FIGURES

ABSTRACT

The pentameric ligand-gated ion channels (pLGIC) are key-players in the early events of electrical signal transduction at chemical synapses. The family codes for a structurally conserved scaffold of channel proteins that open in response to the binding of neurotransmitter molecules. In this way the receptors facilitate the gated diffusion of ions and thus generate a neurotransmitter-dependent electrical signal. All proteins share a pentameric organization of identical or related subunits that consist of an extracellular ligand-binding domain followed by a transmembrane channel domain. The dysfunction of pLGICs in the central and peripheral nervous system results in severe diseases like myasthenic syndromes, epilepsy, schizophrenia and Alzheimer's disease.

The pLGIC family has been studied for decades using electrophysiological and biochemical techniques. To date details about their pharmacological behavior, ion selectivity, the kinetics of ligand binding and gating are known. In contrast to the rich source of biochemical data, the structural knowledge is still scarce. Until recently, detailed structural insight was only available from the crystal structure of the acetylcholine-binding protein, a soluble protein that is homologous to the extracellular domain of the acetylcholine receptor, and from cryo-electron microscopy studies of the full-length acetylcholine receptor at comparatively low resolution. These studies have revealed the chemistry of ligand recognition and the overall topology of the family.

To understand the detailed mechanisms of ion conduction and gating, high-resolution structures are mandatory, which allow to assess the role of single residues for channel function in a structural context. It was the aim of my PhD thesis to determine the first high-resolution structure of any family member and to characterize its function by means of electrophysiology.

The large abundance of prokaryotic genomes has allowed the identification of bacterial homologues of the pLGIC family. I have during the course of my Ph.D. studies succeeded in cloning and overexpression of several prokaryotic pLGICs. In my studies I have focused on the two homologues from *Erwinia chrysanthemi* and *Gloebacter violaceus*, named ELIC and GLIC, respectively. As revealed by electrophysiology, both proteins share functional properties with their eukaryotic counterparts such as ion selectivity and channel block. With respect to its activation, however, GLIC shows an unusual behavior for a pLGIC as it is opened by protons. In the course of this thesis I have crystallized ELIC and GLIC and have determined their three-dimensional structure by X-ray diffraction.

The structure of ELIC revealed the first high-resolution structural insight into the family of pLGICs. Since the ligand opening ELIC is not known, the protein was crystallized in a resting non-conducting state. The structure shows a wide, aqueous cavity within the extracellular do-

main that narrows at the membrane interface to a discontinuous pore, which is constricted by hydrophobic residues that prevent ion permeation. The structure of GLIC, on the other hand, shows a channel in a conducting state, as the protein was crystallized at low pH, a condition where the open probability is high. Structural differences between the two proteins indicate two distinct conformations. Whereas the ion pore in ELIC is restricted at the extracellular entrance, the GLIC structure shows a funnel-shaped opening with a linearly decreasing diameter that places its narrowest part at the intracellular entry of the channel. The difference in pore shape results from a difference in the orientation of the α-helices forming the ion pore, which have moved like a rigid unit to open the extracellular hydrophobic part and to form a region similar to an ion selectivity filter at the intracellular entrance.

In combination, both structures suggest a novel gating mechanism for pentameric ligand-gated ion channels where channel opening proceeds by a change in the tilt of the pore-forming helices. The results of this thesis thus provide a first structural view at high resolution into how a pLGIC may open and selectively conduct ions.

ZUSAMMENFASSUNG

Die Familie der pentameren ligandengesteuerten Ionenkanäle (pLGIC) spielt eine wichtige Rolle in der elektrischen Signalübertragung an chemischen Synapsen. Die Proteine bilden ein konserviertes Grundgerüst für Ionenkanäle, die bei Bindung eines Neurotransmitters öffnen. Dadurch ermöglicht der Rezeptor die geregelte Diffusion von Ionen durch die Membran und erzeugt ein von Neurotransmittern abhängiges elektrisches Signal. Alle Proteine dieser Familie zeigen eine fünffach-symmetrische Anordnung von ähnlichen oder gleichen Untereinheiten, die jeweils aus einer extrazellulären Ligandenbindungsdomäne und einer Transmembrandomäne bestehen. pLGIC sind wichtig für viele verschiedene Funktionen im zentralen und peripheren Nervensystem, und eine Fehlfunktion führt zu schweren Krankheiten wie dem Myasthenie-Syndrom, Epilepsie, Schizophrenie und Alzheimer.

pLGIC wurde bereits jahrzehntelang mit physiologischen und biochemischen Methoden untersucht. Daher sind Details der Pharmakologie, der Ionenselektivität, der Kinetik der Ligandenbindung und der Kanalöffnung bekannt. Im Gegensatz zur Fülle an biochemischen Ergebnissen weiss man nur wenig über die Struktur der pLGIC. Bis vor kurzem basierten strukturelle Erkenntnisse vor allem auf der Kristallstruktur eines zur extrazellulären Domäne homologen Proteins und auf der mit Kryo-Elektronenmikroskopie bestimmten Struktur eines Acetylcholinrezeptors bei vergleichsweise niedriger Auflösung. Während diese Untersuchungen Einblicke in die Chemie der Ligandenerkennung sowie die Gesamttopologie der Familie erlaubten, ist ihre Aussagekraft bezüglich funktioneller Mechanismen begrenzt.

Um die Ionendiffusion und den Öffnungsmechanismus detailliert zu verstehen, sind hochaufgelöste Strukturen nötig, die es erlauben, die Rolle einzelner Aminosäuren für die Struktur und die Funktion des Proteins zu untersuchen. Daher war es das Ziel meiner Doktorarbeit, die erste hochaufgelöste Röntgenkristallstruktur eines Mitglieds der Familie der pLGIC zu bestimmen und diese Proteine funktionell zu charakterisieren. Dank der Fülle verfügbarer prokaryotischer Genome war es möglich, bakterielle Homologe der LGIC-Familie zu identifizieren. Während meiner Doktorarbeit gelang mir die Klonierung und Überexpression einiger prokaryotischer pLGICs. In meiner Arbeit habe ich mich auf zwei Homologe aus *Erwinia chrysanthemi* (ELIC) und aus *Gloebacter violaceus* (GLIC) konzentriert. Wie ich mit elektrophysiologischen Messungen zeigen konnte, haben beide ähnliche Eigenschaften wie die eukaryotischen Proteine in Bezug auf Ionenselektivität und Kanalblock. Allerdings zeigt GLIC die für die pLGIC Familie ungewöhnliche Eigenschaft, dass es durch Protonen aktiviert wird. Es ist mir im Rahmen dieser Doktorarbeit gelungen, ELIC und GLIC zu kristallisieren und ihre dreidimensionale Struktur mit Hilfe der Röntgenkristallstrukturanalyse aufzuklären.

Die Struktur von ELIC zeigt die erste hochaufgelöste Struktur aus der Familie der pLGIC. Das Protein wurde in seinem inaktiven Zustand kristallisiert, da der Ligand, der ELIC öffnet, nicht bekannt ist. Die Struktur zeigt einen weiten, wassergefüllten Hohlraum, der von der extrazellulären Domäne begrenzt wird. Am Übergang zur Membran verengt sich dieser Hohlraum zu einer Pore mit geringem Durchmesser, die von hydrophoben Resten unterbrochen ist und offensichtlich einen geschlossenen Zustand des Kanals darstellt.

Im Gegensatz zu ELIC zeigt die Struktur von GLIC einen Kanal im offenen Zustand. Das Protein wurde bei niedrigem pH und dadurch hoher Öffnungswahrscheinlichkeit kristallisiert. Räumliche Unterschiede zwischen den beiden Strukturen von ELIC und GLIC lassen zwei unterschiedliche Konformationen des Kanals erkennen. Während der Ionenkanal in ELIC am extrazellulären Eingang verschlossen ist, zeigt GLIC einen sich verjüngenden, trichterförmigen Kanal, der zu einer Engstelle am intrazellulären Ende führt. Die Unterschiede in der Konformation der Pore resultiert aus der Neigung der die Pore säumenden α-Helices, die wie ein Hebel den extrazellulären Teil nach außen kippen lassen und so die hydrophobe Hälfte der Pore öffnen und gleichzeitig am intrazellulären Eingang der Pore verengen, um dadurch einen Selektivitätsfilter für Ionen zu bilden.

In Kombination deuten die beiden Strukturen auf einen neuen Öffnungsmechanismus für die Familie der pLGIC hin, in dem die Kanalöffnung auf der Änderung der Neigung der Poren-formenden Helices basiert. Diese Arbeit bietet erste strukturelle Erkenntnisse bei hoher Auflösung, wie LGIC sich öffnen und selektiv Ionen den Fluss durch die Membran ermöglichen.

OUTLINE

This thesis comprises several parts which I would like to outline here.

The introduction provides basic information about the electro-chemical background of signal transmission, followed by a concise overview of the main research areas in the field of pentameric ligand-gated ion channels. The three main chapters in this part focus on ligand recognition, ion selectivity and gating within this protein family, topics which have been in the focus of biochemical, electrophysiological, computational and structural studies. Since research on pentameric ligand-gated ion channels has been carried out for a long time, some aspects are only mentioned briefly. Subsequently, the structural knowledge on the family, several high resolution structures of the acetylcholine-binding protein, a homologous protein resembling the extracellular domain, and cryo-electron microscopy studies of the full-length acetylcholine receptor at medium resolution, is summarized. The discovery of prokaryotic pentameric ligand-gated ion channels, the prerequisite for this project, is concluding the introduction.

The first chapter of the results section describes the problems in the overexpression, purification and crystallization of the protein, which had to be overcome. Subsequently the structure determination of the two pLGICs ELIC and GLIC are discussed. The studies resulted in two publications in *Nature* of the first two high-resolution structures of prokaryotic pentameric ligand-gated ion channels. The two publications are included as reprints here. Additionally to the two publications, supplementary information about certain aspects of the work are explained in more detail.

The discussion and outlook section starts with a comparison of the two prokaryotic protein structures, which was published as review in *Current Opinion in Structural Biology*. In the following the two structures are put in a broader context of previous research, by relating the work to results obtained on the eukaryotic proteins. Additionally, ongoing follow-up studies using the new prokaryotic structures as a starting point, are described briefly.

The outlook, finally, proposes experimental approaches of how to tackle open questions in this field by using the two prokaryotic pLGICs as model systems.

At the end of the thesis a method section provides detailed protocols of the experiments.

CHAPTER 1

INTRODUCTION

The communication between cells is a fundamental process in multicellular organisms. Our nervous system plays a key role in this communication as it conducts electrical signals in the form of an action potential between different parts of our body. As an action potential is transmitted between two nerve cells it has to cross a gap of about 20 nm at a location called the synapse, where it cannot be transmitted as an electrical signal. Therefore it is converted into a chemical signal in form of a neurotransmitter, which is released from the presynaptic cell into the synaptic cleft. The membrane of the postsynaptic cell contains a protein, which converts the chemical signal back into an electrical signal. Upon binding of the neurotransmitter this protein changes its conformation and opens a membrane-spanning channel. The open channel allows charged molecules, ions, to cross the postsynaptic membrane and thus a new action potential is generated. To determine the three-dimensional structure and to study the function of this protein in more detail was the aim of this PhD thesis.

1.1. Transport through the Membrane

The cell membrane is an important barrier to maintain defined internal conditions, which are required for the biochemical processes inside the cell. However, without exchange with the outside solution the cell would not be viable either. Therefore the cell needs mechanisms to facilitate the uptake, excretion, influx and efflux of specific substances. These tasks are carried out by proteins located in the membrane, forming channels or transporters. Transporters carry a specific substance through the cell membrane, often against the chemical gradient of this substance. This process requires energy input either from a chemical source or from the transport of another substance, typically an ion, down its gradient as the driving force.

While transporters carry a wide range of molecules (such as ions, sugars, drugs), different families of channels facilitate the flow of ions down their electrochemical gradients. Ion channels can be selective for one specific ion or for a certain ion (like potassium channels) or for a class of ions (e.g. cations or anions). Because the influx or efflux of ions has to be tightly regulated, channels have usually defined states: non-conducting states, which are impermeable to ions, and conductive states, which allow ions to flow into or out of the cell.

Since the diffusion of ions through the membrane carries a charge from one compartment to another, a current is flowing. The change of the membrane potential in response to the diffusion of ions is the basis for signal transduction within the nervous system.

	Extracellular	Intracellular	Relative Permeability
Na^+	150	15	1
K^+	5	150	25
Protein	0	65	0
Cl^-	120	7	0.025

Table 1.1.: **Ion distribution.** Overview over the distribution of relevant ions in the nerve cell and their relative permeabilities in the resting state. Extracellular and intracellular concentrations are given in mM.

1.2. Electricity in the Nervous System

As any other membrane, the membrane of nerve cells is mostly impermeable to ions. Ions are unevenly distributed between the outside and the inside of the cell. The outside solution is rich in Na^+ ions and Cl^- ions, whereas the inside of the cell has a high K^+ concentration and a high concentration of large negatively charged anions (e.g. proteins and nucleic acids)(see table 1.1). The membrane of nerve cells contains a small number of ion channels, that are selective for K^+ ions and that are open in the resting cell. These leak channels make the membrane permeable for K^+ ions, which follow their chemical gradient and diffuse out of the cell. Since a positive charge is transported to the outside, an electrical gradient in the opposite direction is formed. K^+ ions continue to flow out of the cell as long as the energy in the electrical potential is smaller than the energy in the concentration difference. Once the ions reach their electrochemical equilibrium, the chemical and the elctrical driving forces are in balance. The corresponding membrane potential is called the equilibrium potential for potassium and is described by the Nernst equation:

$$E_K = \frac{RT}{zF} ln \frac{[K^+]_{out}}{[K^+]_{in}}$$

In this equation E_K is the equilibrium potential for K^+ at the given concentrations of K^+ inside and outside of the cell ($[K^+]_{in}$ and $[K^+]_{out}$, respectively). R is the gas constant, T the absolute temperature, F the Faraday constant and z the valence of the ion. The equilibrium potential of a cell whose membrane is permeable to K^+ ions is only determined by the ratio of the K^+ ion concentrations across the membrane. However, the membrane of the nerve cell is also permeable to other ions like sodium and chloride. Therefore, all ions contribute to the membrane potential of a resting cell, which can be described with the Goldman equation. This equation resembles the Nernst equation, in that it takes the charge and the distribution of the ions into account, but also includes the relative permeabilites (P) of the ions:

$$E_m = \frac{RT}{F} ln \frac{P_K[K^+]_{out} + P_{Na}[Na^+]_{out} + P_{Cl}[Cl^-]_{in}}{P_K[K^+]_{in} + P_{Na}[Na^+]_{in} + P_{Cl}[Cl^-]_{out}}$$

Since in the resting state the membrane of nerve cells is much more permeable to K^+ than to other ions, the resting potential is close to the equilibrium potential of potassium, which is close to -60 mV for most animal cells.

As described in the next section the change in membrane potential is used as a signal. In the electrical signal transmission along a nerve cell a local depolarization of the membrane is propagated along the nerve cell and is transmitted from one cell to another. To create an initial electrical stimulus, a specific chemical signal, a neurotransmitter, causes a transmembrane protein to open a selective ion channel, which allows ions to cross the membrane and thus to change the membrane potential. In the case of excitatory signal transmission the ion channel is selective for cations. If the channel opens, Na^+ ions will flow into the cell down their electrochemical potential. By this a positive charge is carried into the cell and the membrane potential depolarizes. To transmit this signal along a nerve cell, downward voltage-gated sodium channels are triggered to open by the depolarization of the membrane before the inactivation of sodium channels and the opening of voltage-gated potassium channels cause the return to the resting potential.

Due to continuous depolarization and repolarization events, the concentration gradient for Na^+ and K^+ would dissipate over time. To maintain the gradient of either ion, a Na^+-K^+-ATPase constitutively hydrolyzes ATP to transport 3 Na^+ ions out of the cell and 2 K^+ ions into the cell, a process that uses about one third of the total energy of a living cell.

1.3. Signal Transmission at Chemical Synapses

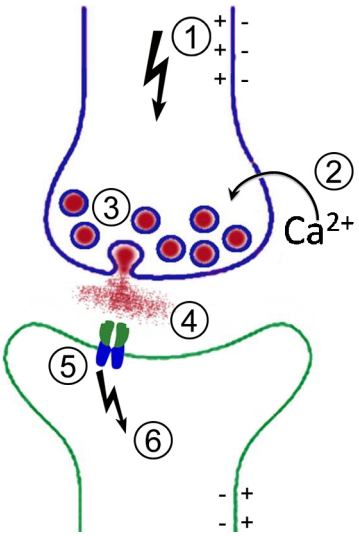

Figure 1.1.: **Signal transmission at chemical synapses.** 1) Electrical signal in form of depolarization of membrane. 2) Influx of calcium ions. 3) Fusion of synaptic vesicles with the presynaptic membranes. 4) Diffusion of neurotransmitter to the postsynaptic membrane. 5) Detection of the neurotransmitter and opening of an ion channel. 6) Newly generated electrical signal.

Nerve cells have next to a cell body and tentacle-like extensions, the dendrites, a long tubular structure, the axon. The axon resembles a cable, which transmits electrical signals over long

distances. At the end of the axon the nerve cell forms contact to a neighboring nerve or muscle cell to which the electrical signal can be transmitted. There are two ways of transmitting the electrical signal: At an electrical synapse the two nerve cells are in direct contact. Their cytoplasms are connected by gap-junction channels, where the change in membrane potential is directly transmitted from cell to cell. At the chemical synapse, in contrast, the two nerve cells are separated by a gap of about 20 nm, which cannot be crossed by the electrical signal. The electrical signal is thus converted into a chemical signal at the axon terminal of the presynaptic cell. This chemical signal is recognized by the postsynaptic cell, which leads to the generation of a new action potential.

The process at the chemical synapse proceeds in the following sequence of events: The action potential which is arriving at the nerve terminal causes a depolarization of the presynaptic membrane (1) (compare figure 1.1). The presynaptic membrane contains voltage-activated calcium channels that open in response to this depolarization. Calcium ions follow their electrochemical gradient and flow into the cell (2). The influx of calcium stimulates the fusion of presynaptic vesicles with the membrane (3) in a way that the content of the vesicles – a specific neurotransmitter depending on the type of synapse – is released into the synaptic cleft and diffuses to the postsynaptic membrane (4).

At the surface of the postsynaptic cell it encounters a protein with a ligand-binding pocket. These proteins are integral membrane proteins with a large extracellular domain that contains a neurotransmitter binding site. The transmembrane domain forms an ion channel, which is closed in the absence of ligands. As ligands bind to the extracellular domain the protein undergoes a conformational change in this domain, which is transmitted to the transmembrane domain. Thereupon the ion channel opens and permits specific ions to flow through the channel down their electrochemical gradient (5). Depending on the specificity of the channel either cations or anions are allowed to pass the channel and therefore give rise to an excitatory or inhibitory signal, respectively. The excitatory signal causes the firing of action potentials, whereas the inhibitory signal suppresses electrical activity (6).

1.4. The Family of Pentameric Ligand-Gated Ion Channels

The family of pentameric ligand-gated ion channels (pLGIC) contains acetylcholine, serotonin (5-hydroxytryptamine or 5-HT_3), γ-aminobutyric acid (GABA) and glycine receptors. They play starring roles in the central and peripheral nervous system and are needed for the fast electrical transmission at many chemical synapses. Within a few microseconds after a neurotransmitter is binding to the extracellular side, they open a selective ion channel to excite or inhibit the postsynaptic cell. They close again a few microseconds after the neurotransmitter is dissociating and they desensitize upon prolonged exposure to neurotransmitters. It is not surprising that these proteins are involved in cognitive processes such as attention, learning and memory and that there are many diseases associated with dysfunction of the receptors such as myasthenic syndromes, epilepsy, schizophrenia, autism, pain, depression, Alzheimer's and Parkinson's disease. In addition pLGICs play a role in addiction to benzodiazepines, barbiturates and nicotine.

Acetylcholine and serotonin receptors are cation selective and thus excitatory, whereas GABA and glycine receptors are anion selective and thus inhibitory. All plGICs share the same archi-

tecture and the basic mechanisms of ligand recognition and gating. They are formed by five subunits, which are either identical or highly homologous and have presumably evolved from a common ancestral gene.

1.5. The Nicotinic Acetylcholine Receptor

Due to its abundance in the electric organ of the electric ray *Torpedo marmorata*, the nicotinic acetylcholine receptor (nAChR) has played a pivotal role for the investigation of pLGICs and is by far the best studied member of the family. Following I will give a short historical overview, before I focus on mechanistic details of this protein.

1.5.1. Historical Overview

As early as 1904 T. R. Elliot has made the suggestion that the signal transmission between nerve and muscle cell occurs by means of a 'specific chemical stimulant'. Between 1905 and 1907 his mentor John Langley developed the idea of transmitter receptors as a 'receptive substance'. Several years later Sir Henry Dale coined the phrase of 'chemical transmission'[1] and in 1936 he and his coworkers identified acetylcholine as the transmitting agent[2].

In parallel to these studies on different types of tissues, the electroplax organ of *Torpedo marmorata* was recognized to be activated by similar means[3]. In 1970 Katz and Miledi described a 'membrane noise produced by acetylcholine'[4]. Neher and Sakmann developed the patch-clamp technique to carry out single channel recordings in 1976[5], for which they received the nobel prize in 1991. By then the acetylcholine receptor from the neuromuscular junction was the best described channel in biological membranes.

Research on the acetylcholine receptor did not slow down since then. In 1974 it was purified to homogeneity from *Torpedo californica* and the different subunits were isolated[6]. In the beginning of the 1980s Noda and coworkers determined the primary sequence of all subunits and proposed the topology with four transmembrane helices in each subunit[7–9]. The first experiments with reconstituted receptor were carried out in the 1980s and in 1984 the protein was expressed heterologously in COS monkey cells and *Xenopus* oocytes[10]. Kistler and coworkers were the first to report structural data from electron microscopy studies of two-dimensional crystals[11], followed shortly by Brisson and Unwin[12], and the overall shape of the protein and its orientation within the membrane was established. Nigel Unwin continued to study the nAChR using electron microscopy for many years. He was able to gradually improve the resolution, finally providing electron density at 4 Å[13]. His results were the basis for many functional studies and have provided the framework to locate single residues. A more detailed overview of this work follows in section 1.6.2.

The in-depth analysis of the nicotinic acetylcholine receptor has revealed many aspects of its pharmacological behavior, its activation, inactivation and desensitization. To date the overall assembly of the protein and the estimated positions of specific residues are known.

The nAChR is encoded by at least 17 human genes termed α1–α10, β1–β4, γ, δ and ϵ, which assemble to about 20 distinct subtypes found in humans. The nAChR from the neuromuscular junction, which controls the voluntary movement of muscles, is formed by five homologous

subunits with a stoichiometry of two $\alpha 1$ subunits and one $\beta 1$, γ and δ subunit each (in its fetal form, in the adult protein the γ subunit is replaced by an ϵ subunit)[14]. This arrangement is essentially identical to the subunit stoichiometry in the nAChR of *Torpedo* which makes the results from the *Torpedo* nAChR highly relevant for the human protein from the neuromuscular junction. The remaining nAChR subunits are found in receptors within the central nervous system. These 'neuronal' nAChRs are less well defined in their subunit assembly, formed by at least two $\alpha 2$–$\alpha 10$ subunits in various combination with the $\beta 2$–$\beta 4$ subunits, but also in a homopentameric assembly like in the $\alpha 7$ receptor (1.2).

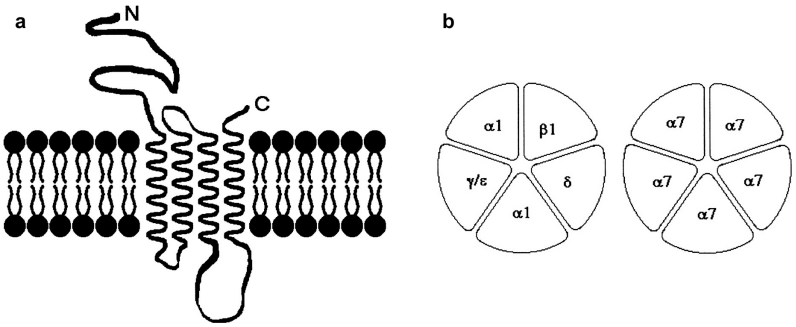

Figure 1.2.: **Subunit topology and receptor assembly. a** Schematic drawing of the topology of the pLGIC family. The N-terminal domain is followed by the ion pore domain consisting of 4 transmembrane helices. Between α-helix 2 and 3 there is a large cytoplasmic loop. **b** Receptor assembly showing the muscle type (left) and the homopentameric $\alpha 7$ assembly (right). Figure adapted from Lukas et al.[15].

Each subunit contains an N-terminal extracellular domain, followed by a transmembrane domain, into which a long intracellular region is inserted as loop between two transmembrane helices (see figure 1.2). In the channel the five subunits are arranged in a circle around the central ion permeation pore, forming a protein with dimensions of 80 Å in diameter times 110 Å in length. The extracellular domain behaves functionally as a separate unit from the transmembrane domain. In 1993 the first functional chimera between the N-terminal ligand-binding domain of the nAChR and the transmembrane domain of the serotonin receptor was studied[16]. In their experiments Eisele and coworkers could show for the first time the independence between the two domains, each contributing specific characteristics to this chimeric protein.

The extracellular ligand-binding domain (LBD) recognizes the ligand and undergoes a conformational change that is transmitted to the transmembrane domain (section 1.5.2). Because of its pharmacological importance, the ligand-binding pocket was studied thoroughly for many years. A more detailed description of its structure and the chemical interactions important for ligand-binding can be found in section 1.6.1.

The conformational change upon ligand-binding to the extracellular domain is transmitted to the transmembrane domain via an interface that is highly conserved and contains the signature sequence of the family in the so-called Cys-loop. The Cys-loop is connecting two β-strands ($\beta 6$ and $\beta 7$) of the extracellular domain and got its name from the two flanking cysteines located 13

residues apart from each other. Residues in the Cys-loop interact with residues in the extracellular loops of the transmembrane domain and are indispensable for gating (section 1.5.3).

The transmembrane domain is formed by four α-helices from each of the five subunits. It was discovered early on that residues in the α2-helix (named M2) are important for the rate of ion transport[17], for the affinity of voltage-dependent blockers[18]. The ion selectivity is influenced by several factors as determined in experiments, where the selectivity was converted from cation- to anion-selective channels (see also section 1.5.5). The pore lining properties and the α-helical character of the α2-helix were identified in several studies using the substituted cysteine accessibility method (SCAM)[19–23]. The pore-lining α2-helix is surrounded by a concentric ring formed by helices α1 and α3. Helix α4 is located at the periphery of the channel and is not involved in intersubunit contacts.

The role of the intracellular domain, the long cytoplasmic loop connecting the helices α3 and α4, is not well understood. Kottwitz and coworkers tried to access the structure of the isolated intracellular domain from the nAChR δ subunit from *Torpedo* and the homologuos protein from rat, but came to the conclusion that this part of the protein is mostly unstructured[24]. It was proposed that the intracellular domain is involved in expression[25], assembly[26], targeting[27,28] and function[29,30] of the receptor. However, Jansen and colleagues recently showed that a serotonin and GABA receptors are expressed in the membrane and show very similar functional properties as the wild type, even if the intracellular domain is replaced by a short linker[31].

The functionally important steps of ligand recognition, gating and ion selectivity will be discussed in more detail in the following sections.

1.5.2. Ligand Recognition

Before any structural data of the full-length receptor was available, one pharmacological important focus of different studies concerned the location of the ligand-binding pocket (LBP). The techniques employed in the task to identify the LBP included photoaffinity labeling, EPR spectroscopy, FRET measurements and mutagenesis combined with electrophysiological recordings. A residue was reckoned as being located within the LBP since the efficiency of labeling by ligands was inhibited in the presence of agonists or competitive antagonists such as α-bungarotoxin, and at the same time was not affected by non-competitive inhibitors. The first of these studies was carried out by Changeux and coworkers in 1967[34].

Several other studies involved the mutagenesis of single residues and measuring single channel properties in recordings of *Xenopus* oocytes injected with the mutant mRNA and comparing the results to the wild-type behavior. A drawback of these studies is that an effect cannot be unambiguously attributed to ligand-binding, since allosteric coupling can also be affected and result in similar behavior of the protein. FRET measurements were used to measure the distance between the ligand-binding site and the membrane plane, or to determine the distance between the non-competitive inhibitor-binding sites and the agonist-binding site or the membrane. All these studies revealed the location and chemical nature of the LBP for the nAChR.

The nAChR contains two ligand-binding sites in each pentamer, each of which has to be occupied by an agonist for efficient channel gating. The sites are located in the interface between an α-subunit and the neighboring γ- or δ-subunit about 30–35 Å above the membrane plane[35]. The LBP is formed by six loops which have been termed A-, B- and C-loops in the α-subunit,

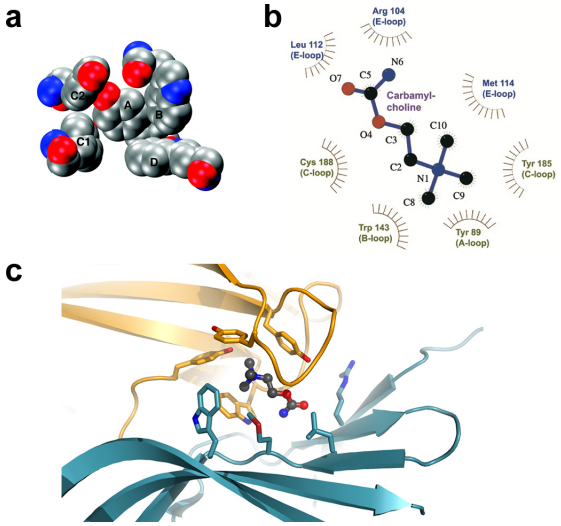

Figure 1.3.: **Cation-π interaction.** **a** The 'aromatic box' comprising the nAChR active site, based on AChBP coordinates. **b** Schematic drawing of carbamylcholine binding to the AChBP. **c** Details of the LBP illustrating the prevalence of aromatic residues between the two β-sheets forming the binding site. (PDB-ID 1UV6). Figure taken from Celie et al.[32] and Beene et al.[33]

and D, E and F in the other participating subunit[36–41]. The C-loop is the loop shielding the LBP from the outside of the protein, thereby forming a lid on top of the ligand-binding site. It undergoes the largest conformational change within the region of the LBP upon ligand binding (see chapter 1.6.1). The LBP itself is formed by a box consisting of five aromatic residues from different loops, which surround the cationic ligand (see figure 1.3).

The chemical properties of the ligand-binding site have been studied very thoroughly by Dougherty and colleagues. A cation-π interaction was already predicted in 1990 as being important for the ligand-protein interaction in the nAChR. In an isolated system Dougherty and coworkers carried out studies on cation-π interactions, where it was shown that a fluorine substituent at an aromatic residue is weakening the cation-π interaction and that the effect of several fluorine substituents accumulates. In 1995 they were the first to describe the incorporation of an unnatural amino acid into a living cell[42]. By incorporating fluorinated tryptophanes or tyrosines into the LBP of the nAChR they could study the effect of the cation-π interaction on ligand binding. In every receptor one aromatic residue is dominant for ligand coordination, although there are several aromatic residues in the LBP. Interestingly, the residues providing the π-electrons for the ligand coordination are not the same in different receptors and for different ligands[43](and references therein).

Thus, even if the overall layout of the LBP and also the number and type of the involved protein side chains is highly conserved between different members of the family, the interactions between the ligand and the protein side chains varies and cannot be predicted, which complicates the efforts taken in homology modeling and drug discovery studies.

In 2001 the first structural information on the extracellular part of the acetylcholine receptor was obtained from the acetylcholine-binding protein, a protein resembling the isolated extracellular domain[44]. The structure and follow-up structures of complexes with different ligands confirmed many previous observations and have provided detailed insight into the chemistry of ligand binding (see section 1.6.1).

1.5.3. Gating

As the ligand is bound to the extracellular LBD a conformational change is triggered that leads to channel opening within microseconds. During this time the signal is transmitted from the LBP to the gate over a distance of about 60 Å. Several studies have focused on this allosteric coupling and the events involved in gating with different methods. In the gating process the nAChR oscillates rapidly between – at least – two states, closed and open. Since these two states interconvert so rapidly the energy difference between them has to be very small as has been proposed by Bernd Sakmann in 1981[45].

Anthony Auerbach has studied the linear free energy relationship (LFER) of residues in the nAChR during gating over several years. With this method detailed kinetic data of point mutations obtained from patch-clamp recordings are used to determine the degree to which a mutation perturbs the channel-opening rate constant (β) and the open-closed channel equilibrium (Θ). If a plot of β versus Θ for a series of mutants at a given site is linear, the slope corresponds to ϕ, which is a measure whether the effect of the mutation happens early or late in the transition. The studies from Auerbach and coworkers have led to the proposal of a conformational wave, in which a conformational change induced by agonist binding in the extracellular domain propagates down the receptor over the interface to reach the gate[46–50].

The importance of the interface was confirmed by Bouzat and coworkers. They demonstrated that a chimeric protein between the AChBP and the transmembrane domain of the serotonin receptor can form a functional ligand-gated ion channel if three loops, $\beta1$–$\beta2$, $\beta6$–$\beta7$ and $\beta8$–$\beta9$, of the AChBP facing the interface are replaced by the respective sequences from the serotonin receptor[52], which emphasizes the need for specific contacts between the extracellular and the transmembrane domain.

Based on these results other groups proposed different mechanisms for the transmission of the signal from the extracellular LBD to the transmembrane domain. Dennis Dougherty and coworkers divided the residues in the interface and showed that the group of residues in the LBD has an overall negative charge, whereas the residues on top of the transmembrane domain have an overall positive charge. In several studies they mutated residues in this interface and found out that charge reversal, charge neutralization, and charge introducing mutations were well tolerated in general, as long as they did not disturb the overall charge pattern[53]. Based on this finding they proposed a model based on 'global electrostatic attraction' between the two interfaces. In this model, clusters of charged residues define a structural unit, which form contacts in diffuse electrostatic interactions bridging the gating interface. This model would allow the fast oscillating change between the open and the closed state of the receptor, since the two domains could slide past each other without high energetic penalties, but it is in contrast to other studies, where strong, specific ion pair interactions were proposed to be important in the gating interface.

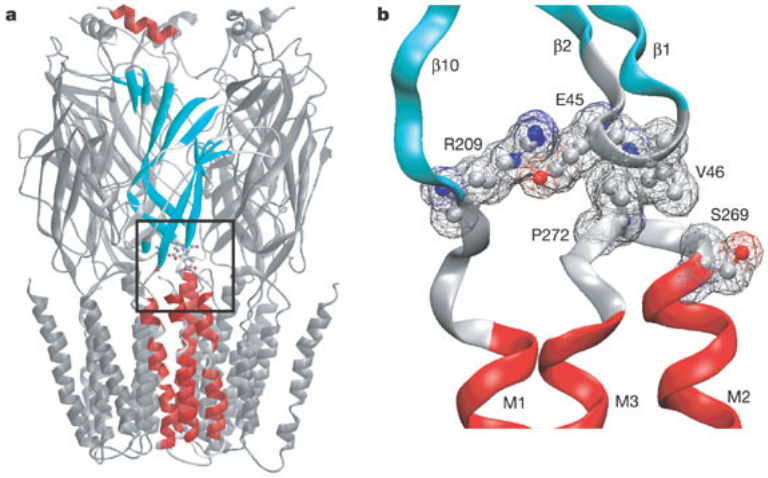

Figure 1.4.: **Principal pathway.** **a** Cartoon representation of the pentamer. The secondary structures of one α-subunit are highlighted (α-helices, red. β-sheets, cyan. loops, grey). **b** Close-up view of the principal pathway in the α-subunit. Atoms of key residues are highlighted according to electrostatic charge (blue, positive. red, negative. grey, neutral). Van der Waals surfaces are rendered as a wire mesh. The key residues belonging to the 'principal pathway' are shown. The Cys-loop, β8–β9 linker and α4 helix have been removed for clarity. Figure taken from Lee and Sine[51].

Kash and colleagues demonstrated the importance of specific electrostatic interactions in the $GABA_A$ receptor by measuring current responses to GABA in different point-mutants[54]. They suggested that a saltbridge network between a lysine from the α2–α3 loop and aspartates from the β1–β2 and β6–β7 loop is required for efficient gating. Lee and Sine have investigated the coupling residues in the nAChR of the human skeletal muscle[51]. They measured single-channel currents in patch-clamp recordings and analyzed the open and closed dwell times to determine rate constants by assuming a mechanism in which acetylcholine binding and channel gating are separate, sequential events. In mutant-cycle analysis they studied interactions between conserved residues. In these experiments the term 'principal pathway' was coined, describing the molecular links between the LBD and the transmembrane domain, which are required for gating. In their model the event of ligand-binding leads to closure of the C-loop. This conformational change is conveyed as a rigid body movement along the β-strand 10. Close to the membrane surface an arginine in β10, R209, is buried in a pocket formed by the surrounding loops and forms a saltbridge with glutamate E45 in the β1–β2 loop. E45 and the neighboring V46 in turn stack hydrophobically on proline P272 from the transmembrane domain, which is located in the extracellular loop following the pore forming α2-helix. V46 fits into a gap surrounded by P272 and a serine in the same loop, S269 (Figure 1.4). The saltbridge between an arginine in the β10-strand and a glutamate in the β1–β2 loop is highly conserved within the family, whereas

the following hydrophobic contacts are conserved within the single subclasses. Overall Lee and Sine identified a molecular continuum that links ligand-binding to gating with an interdependent network in the interface between the two domains.

A different gating switch was proposed for serotonin receptors. Lummis and coworkers[55] studied the role of the proline in the $\alpha 2$–$\alpha 3$ loop in the homopentameric 5-HT_3 receptor. By introducing proline analogues, with different propensities for the cis or trans configuration, they found that the proline analogues with a higher cis bias show a drop in EC_{50} for activation with serotonin and influence the open-closed gating equilibrium. However, the serotonin receptor opening rate constant lies around 10–100 s^{-1}, whereas the proline cis-trans isomerization is slower by a factor of 10. Even in case the isomerization rate would be accelerated by a hydrophobic receptor environment or a hydrogen bond, making the cis-trans isomerization a possible gating-switch for the serotonin receptor, the same mechanism is not feasible for other members of the family. The opening of the nAChR would be much too fast (around 50000 s^{-1}) to involve a cis-trans isomerization of a proline, whereas in the GABA and glycine receptors an analogous proline is not conserved in the sequence.

1.5.4. Location of the Gate and Opening movements

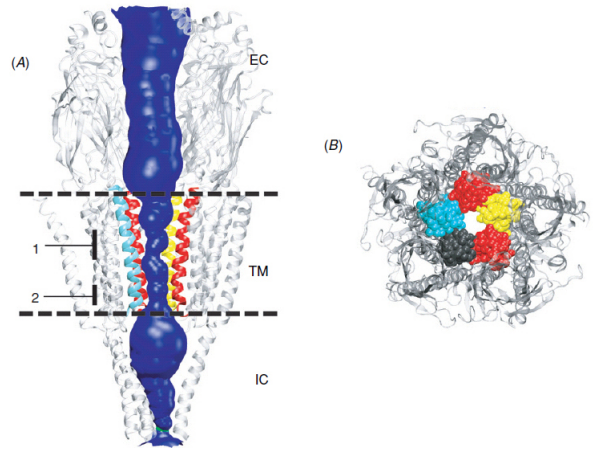

Figure 1.5.: **The gate in the *Torpedo* nAChR. a** Overall architecture of the nAChR (PDB ID 2BG9) as determined by cryo-electron microscopy[13], showing the surface of the pore (calculated with HOLE[56]). Membrane boundaries are indicated. The $\alpha 2$-helices are highlighted; the front subunit is omitted for clarity. **b** Structure of the nAChR TM domain viewed down the pore axis from the extracellular end, with the $\alpha 2$-helices in space-filling format (images produced with VMD[57] and RASTER3D[58]). Figure taken from Beckstein et al.[59].

The location of the gate of the nAChR has been under debate for a long time. The electron microscopy structure of the *Torpedo* nAChR was determined in the absence of ligand and presumably shows the closed state of the channel[13]. However, it shows a continuous water-filled pore with two constrictions with a minimum diameter of 3 Å each (see figure 1.5). One con-

striction is located about half way through the membrane and lined by hydrophobic residues (L, V; indicated with (1) in figure 1.5), the other one is located closer to the intracellular end of the channel and lined by hydrophilic residues (S, T; indicated with (2) in figure 1.5). There are experiments pointing towards either of these two positions acting as a barrier for ion diffusion, while both regions are sufficiently wide to accommodate a Na^+ ion and two water molecules side by side. Thus the structure shows a functionally closed pore which is not fully occluded. A solution to this paradox has been proposed by the mechanism of 'hydrophobic gating'. A hydrophobic gate has to be small enough (<4 Å) that the passing ion has to shed at least one of its hydrating water molecules. Since the energy of dehydration is rather high, the ion cannot pass as long as there are no hydrophilic groups within the protein channel which could substitute for the water molecule. Thus the constriction of the channel must be lined by hydrophobic residues to function as a gate. The central part of the pore (1) is lined by hydrophobic residues with a highly conserved sequence motif LxxxVxxxV/L (starting at residue 9′*), which indicates that this region could restrict the flow of ions. Several computational studies suggest that this narrow hydrophobic region could indeed function as a gate that prevents ion conduction [59,61,62].

A hydrophobic gate can fulfill the requirements for rapid pore opening, since a small change in diameter of about 1.5 Å would be sufficient to change from a completely closed conformation to a conformation with maximum conductance in an 'all-or-nothing' type [62,63]. Experiments using time-resolved photoaffinity labeling show that the residues at positions 9′, 13′ and 16′ line the closed pore of the channel [64,65], which would support the prediction that the gate is located at this position.

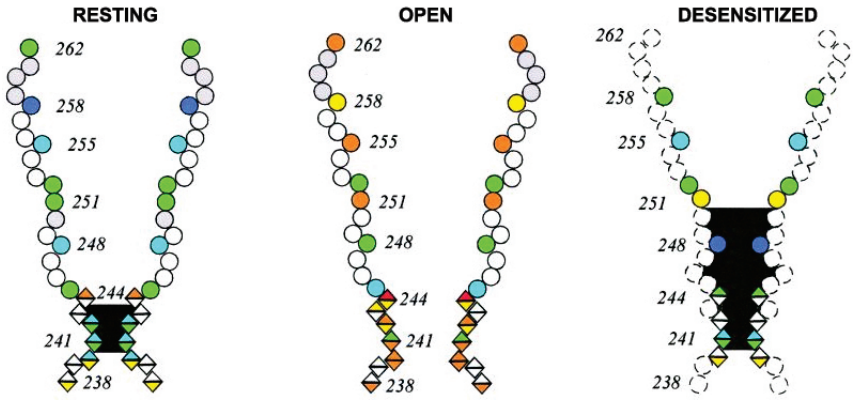

Figure 1.6.: **Pore conformations as proposed by Wilson and Karlin.** The reactivities of Cys substituted for the residues in α2 and the α1–α2 loop in resting, open, and desensitized states. Two α2 segments are represented schematically, facing the channel lumen. Where the lumen is black, the channel is relatively impermeable to MTSEA and presumably to inorganic cations. Warmer colors indicate a higher reactivity. Figure taken from Wilson and Karlin [66].

*Numbers indictated with ′ refer to the internal numbering of the α2-helix, starting with 1′ in the α1–α2 linker at the intracellular end. Compare to Miller [60]

Other experiments propose the intracellular end of the pore as the location of the gate in the closed state. Wilson and Karlin used the substituted cysteine accessibility method (SCAM) to probe the accessibility of residues in the pore region and the $\alpha1$–$\alpha2$ linker in different states of the receptor of the mouse muscle nAChR[66,67]. In a broad screen they mutated every residue in this region to cysteine and measured the reactivity to small cationic sulfhydryl-specific reagents (methanethiosulfonates, MTS), which can be used as a substitute for small permeant cations. In the open state all residues are accessible to these MTS reagents, whereas in the closed state the residues from -3′ to 2′ are not accessible, which would correspond to a gate at the intracellular end of the pore. Additionally they showed that MTS cannot pass the midpore of the channel in the desensitized state, based on which they proposed a conformation for the desensitized state where the gate of the resting state is broadened encompassing residues from -3′ to 9′ (see figure 1.6). This led to the assumption that the electron microscopy structure is in a desensitized state rather than in a resting closed state.

Paas and colleagues probed the conformation of the ion pore with a histidine scan measuring state-dependent Zn^{2+}-channel interactions in a chimeric $\alpha7$-5HT$_{3A}$ receptor[68]. With their experiments they propose a constriction at the intracellular end of the ion pore in the resting state, similar to the conformation concluded by Wilson and Karlin, which was described as an 'inverted teepee'. In the open state the channel was estimated to have a conformation with a wider diameter at the bottom of the pore and a narrower diameter in the extracellular half, a conformation that can be reached by a tilt of the $\alpha2$-helices around an axis parallel to the membrane.

Earlier electrophysiological studies determined the concentration dependence of permeability ratios and streaming potentials, that in combination resulted in a model of the channel in the open state with a short constriction at the intracellular end of the pore with one ion-binding site[69].

Based on the different conformations proposed for the resting, open and desensitized state several different models for the movements accompanying gating were developed. Unwin and coworkers proposed a rotational movement of the inner helices lining the pore, based on comparison of the different conformations seen in the electron-microscopy structures of the *Torpedo* nAChR, which have been imaged in assumed resting[73], desensitized[74] and open[72] states. In their model the $\alpha2$-helices are loosely packed and mainly separated from the outer protein wall, which is formed by the α-helices 1, 3 and 4. The $\alpha2$-helices are connected to the rest of the protein by flexible loops containing glycine residues and fixed by a covalent link formed by the Cys-loop, which also serves as a hinge. Ligand binding induces a rotational change in the 2 α-subunits which is transmitted to the $\alpha2$-helices[75]. The helices rotate and thus destabilize the gate which is formed by hydrophobic residues as a kink in the $\alpha2$-helices about halfway through the membrane (see **c** and **d** in figure 1.7) (see also section 1.6.2). While in the extracellular domain only the α subunits undergo a conformational change, in the transmembrane domain all 5 pore helices show the same contribution to channel opening[76].

Several computational studies used the electron-microscopy structure of the *Torpedo* nAChR or homology models based on it to assess the opening movements. Taly and colleagues performed normal mode analysis of a homopentameric $\alpha7$-receptor and observed a 'concerted symmetrical quaternary twist motion of the protein with opposing rotations of the extracellular and transmembrane domains'[77](see **b** in figure 1.7), a movement which was supported by

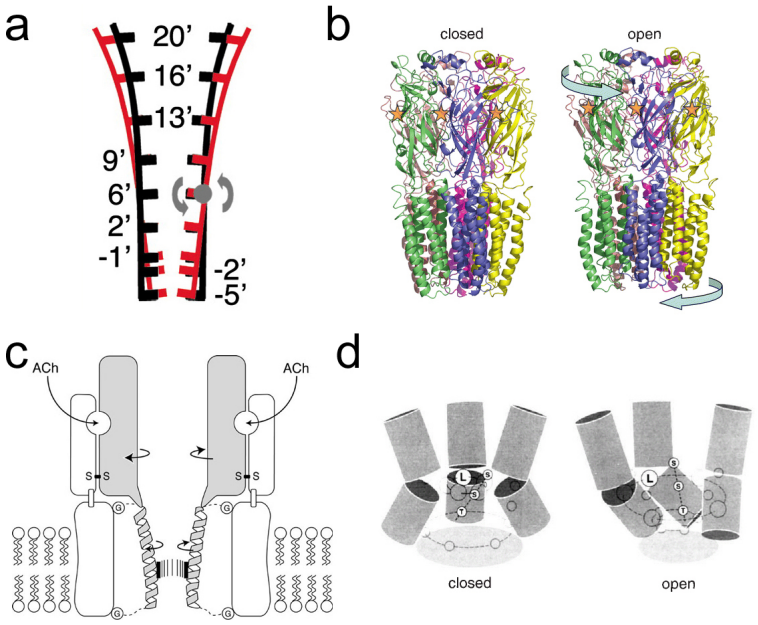

Figure 1.7.: **Proposed models of the gating process a** Red and black lines represent the closed and open states, respectively. The gray arrows indicate the motions around an axis of tilting. Paas et al.[68] **b** The comparison of the closed structure and the open model after energy minimization demonstrates the quaternary twist motion between the structures (following the arrows). Taly[70]. **c** The rotations in the α-subunits are transmitted to the gate through the α2-helices. The helices move freely during gating because they are mainly separated from the outer protein wall and connected to it by flexible loops, containing glycine residues (G). The relevant moving parts are shaded. Miyazawa et al.[71]. **d** Closed and open configurations of the α2-helix, with the pore-lining residues indicated. Relative to the closed state the open configuration has moved back the leucines, reoriented the line of polar residues, and brought T244 closer to the axis of the pore. Unwin[72].

later studies[78,79]. These rotational movements would be large enough to open the channel and are in agreement with several functional studies[66,75,80,81].

Contrary to these models there are studies which disagree with a rotational openening mechanism. By measuring the accessibility of residues in the α2-helix by SCAM, photoaffinity-labeling or a protonatable mutagenesis study developed by Cymes and Colleagues, it was found that the residues lining the pore are the same in the open and in the closed conformation, suggesting that there is only a minimum rotation involved[66,82] (see also figure 1.6). Referring to the work of Miyazawa[71] Cymes and coworkers propose an opening mechanism which involves a widening of the pore that changes the location of the narrowest constriction from the middle of the membrane to the intracellular exit.

Since Paas and coworkers find the constriction of the closed state at the intracellular end of the pore and a smaller tilt of the helices in the open state, they propose an opening mechanism

as a concerted rigid-body tilting movement of the pore lining helices around an axis parallel to the membrane away from the pathway of ion conduction. This movement opens the bottom of the pore, while at the same time it narrows the extracellular half of the pore (see **a** in figure 1.7).

To sum up, even if many studies have probed the location of the gate, the conformations of different states and the gating movements, there are several contradictory models. It is clear that the ambiguity will only be resolved with high-resolution structural information of defined states of the receptor.

The conformational changes that lead to channel opening originate in the extracellular domain upon ligand binding. These changes have not been studied in as great detail as for the pore domain. However, Nigel Unwin proposed a rotation within the extracellular domain of the α subunit upon activation based on the difference in the conformations between α and non-α subunits observed in the electron density[75]. In his model the α subunits in the resting state adopt a characteristic conformation different from the other subunits, which is stabilized by specific interactions with the neighboring subunits. Upon activation the α subunits rotate to adopt the same conformation as seen in the non-α subunits.

1.5.5. Ion Selectivity

As the gate of the ion channel opens, ions are allowed to flow down their electrochemical gradient. However, the channels do not allow all ions to pass, they are usually selective since an unselective ion channel would quickly dissipate all ionic gradients, which would be fatal for the cell. The mechanism by which ion channels specifically catalyze the rapid permeation of certain ions, which is a prerequisite for fast signaling, while they exclude others, is an important topic in ion channel research. While a strong binding site would allow for high selectivity, it would at the same time restrict the ion flow. A fine-tuned mechanism is needed to account for high selectivity and fast ionic flux. The selection for a specific ion is based on its size and charge and it requires to either partly or fully release its hydration shell and coordinate it by hydrophilic protein atoms in a narrow region of the channel called the selectivity filter.

Several examples of selectivity filters have been studied in great detail in different classes of ion channels. The first selectivity filter at atomic resolution was seen in the K^+-channel KcsA, a structure that was determined by Zhou et. al[83]. The selectivity filter of KcsA is formed by several backbone carbonyl oxygens, which point into the pore. A hydrogen bond network stabilizes the carbonyl atoms in a conformation that stabilize K^+ ions efficiently while it prevents Na^+ ions to pass the pore. In this way four K^+ ion-binding sites are formed, which can be occupied by two K^+ ions either in a 1–3 or a 2–4 configuration, where the cations have shed most of their hydration shell and are coordinated by the carbonyl atoms. The selectivity filter of the chloride channel homologue from *E. coli* (EcClC), on the other hand, is formed by amide nitrogen atoms and protein side chains (Ser and Tyr) within a 15 Å long neck of an hourglass-shaped pore[84]. Two Cl^--binding sites are freely accessible and a third one is released as soon as the fast gate of the channel, a glutamate that blocks an ion-binding site exposed to the extracellular solution, opens. In this site the Cl^- ion is surrounded by aminde nitrogen atoms of two juxtaposed helix termini (see figure 1.8).

It is an important question how ion selectivity in the family of pLGICs is accomplished. The transmembrane helix $\alpha 2$ has long been known to line the central ion pore, which makes

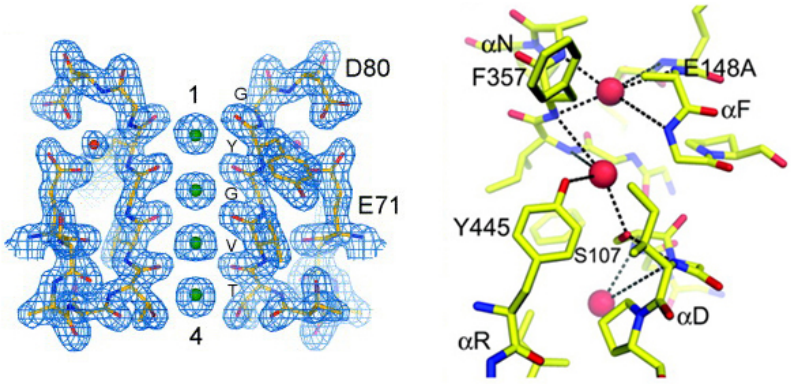

Figure 1.8.: **Selectivity filters in KcsA and EcClC. a** The selectivity filter region (two subunits) of KcsA. Residues surrounding the selectivity filter (from E71 to D80) are shown. The four K^+-binding sites are represented as green spheres and numbered 1 through 4. The $2F_o$-F_c electron density map is colored in blue. K^+ ions are coordinated by backbone oxygen atoms. **b** View of the ion-binding sites of the EcClC E148A mutant. Selected residues in the vicinity of the bound Cl^- ions are shown. Hydrogen bonds between the protein and Cl^- ions (red spheres) are shown as dashed lines. Cl^- ions are coordinated by serine, threonine side chain atoms and amide backbone atoms. Figures taken from Zhou and MacKinnon[85] and Dutzler et al.[86].

it relevant for ion permeation and also for selectivity. The nAChR is cation selective with a poor discrimination between different cations[87–92]. Depending on the subtype of receptor it also allows Ca^{2+} ions to pass the ion channel to different extents[92]. The narrowest part of the pore is believed to be around 7.4 Å for the *Torpedo* nAChR[93] or 8.4 Å for the nAChR homologue from the mouse[91], whereas in the anion-selective branch of the family the diameter is suggested to have a smaller size of about 5–6 Å[94,95]. The narrowest part of the pore of the nAChR, which most likely represents the selectivity filter, has been assigned a longitudinal dimension of 3–6 Å, which would correspond to two or three turns of an α-helix pointing amino acids into the pore[69].

Residues that are important for ion selectivity have been identified by sequence alignment, followed by mutational analysis. Three rings of conserved residues, mostly glutamates, within the α2-helix are highly conserved. They were termed the extracellular (at amino acid 20′), intermediate (-1′) and cytoplasmic (-5′) ring of charges (compare to figure 1.9)[96]. A decrease in the net charge at these positions leads to a decrease in channel conductance, an effect which is strongest for mutations at the -1′ position[97], a fact that suggests this position as candidate for the selectivity filter.

By using electrophysiology it was also determined that the amino acid at position 2′ that contains a conserved polar residue (Ser or Thr) is involved in a narrow constriction of the ion-conduction pathway[99,100]. It was suggested that this 'polar ring' participates in coordination of the partially dehydrated cations[101]. Mutations in this position reduce the single-channel conductance depending on the size of the side chain of the introduced amino acid[100,102]. Mutation

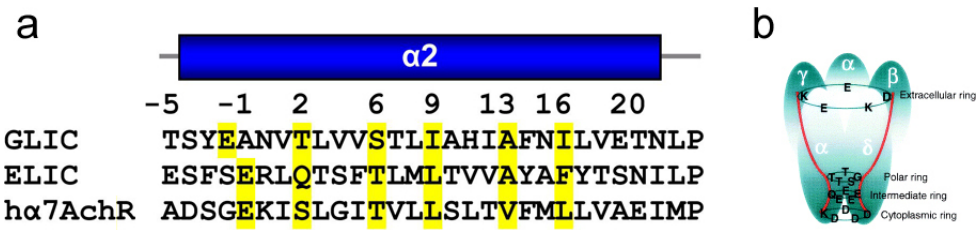

Figure 1.9.: **Sequence alignment of the α2-helix region.** **a** Alignment of the pore lining residues of the human α7 nAChR, ELIC and GLIC. Conserved rings are indicated. **b**. The amino acid residues implicated in the different charged rings of the muscular nAChR. **b** taken from Jensen et al.[98].

in positions further along the pore (at 4′, 6′, 10′ and 12′) do not influence the conductance, which suggests a wider channel diameter in these regions in the open pore[99] (see also section 1.5.4).

Overall the intracellular and extracellular ring of charges influence channel conductance, whereas the residues at -1′ and 2′ form a narrow region typical for a selectivity filter, which facilitates ion conduction and selection. Apart from α-helix 2 the linker between the α1 and α2-helices is also important for electrostatics and the determination of the pore size. The dimensions and shape of the pore as well as the distribution of charges correspond well to what has been predicted by Dani based on measurements of streaming potentials in the nAChR[69,103].

How anions are selected in the anion selective branch of the family is less clear. A comparison shows that these channels often do not contain charged residues in the same positions. The position -1′, for example, does not carry a positively charged residue. The cytoplasmic ring at -5′ is negatively charged, whereas positively charged residues can be found at positions 0′ and 19′. Interestingly, some of the anion selective channels contain an additional proline within the α2-helix close to the intracellular exit.

By mutating all seven residues that were predicted to face the pore in the α7 nAChR to the respective residues from the anion selective GlyR, the α1 channel switched its ionic preference from cation selective to anion selective. It was also possible to reduce the number of necessary mutations to three: Glu-1′ to Ala, Val13′ to Thr and a proline insertion at position -2′ to convert the ion selectivity[104]. Different combinations of these mutations were studied in more detail[104,105]: whereas E1′A and V13′T were termed permissive, proline insertion was termed exclusive for anion selectivity, even if the position for insertion was found to be flexible between -4′ and -1′[105]. None of the mutations were able to change ion selectivity gradually, which proposes a switch of selectivity that might occur due to a structural reorganization upon proline insertion as a key determinant for ion selectivity.

The proline residue was also proposed to be important for determining the pore diameter[106]. It was argued that a larger pore size might allow cation permeation, whereas a smaller pore would still be permeable to anions due to their bigger size and the lower energy requirements for dehydration. Several follow-up studies have focused on the insertion of a proline in the pore forming helix, but the role of this rigid residue remains unclear, since its importance could not be shown for other family members. A serotonin receptor was turned to be anion selective without a proline insertion, glycine and different GABA receptors stayed anion selective even if

the proline was removed and a cation selective GABA receptor could be constructed containing a ring of proline residues[98]. Another interesting feature is that the 'missing' proline residue in cation selective channels is more conserved than the existent residue in anion selective channels.

While most of the experiments to switch ion selectivity have been carried out in homopentameric serotonin, glycine and GABA receptors, the first study on a heteromeric pLGIC was using a GABA receptor ($2\alpha_2 2\beta_3\gamma_2$), which was switched to be cation selective with mutations only in the β subunit, while leaving the α and γ subunits in their native state[107]. This asymmetric behavior has also been shown for the heteromeric muscle nAChR, where mutations at the -1′ position have a stronger effect if they occur in the γ subunit than in any of the other subunits[93,96,102]. The asymmetry in most channels from the pLGIC family offers fine tuning possibilities regarding ion selectivity and conductance.

A recent study has probed the ion selectivity within the extracellular domain of the family of pLGIC[108]. It was found that a conserved ring of charged residues about 24 Å above the membrane plane at the inner face of the vestibule could function as a first selectivity filter, prescreening the ions before they enter the narrow ion conduction pore.

1.5.6. Desensitization

A functional property of the nAChR, which is poorly understood, is the purpose and mechanism of desensitization. Desensitization is a reversible reduction or loss of biological response during prolonged or repetitive agonist application. On a macroscopic level it can be observed as the decline in macroscopic response during continuous exposure to neurotransmitter and a decrease in the absolute responsiveness of the muscle cell to agonist. On a microscopic level it reflects the time-dependent accumulation of receptors in long-lived non-conducting states[109,110]. It is an intrinsic property of the receptor, since reconstituted proteins show the same behavior[111].

Katz and Thesleff have carried out a detailed kinetic analysis of desensitization onset and recovery[112]. The resulting model describes the nAChR existing in two states: one resting or activatable state (R) and a desensitized state (D). The R state has a relatively low affinity and requires high agonist concentrations for activation, whereas the D state has at least a 20-fold higher affinity for the agonist. Desensitization occurs through binding of agonist in very low concentrations to the D state and in this way removing the receptor from the open-close equilibrium. There are different estimations about the fraction of receptor in the D state in the absence of agonist ranging from «1%[113] up to 60%[114]. Desensitization can thus be described as a classical form of allosteric protein behavior.

Desensitization depends heavily on the receptor subtype and can be distinguished between α7-receptors, which desensitize rapidly (in milliseconds) and non-α7 receptors, which desensitize slowly (in seconds). Classical desensitization happens in the presence of high agonist concentration, which first activates the receptor and subsequently leads to desensitization until the agonist is cleared from the synaptic cleft. If agonist is present in low concentration 'high-affinity desensitization' can occur, a slow process which happens during prolonged exposure to agonist.

The physiological role of desensitization still remains unclear since the neurotransmitter is usually not long enough in the synaptic cleft for desensitization to occur[115]. It could only be relevant in the α7-receptor, which desensitizes rapidly, or in receptors with a high agonist affin-

ity, where the agonist remains bound even after the free transmitter has been cleared from the synaptic cleft. It was speculated that desensitization is a use-dependent, readily reversible form of signal plasticity or that it provides a mechanism to protect cells from uncontrolled excitation[111], which would lead to excitotoxicity due to the high Ca^{2+} permeability of most nAChRs. This process might also be relevant to control cholinergic activity and induce adaptive changes, which might play a role in chronic modulation of nAChRs in the brain of tobacco smokers.

The occurence and timecourse of desensitization is highly subtype and agonist specific and has been studied thoroughly with radiolabeled ligand-binding assays and physiological measurements, leading to a detailed understanding which is summarized in a review by Giniatullin and coworkers[116]. It will not be discussed in detail in this thesis, since the prokaryotic homologues studied in this PhD project do not show desensitization (see section 1.7).

1.6. Obtaining Structural Information on the pLGIC Family

Structural studies of members of the pLGIC family were lacking for many years. Various attempts towards the structure determination of these eukaryotic membrane proteins failed because of difficulties to obtain sufficient amount of protein in a pure and stable state. More recently structural information was obtained due to the discovery of the acetylcholine binding protein (AChBP), a soluble protein that resembles the extracellular domain of the receptor, and due to the advances in cryo-electron microscopy to image the nAChR from *Torpedo* electric ray.

1.6.1. Soluble Acetylcholine Binding Proteins

In 2001 a soluble protein from Glia cells of snails was discovered[117], which modulates synaptic activity by binding acetylcholine and in this way preventing it from binding to the receptor. On the sequence level this protein shows high homology to the N-terminal extracellular LBD of pLGICs, but it lacks the transmembrane and intracellular domains of the receptors. This acetylcholine binding protein (AChBP) is most closely related to the α-subunit of the nAChR, containing nearly all residues, which are conserved within the family. It was also shown that AChBP binds known agonists and antagonists of the nAChR as acetylcholine, nicotine and α-bungarotoxin. The first X-ray structure of this protein was determined in 2001 by Brejc and coworkers[44].

The overall structure of the AChBP is shown in figure 1.10. Each subunit consists of an N-terminal α-helix, two short 3_{10}-helices and a core of ten β-strands, which form a β-sandwich. The β-sandwich can be described as modified immunoglobulin fold, where the β-strands have been rotated with respect to each other. The view along the five-fold axis shows a windmill toy-like shape with a diameter of 80 Å. The inner diameter of the central hole is ~18 Å, the height of the cylinder 62 Å. The ligand-binding site was identified in the interface between two protomers surrounded by residues, which have been shown to be important for ligand-binding. In this first structure the ligand-binding site is occupied by a HEPES molecule, which stacks with its quaternary ammonium cation onto a tryptophane residue making cation-π interactions as expected for nicotinic agonists[118].

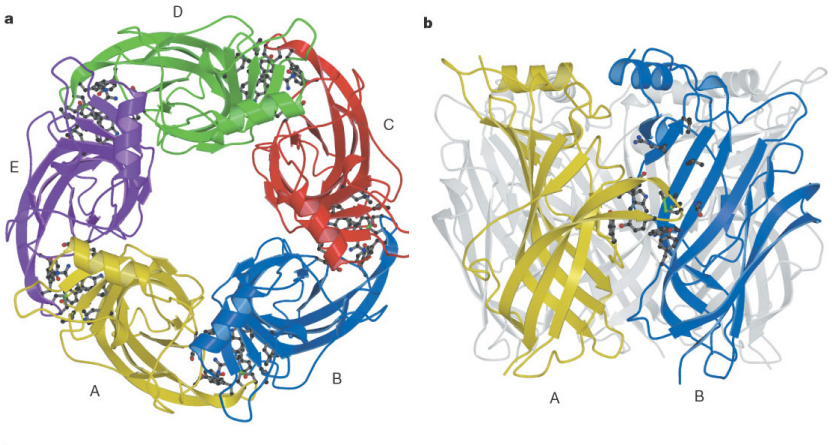

Figure 1.10.: **Structure of the AChBP.** Cartoon representation of the structure of the acetylcholine binding protein. Each subunit is shown in a different color. Residues lining the ligand-binding site are shown in ball-and-stick representation. **a** View along the five-fold axis. **b** View of the AChBP pentamer perpendicular to the five-fold axis. Figure taken from Brejc et al.[44].

The conserved residues in the LBD can be classified in three clusters, which are involved in packing of the N-terminal α-helix against the core and in the upper and lower half of the core of the β-sandwich, respectively. Most of the conserved residues in the family are hydrophobic and with the structure of the AChBP it becomes obvious that they are important for maintaining the overall fold of the protein. The residues in the interface between the subunits, however, are not conserved, which opens possibilities for varying interactions between different receptor subunits to create a variety in allosteric contacts and movements upon activation. Another feature which is highly conserved in the pLGIC family are the residues in the Cys-loop, that forms contacts to the transmembrane domain, which are important for gating of the ion channel. Since in the AChBP this loop is exposed to solvent instead, the respective residues are not conserved and are replaced by hydrophilic residues.

While the structure of the AChBP does not provide insight into the allosteric movements upon activation of a full-length receptor, it can give valuable insight into conformational changes and the chemistry of ligand-protein interaction during agonist or antagonist binding. Following-up on the first structure, several structures in complex with different ligands have been determined by X-ray crystallography[32,119–122]. The structures of AChBP in complex with different agonists and antagonists revealed the important role of the C-loop, which is closing the LBP upon ligand-binding. Hansen and coworkers determined the structure of the *Aplysia californica* homologue (A-AChBP) in the apo-form, in the presence of agonists and antagonists[119]. In the absence of ligand the C-loop adopts an open conformation, which allows ligand to enter the binding pocket. Binding of agonists leads to loop closure, whereas binding of antagonists stabilizes the open conformation or displaces the loop even further away from the protein core. This ligand

induced structural change of the C-loop has been attributed to induce conformational changes, which finally lead to channel opening.

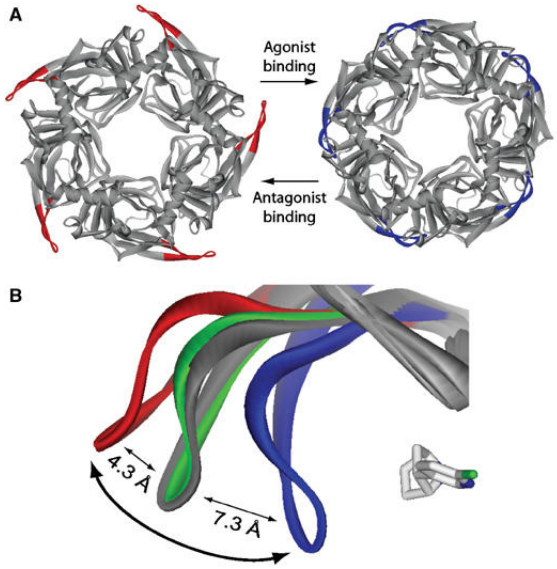

Figure 1.11.: **Conformational fit mechanism. a** Top views of the antagonist-bound (red loops C) and agonist-bound A-AChBP pentamers (blue loops C) showing two distinct conformations. **b** Overlay of loop C in apo A-AChBP (gray) and the antagonists (red) and (green), as well as the agonist complexes (blue); the bound agonist molecule is shown in light gray. The curved arrow denotes opening and closure of loop C upon antagonist and agonist binding. Figure taken from Hansen et al.[119].

1.6.2. The nAChR from Torpedo marmorata

The only abundant, natural source of any pLGIC family member, is the electric ray *Torpedo marmorata*, which contains staples of membranes in its electroplax organ which are packed densely with the nAChR. Due to this high concentration of almost pure nAChR in its membrane, Chris Miller once called *Torpedo* a "swimming purified acetylcholine receptor"[124]. The natural abundance of the nAChR from *Torpedo* allowed structural studies by electron microscopy, work which was carried out during many years in the laboratory of Nigel Unwin.

The isolated membranes from *Torpedo* convert readily into long tubular crystals if left standing at 4–17°C for 4 weeks, arranging the receptor and the surrounding lipids on a helical surface lattice suitable for cryo-electron microscopy (see **a** in figure 1.12). The first images were obtained from negatively stained flattened tubular vesicles (1980s). Later the tubes were suspended in layers of thin ice to conserve the helical symmetry. The tubular arrangement allows the receptor to be seen from many different possible angles which allowed to determine the pentameric symmetry of the protein[125]. With continuous refinement of technical details, like an improved cold stage, the correction of distortion of the crystal lattice and computational image analysis, the structural information obtained from the tubular crystals could be improved over the

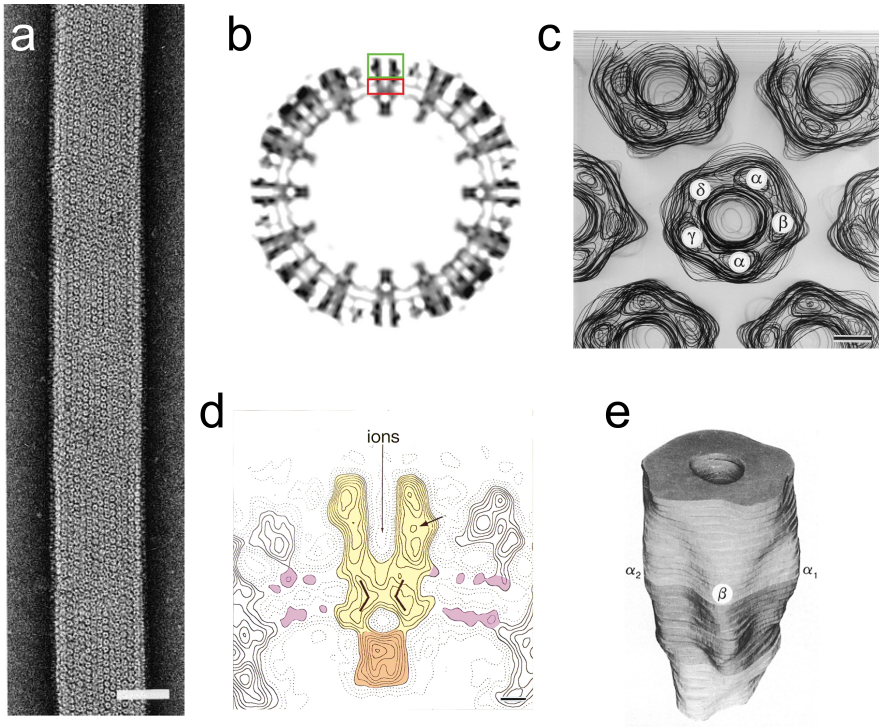

Figure 1.12.: **Electron Microscopy of the nAChR. a** Tight lateral packing of nAChR grouped into a regular p2 surface lattice in tubular crystals. Scale bar 500 Å. **b** Cross-section of a tubular crystal at low resolution. **c** Extracellular domain viewed from the synaptic cleft after activation by ACh, made by stacking successive 2 Å-spaced sections on top of one another. **d** nAChR at 9 Å resolution in a section normal to the tube axis. **e** Balsa-wood models of the nAChR before exposure to carbamylcholine. Figures taken from Unwin et al.[71,72,74,123].

years[13,72–74,126–131] to finally give rise to a cryo-electron microscopy structure of the receptor at 4 Å resolution[13] (see **a** and **b** in figure 1.13). The identification of the different subunits was achieved by using labeled ligands or FAB fragments, which bind to specific subunits[132]. Images of the receptor in specific states were determined by different methods. While the untreated receptor adopts the closed resting state[13,73], a prolonged (several minutes) treatment with carbamylcholine, an acetylcholine analogue, shifts the receptor in the ligand-occupied, desensitized state[74] (see **e** in figure 1.12). By a very fast incubation with acetylcholine and immediate freezing of the receptor it was assumed to image the receptor in the open state[72] (see **c** in figure 1.12).

The structures in the different states were used to predict possible conformational changes upon gating of the channel. Comparing the 4 Å resolution structure in the resting state with the structure of the presumably open state, several differences can be detected. The rapid spray-freezing technique leads to a local disturbance around the ACh-binding sites in the extracellular domain, and to rotational movements in the LBD of the α subunits, mainly in the inner β-sheet.

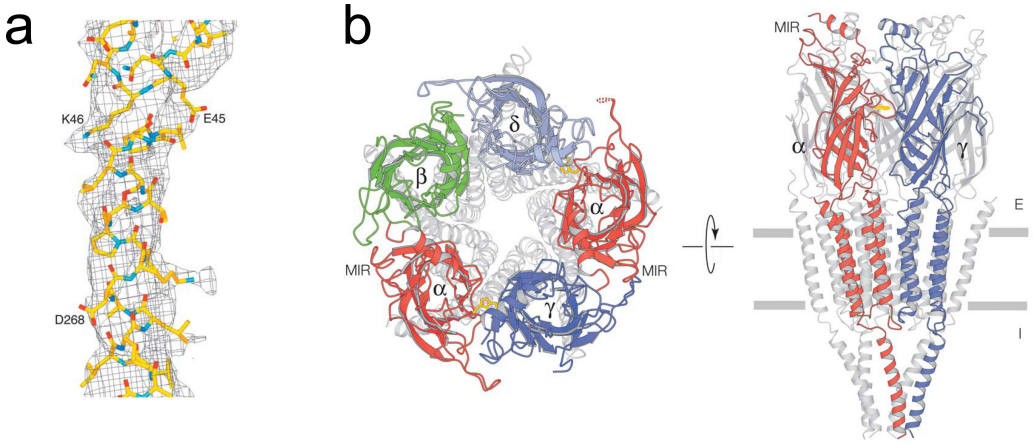

Figure 1.13.: **4 Å resolution structure of the nAChR. a** Protein chains superimposed over the refined and improved density map at 4 Å resolution. **b** Cartoon representation of the nAChR viewed from the synaptic cleft (left) and parallel with the membrane plane. Figures taken from Unwin[13].

Additionally to this the α2-helices in the transmembrane domain change their location, so that the lumen of the ion pore is widened in the middle of the membrane.

The structure in the resting state prior to activation shows a distinct conformation: the inner sheet is rotated anticlockwise by about 11° around an axis normal to the membrane that passes between the 3 α-helices 1, 3 and 4, whereas the outer β-sheets tilt more steeply in the α subunits. This difference in tilt is mainly based on a different twist of the β9-β10-strands. The C-loop, closing the LBP, is mostly undefined in the α subunits, which indicates that it is flexible in the ligand unbound form.

It was proposed that the α subunits are distorted in the resting state and stabilized in this conformation by inter- and intra-subunit interactions, while the energy of ligand-binding induces a conversion into the relaxed form, as seen in the non-α subunits. In this way the extracellular domains of the α subunits induce channel opening, while the other subunits can influence this process by direct participation in the ligand-binding process or by stabilizing specific conformations of the α subunits. In the transmembrane domain, however, all subunits participate equally to break the hydrophobic gate seen in the middle of the membrane[76].

The transmission of the signal from the LBD to the transmembrane domain cannot be deduced from the electron microscopy data, since the relatively low resolution (9 Å) does not allow clear insight into the region of the domain interface and since there is no data at high-resolution on the receptor in the open state. However, it was proposed from the structure that Val-46 serves as a direct link between the extracellular domain and the transmembrane domain. This residue is located in the β1–β2 loop and fits well into a hydrophobic pocket on top of the α2–α3 loop. Additionally to this valine the neighboring glutamate E45 forms conserved interactions to another region of the extracellular domain, as has been proposed by Lee and coworkers[51] (compare figure 1.4). However, much of these ideas are mere speculation and even if a resolution of 4 Å is remarkable for cryo-electron microscopy, it is not sufficient to unambiguously locate

individual residues. The detailed positions of amino acid side chains are thus uncertain and even the register might be shifted. Thus, high-resolution structures of a pLGIC at different states of the gating process are needed to obtain definite answers about conformational changes and signal transduction in pLGICs.

1.7. Prokaryotic Homologues

Prokaryotic homologues have frequently been used as model systems for soluble protein families and as structural surrogates to gain insight into conserved mechanistic features. Results obtained from homologous prokaryotic proteins have thus proven to be valuable for the understanding of their eukaryotic counterparts. For ion channels, however, prokaryotic homologues were for a long time unknown which prevented them to serve as alternative for functional and structural studies. One of few eukaryotic ion channels of natural abundance was the nAchR from *Torpedo*, which despite the large experimental efforts did not allow to obtain structural data at high resolution. The high-level heterologous expression of eukaryotic proteins, in contrast, was not within reach and still is in its infancy. While ion channels were studied with highly-developed electrophysiological equipment in unprecedented detail, their structural understanding was lagging behind due to the lack of sufficient material, a situation well described by Chris Miller: a 'functional paradise, structural hell' [133].

The first glimpse of hope was seen in 1994, when the first bacterial K^+-channel was discovered [134], followed four years later by the first high-resolution structure of any ion channel solved in the laboratory of Roderick MacKinnon [135].

For a very long time it was believed that pLGIC only exist in higher eukaryotes until in 2005 Tasneem and colleagues discovered the first pLGIC in prokaryotes [136]. In sequence-profile searches they identified pLGICs in several bacteria and a single archaeal genus, but only about 1 % of all available prokaryotic genomes contain a copy of this gene. The homology between eukaryotic and prokaryotic pLGICs proteins extends to the extracellular LBD and the transmembrane domain, whereas a short N-terminal α-helix and the intracellular $\alpha3$–$\alpha4$ loop are missing. Even if the sequence identity is low (<20%) and the eponymous Cys-loop cysteines are missing, several key residues are conserved throughout species, e. g. the charged residues in the $\alpha2$-helix as key determinants for ion selectivity, aromatic residues forming the LBP, an acidic residue in the Cys-loop and the basic interaction partner in $\beta10$ as a network indispensable for gating. Due to the presence of functionally important residues the prokaryotic proteins are likely to share structural and mechanistic properties with their eukaryotic homologues.

Some of the bacterial homologues are fused to an additional N-terminal domain of the periplasmic binding protein type I superfamily or in more distantly related homologues to a methyl accepting chemotaxis protein-N domain or Cache domain. In the genomic context genes coding for periplasmic binding proteins type II can be found in the same operon. All these additional domains are ancient sensory modules, which are also used in animal neural systems. Based on this it was proposed, that in their native environment the bacterial pLGIC might be involved in chemotaxis of low molecular weight solutes.

Bocquet and coworkers studied the homologue from *Gloebacter violaceus* and established its function as a proton-gated ion channel from the pLGIC family [137]. The *Gloebacter* ligand-

gated ion channel (GLIC, former Glvi) was expressed in HEK293 cells and *Xenopus laevis* oocytes. In functional studies the channel can be opened by low pH, with a midpoint of activation around pH 4.9. It shows robust cationic currents without desensitization and a single channel conductance of 8 pS. Currents can be inhibited by tetraethylammonium (TEA) and QX-222, a quarternary ammonium derivative of lidocaine, which both are typical Na^+-channel blockers, but are also known to inhibit the nAChR. In contrast to the eukaryotic proteins, GLIC shows a slow activation and a rapid offset. Studies of the L9'I mutant of GLIC showed functionally similar behavior as has been seen in eukaryotic family members, like increased sensitivity to agonist and a slower inactivation rate. GLIC could be expressed in *E. coli* as a fusion to an N-terminal maltose binding protein (MBP) and forms a pentamer in solution, which could be crosslinked and detected by electron microscopy. GLIC was the first prokaryotic pLGIC which could be expressed in a functional state for electrophysiological recordings and it provided a model system to tackle structural studies, since it is readily overexpressed in *E. coli*.

1.8. Aim of this thesis

The aim of this PhD thesis was to solve an X-ray structure and to obtain high-resolution structural data of a prokaryotic member of the pLGIC family and to study functional properties of ion selectivity and gating. Prokaryotic membrane proteins have previously proven to facilitate structural studies due to their comparatively higher stability when extracted from the membrane and due to the more compact structure, features that were also seen in GLIC. Since key residues are conserved, it is likely that in the overall structure elementary functional properties are shared between the prokaryotic and eukaryotic counterparts. Thus the prokaryotic pLGICs provide important model systems to allow a deeper understanding of the open questions in the field.

CHAPTER 2

RESULTS

2.1. Expression Studies

The pLGICs have an unusual topology for bacterial membrane proteins in that both termini of the protein reside on the periplasmic side. The extracellular N-terminus is followed by a soluble domain of about 200 amino acids and a four helices containing transmembrane domain. For overexpression 10 identified bacterial homologues (see chapter 4 and sequence alignment in figure 2.1) were cloned into a pET-based expression vector for expression under the control of the T7 promoter (see section 4.1.1). None of these constructs showed any expression on a whole cell SDS-PAGE/Western blot using an antibody detecting the His-tag attached to the C-terminus of the protein. All constructs included the full length sequence starting with the first possible methionine, which for most of the homologues starts with a secretion signal sequence as predicted by the SignalP prediction server[138]. This signal sequence is required in the host organism to target the protein to the membrane and to export its N-terminus out of the cell. It is recognized by the protein translocation machinery of the native organism and even if there are conserved features between different bacterial export mechanisms, the sequence specificities for the recognition sequences differ. To exclude the possibility that the native signal sequences is not recognized by the *E. coli* secretion machinery, several genuine *E. coli* signal sequences were investigated using commercially available vectors that either contain the signal sequences for pelB and the secreted fusion proteins DsbA and DsbB including their respective signal sequences. Except the *R. palustris* pLGIC with the pelB signal sequence, none of these constructs showed any expression under several different expression conditions. The *R. palustris* pLGIC was expressed in very small amounts and this protein turned out not to be localized in the membrane.

It is speculative to reason why none of these proteins are properly expressed in *E. coli*. The topology of the pLGIC with a large extracellular N-terminal domain followed by a transmembrane domain might cause problems, since a similar topology is not common in bacteria. While there are multiple examples of secreted proteins that are exported from the cell into the periplasm, membrane proteins which have their N-terminus outside are rare.

A solution to this problem was proposed by Bocquet and coworkers[137], who were able to express the pLGIC homologue from *G. violaceus* as a fusion protein to the maltose-binding protein (MBP). Recloning of the prokaryotic pLGICs into an expression vector after an N-terminal histidine tag followed by the well expressed MBP (His_6-MBP-3C-pLGIC-His_6) gave rise to high-level expression of all homologues (see figure 2.2 **b**). These proteins are located in the membrane, are extractable with mild detergents like DDM, but are without exception aggregated when analyzed by size exclusion chromatography (SEC)(see figure 2.2 **c**). New constructs

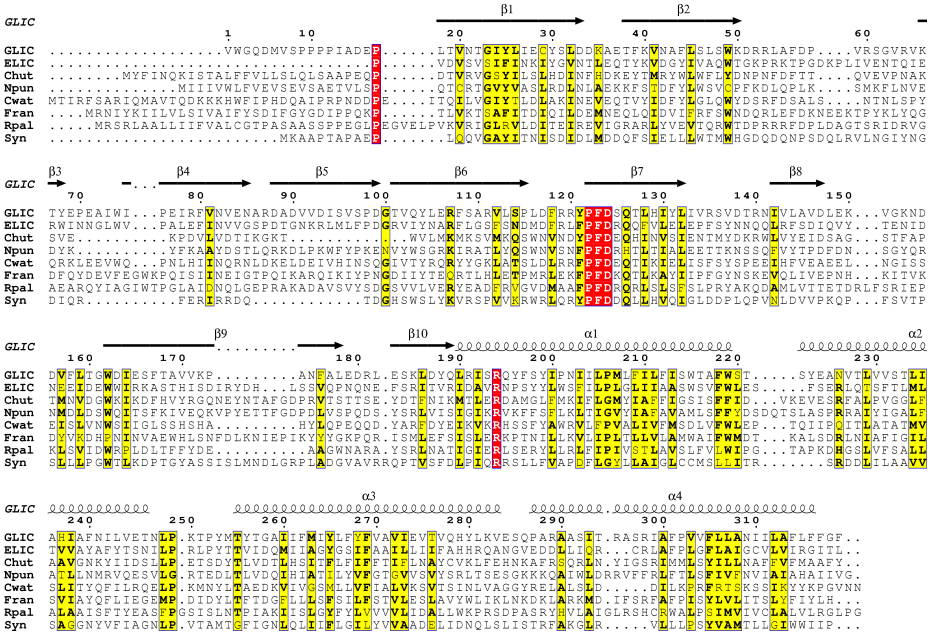

Figure 2.1.: **Sequence alignment of bacterial pLGICs.** 8 bacterial homologues aligned with ClustalW[139]. Identical residues are colored in red, similar residues in yellow. Secondary structural elements from the GLIC structure are indicated above the alignment. Species are abbreviated as follows: Chut *Cytophaga hutchinsonii*, Npun *Nostoc puntiforme*, Cwat *Crocosphaera watsonii*, Fran *Francisella sp.*, Rpal *Rhodopseudomonas palustris*, Syn *Synechococcus sp.*. Homologues from *Methanosarcina barkeri* and *Methanosarcina acetivorans* were not included due to their additional extracellular domain and low sequence conservation. ESPript 2.2[140,141] was used to visualize the alignment.

that include the pelB signal sequence at the N-terminus of the expressed protein, followed by a His_{10}-tag to improve the purification properties (figure 2.2 **a**), overall decreased the expression yield. However, these improved expression constructs allowed the purification of pentameric proteins of two of the homologues that eluted at a volume of ~11.5 ml on a Superdex S200 column (figure 2.2 **d**). The purification, crystallization and structure determination of the two pLGIC homologues from *Erwinia chrysanthemi* (ELIC) and *Gloebacter violaceus* (GLIC) is described in sections 4.2.1, 4.2.2 and 4.2.3.

2.2. The *Erwinia chrysanthemi* pentameric ligand-gated ion channel

Of all investigated homologues the pLGIC from *Erwinia chrysanthemi* (ELIC) was the best expressed candidate with a final yield of about 3 mg of purified protein for 10 l of culture. Its expression was very reproducible and the protein proved to be stable once purified. ELIC showed a comparably high stability in various detergents including several maltosides with different

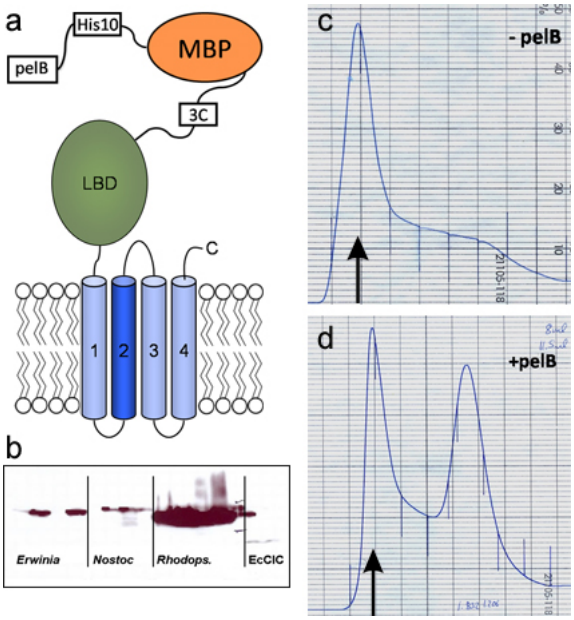

Figure 2.2.: **Expression and Purification of prokaryotic pLGIC in *E. coli*. a** Scheme of final construct including an N-terminal pelB signal sequence followed by a His_{10}-tag, the MBP, the HRV 3C protease cleavage site and the pLGIC. **b** Full-cell western stained with an Anti-His-tag antibody showing the expression of the prokaryotic pLGIC of *Erwinia chrysanthemi*, *Nostoc punctiformis*, *Rhodopseudomonas palustris* without the pelB signal sequence and the chloride channel from *E. coli* EcClC as a control. **c** and **d** Gelfiltration profile on a Superdex S200 column. The void volume is indicated (arrow) **c** ELIC construct as in **a** without the pelB signal sequence and **d** with the pelB signal sequence.

chain-lengths ranging from C_8 to C_{13}, whereas detergents with different head-groups like LDAO or $C_{12}E_8$ led to aggregation of the protein. Figure 2.3 shows samples of a typical purification of ELIC on an SDS-PAGE starting from the elution of the fusion protein from the Ni-NTA column. Due to the high affinity binding of the comparably long His_{10}-Tag to the resin, the Ni-NTA column was washed stringently with 55 mM imidazole to remove non-specifically bound background. Thus, after elution of the protein from the Ni-NTA column by addition of 300 mM imidazole, the protein was already relatively pure (**1**). Subsequently, the protein was digested for 2h with HRV 3C protease and dialyzed to lower the imidazole concentration. During the time of protease incubation the protein is almost completely cut (**2**). It is remarkable at this step that the apparent ratio of the MBP to ELIC often appears not to be stoichiometrical, but instead shows an excess of the MBP. This might be due to the fact, that ELIC might degrade during the purification. After cleavage, the protein is reloaded on the Ni-NTA column, where the MBP and the HRV 3C are rebound, whereas ELIC remains in the flow-through. Apart from the MBP-His fusion this step also removes some impurities, which were co-purified on the first Ni-NTA column (**3**). The His-tagged MBP, the HRV 3C protease and the non-specific impurities bound

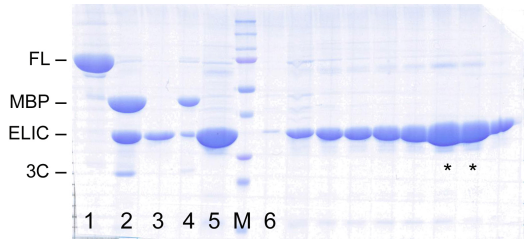

Figure 2.3.: **Coomassie-stained SDS-gel of a typical purification of ELIC.** Samples from different steps of the purification. The size of the fusion protein (FL), the MBP, ELIC and the HRV 3C are indicated. **1** elution from the Ni-NTA column. **2** after 2h cutting with the HRV 3C protease. **3** after removal of the MBP and the 3C, **4** rebound MBP. **5** injection onto the SEC. **6** fractions from the SEC. Fractions indicated with $*$ were taken for crystallization. **M** standard molecular weight marker (BioRad) with 75 (red), 50, 37 and 25 (red) kDa.

on the second Ni-NTA column, can be identified in lane **4**. A small amount of ELIC is found in this fraction as well, which might be either due to traces of uncut protein, which assemble as mixed pentamers or due to aggregated protein. Lane **5** shows ELIC as it is loaded on the size exclusion chromatography (SEC) column. Due to the high concentration of the protein sample some remaining impurities are visible here. The right half of the gel (starting from lane **6**) shows the fractions of the SEC, starting with the first fraction at the beginning of the peak in the void volume. Varying amounts of ELIC found in all fractions indicate that the protein is not only eluting as pentameric species. By comparing the quantities of ELIC on the gel with the SEC absorption profile in part **d** of figure 2.2, it is apparent that the high aggregation peak at the

Figure 2.4.: **Sequence alignments. a** Structure based alignment of the pLGIC of *E. chrysanthemi* (ELIC), the acetylcholine-binding protein from the snail *Lymnea stagnalis* (AChBP, PDB code 1i9B) and the α chain of the nicotinic acetylcholine receptor from *T. marmorata* (nAChRα, PDB code 2BG9). Secondary structure and numbering of ELIC are indicated below and above the sequences. Secondary structure elements contributing to the two sheets in the β-sandwich of the extracellular domain are colored in red and green, respectively. α-helices of the pore domain are colored in blue. Regions of non canonical H-bonding in these helices are marked in cyan. Strictly conserved residues between ELIC and any of the other proteins are colored in blue. Residues of ELIC that are not defined in the electron density are colored grey. Aromatic residues in the acetylcholine-binding site of AChBP are highlighted in yellow, other residues in the surrounding of this site in ELIC in cyan. Residues contributing to the pore lining in ELIC are highlighted in green. Regions of the α3–α4 linker of nAChR not present in the structure are indicated (XXX). **b** Sequence alignment between ELIC and GLIC. Secondary structure elements of ELIC are shown below the sequences. The color coding is as in **a**. Figure **S1**

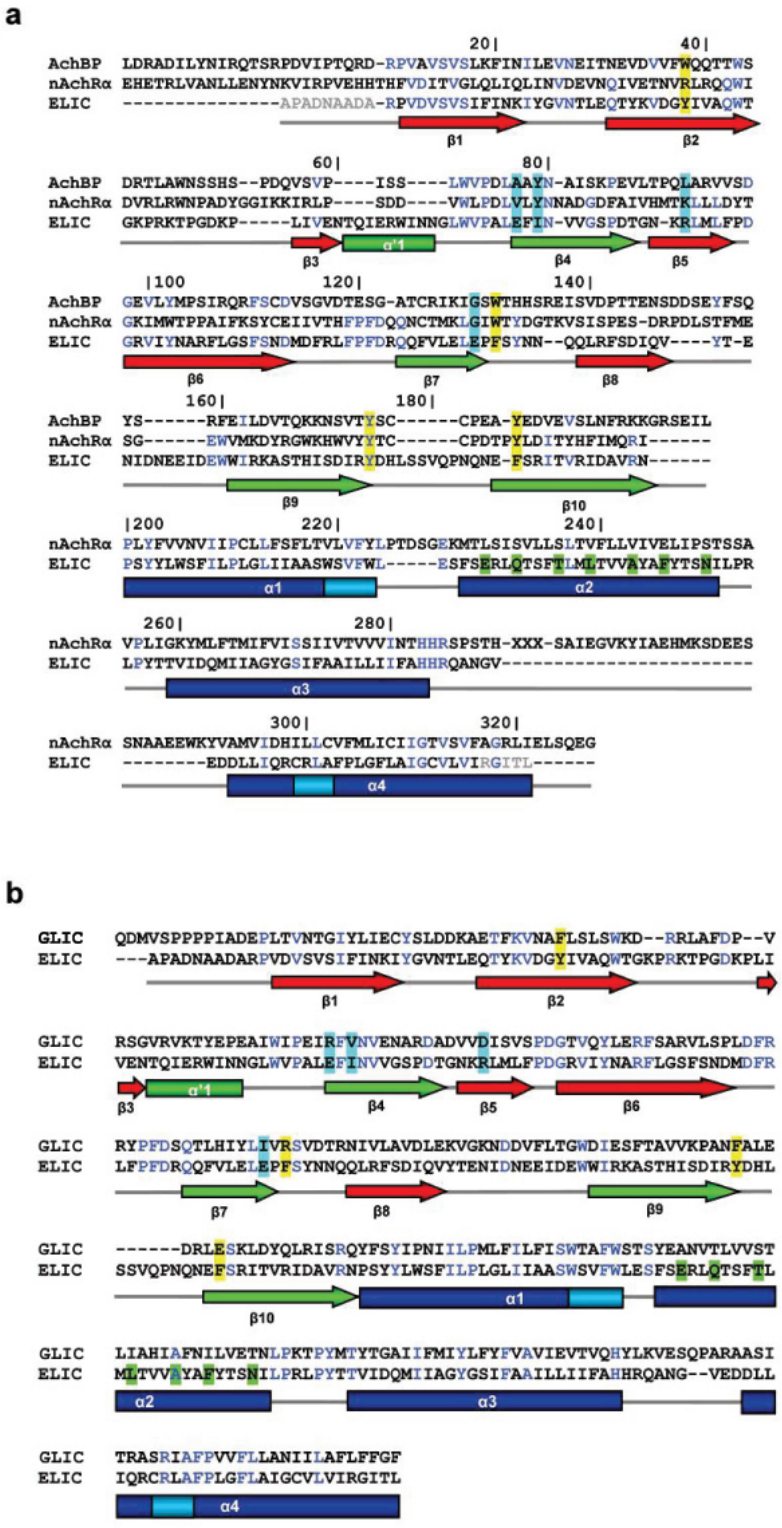
a
AchBP LDRADILYNIRQTSRPDVIPTQRD-RPVAVSVSLKFINILEVNEITNEVDVVFWQQTTWS
nAchRα EHETRLVANLLENYNKVIRPVEHHTHFVDITVGLQLIQLINVDEVNQIVETNVRLRQQWI
ELIC ----------APADNAADA-RPVDVSVSIFINKIYGVNTLEQTYKVDGYIVAQWT
β1 β2
AchBP DRTLAWNSSHS--PDQVSVP----ISS----LWVPDLAAYN-AISKPEVLTPQLARVVSD
nAchRα DVRLRWNPADYGGIKKIRLP----SDD----VWLPDLVLYNNADGDFAIVHMTKLLLDYT
ELIC GKPRKTPGDKP-----LIVENTQIERWINNGLWVPALEFIN-VVGSPDTGN-KRLMLFPD
β3 α'1 β4 β5
AchBP GEVLYMPSIRQRFSCDVSGVDTESG-ATCRIKIGSWTHHSREISVDPTTENSDDSEYFSQ
nAchRα GKIMWTPPAIFKSYCEIIVTHFPFDQQNCTMKLGIWTYDGTKVSISPES-DRPDLSTFME
ELIC GRVIYNARFLGSFSNDMDFRLFPFDRQQFVLELEPFSYNN--QQLRFSDIQV----YT-E
β6 β7 β8
AchBP YS------RFEILDVTQKKNSVTYSC------CPEA-YEDVEVSLNFRKKGRSEIL
nAchRα SG------EWVMKDYRGWKHWVYYTC------CPDTPYLDITYHFIMQRI------
ELIC NIDNEEIDEWWIRKASTHISDIRYDHLSSVQPNQNE-FSRITVRIDAVRN------
β9 β10
nAchRα PLYFVVNVIIPCLLFSFLTVLVFYLPTDSGEKMTLSISVLLSLTVFLLVIVELIPSTSSA
ELIC PSYYLWSFILPLGLIIAASWSVFWL-----ESFSERLQTSFTLMLTVVAYAFYTSNILPR
α1 α2
nAchRα VPLIGKYMLFTMIFVISSIIVTVVVINTHHRSPSTH-XXX-SAIEGVKYIAEHMKSDEES
ELIC LPYTTVIDQMIIAGYGSIFAAILLIIFAHHRQANGV----------
α3
nAchRα SNAAEEWKYVAMVIDHILLCVFMLICIIGTVSVFAGRLIELSQEG
ELIC --------EDDLLIQRCRLAFPLGFLAIGCVLVIRGITL------
α4
b
GLIC QDMVSPPPPIADEPLTVNTGIYLIECYSLDDKAETFKVNAFLSLSWKD--RRLAFDP--V
ELIC ---APADNAADARPVDVSVSIFINKIYGVNTLEQTYKVDGYIVAQWTGKPRKTPGDKPLI
β1 β2
GLIC RSGVRVKTYEPEAIWIPEIRFVNVENARDADVVDISVSPDGTVQYLERFSARVLSPLDFR
ELIC VENTQIERWINNGLWVPALEFINVVGSPDTGNKRLMLFPDGRVIYNARFLGSFSNDMDFR
β3 α'1 β4 β5 β6
GLIC RYPFDSQTLHIYLIVRSVDTRNIVLAVDLEKVGKNDDVFLTGWDIESFTAVVKPANFALE
ELIC LFPFDRQQFVLELEPFSYNNQQLRFSDIQVYTENIDNEEIDEWWIRKASTHISDIRYDHL
β7 β8 β9
GLIC ------DRLESKLDYQLRISRQYFSYIPNIILPMLFILFISWTAFWSTSYEANVTLVVST
ELIC SSVQPNQNEFSRITVRIDAVRNPSYYLWSFILPLGLIIAASWSVFWLESFSERLQTSFTL
β10 α1
GLIC LIAHIAFNILVETNLPKTPYMTYTGAIIFMIYLFYFVAVIEVTVQHYLKVESQPARAASI
ELIC MLTVVAYAFYTSNILPRLPYTTVIDQMIIAGYGSIFAAILLIIFAHHRQANG--VEDDLL
α2 α3
GLIC TRASRIAFPVVFLLANIILAFLFFGF
ELIC IQRCRLAFPLGFLAIGCVLVIRGITL
α4

void volume of the SEC is only partly consisting of ELIC and also contains other impurities. The pooled fractions containing the largest amount of ELIC were concentrated and subjected to crystallization screening.

Electrophysiological recordings of ELIC in artificial lipid bilayers

The sequence conservation between ELIC and the acetylcholine-binding protein (AChBP) and the *Torpedo* acetylcholine receptor (nAChR) can be appreciated from an alignment of the three proteins (figure 2.4). Whereas the overall sequence identity is low (with about 18 % of all residues being conserved between species), important stretches, such as the signature sequence of the family, which is part of the Cys-loop (FPFDRxQ) and several aromatic residues surrounding the ligand-binding pocket are conserved. The conservation of important regions suggests that the main functional and structural features are shared between prokaryotic and eukaryotic channels and that ELIC can serve as a model system for the family. To investigate the functional properties of ELIC, the protein was reconstituted into liposomes and studied by electrophysiology in artificial lipid bilayers.

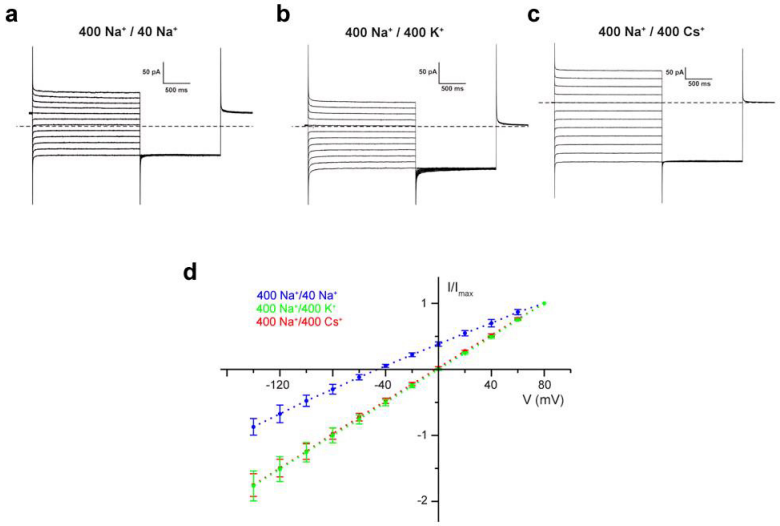

Figure 2.5.: **Electrophysiological recordings of ELIC in artificial lipid bilayers.** Currents were measured as described in section 4.4.1. The position of 0 current is indicated (- - - -). Macroscopic currents mediated by ELIC under asymmetric salt conditions in **a** 400 mM Na^+/ 40 mM Na^+(cis/trans), **b** 400 mM Na^+/ 400 mM K^+, **c** 400 mM Na^+/ 400 mM Cs^+. **d** I-V curve of macroscopic currents mediated by ELIC. Blue: current measured in asymmetric Na^+conditions (as defined in **a**). Green: Currents recorded in Na^+/ K^+gradient (as defined in **b**). Red: Currents recorded in Na^+/ Cs^+gradient (as defined in **c**). Figure **S2**

In these experiments the currents mediated by ELIC were investigated with respect to their ion selectivity. To increase the purity of the protein and to avoid any co-purification of contaminants that would affect the results, an additional ion exchange chromatography step was included af-

ter Ni-affinity purification and prior to SEC. Subsequently, the reconstituted protein eluted as a single peak from the gel filtration and is very pure as judged by SDS-PAGE. When reconstituted into liposomes at a relatively high protein to lipid ratio of 5 μg protein per mg of lipids, ELIC usually gives rise to macroscopic currents at 80 mV ranging from 80 to 200 pA, depending of the number of vesicles fusing with the bilayer. The average current scales with changes in the protein to lipid ratio, it is about five times lower for protein reconstituted at 1 μg/mg of lipids and it doubles at 10 μg/mg of lipids. The observed currents, however, are small for ion channels with high open probability and probably reflect macroscopic currents passed by channels with low open probability as has been reported for pLGICs in the absence of ligands. When assuming a conductance of about 10^7 ions / sec, which was reported for GLIC[137], and when comparing the currents measured in our experiments with currents of similar size obtained from the analysis of the bacterial transporter EcClC (turnover ~$4{\cdot}10^4$ ions / sec) the assumption of a low open probability is clearly justified. The low open probability, however, does not prevent the characterization of functional properties as ion selectivity. By measuring the reversal potential at different ion concentrations, which is independent of the open probability, it is possible to investigate the ion selectivity of the channel. The current measured in an asymmetric Na^+ gradient reverses at a negative potential close to the Nernst potential of sodium indicating a cation selective channel. The reversal potential of -45 mV is somewhat below the Nernst potential of Na^+, probably due to the deviation of the activity coefficient from one for high sodium concentrations. The reversal potential at 0 mV in Cs^+/Na^+or K^+/Na^+gradients indicates a similar permeability of the three cations. Overall this behavior resembles the typical charge selectivity for cation-selective pLGICs.

2.2.1. Crystallization of ELIC

ELIC crystallized readily in many different conditions, however, crystals set up on the day after purification did not grow or did grow in showers of smaller crystals. The addition of lipids in a concentration of 0.5 mg / ml improved the growth and the diffraction properties of the crystals. The crystals were physically stable and tolerated the transfer into solutions containing different ions or cryo-protectant. Soaking into solutions containing heavy atoms, however, destroyed the diffraction.

Like many other membrane proteins the diffraction quality was strongly dependent on the detergent used for purification. Remarkably, ELIC crystals diffracted best (to 3.3 Å) in UDM, even if crystals were also growing in shorter-chain detergents in the same reservoir solution. The protein crystallized in the $P2_1$ space group and packs as shown in figure 2.6. The protein forms chains with pentamers interacting in a head-to-tail arrangement running in four directions and forming crystal contacts with several residues of the extracellular ligand-binding domain. There are two pentamers in the asymmetric unit creating the tenfold non-crystallographic symmetry (NCS), which was important for NCS averaging and phase extension.

Since initial phasing attempts by molecular replacement with models of the AChBP or a truncated nAChR failed to provide any meaningful solution, the measurement of experimental phase information was mandatory. The experimental phases were determined by single anomalous dispersion (SAD) from Se-methionine containing protein, that was grown in minimal medium, where methionine was replaced by Se-methionine. The incorporation of Se-methionine was con-

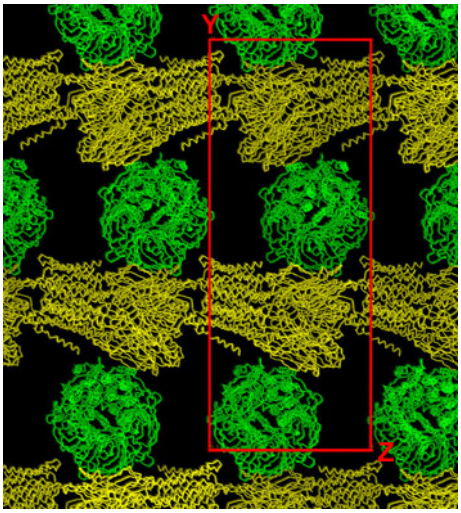

Figure 2.6.: **Packing of ELIC in the $P2_1$ crystal form.** The view is along X. The two pentameric channels in the asymmetric unit are colored in green and yellow. Figure **S4**

firmed by MALDI mass spectrometry. The crystals of Se-methionine substituted protein grew under the same conditions and unexpectedly had superior diffraction properties compared to WT crystals. It is still unclear whether the improvement by 0.3 Å was due to the slower expression in minimal medium. One large, rod-shaped Se-Met protein containing crystal allowed data collection at 3.3 Å, and was at the same time used for anomalous data collection and as a native dataset. It also served as a native dataset for a protein crystal that was incubated with xenon gas at high pressure. Experimental phases were obtained from the isomorphous contributions between the Se-methionine-dataset and the Xe-dataset and the anomalous contributions of the two datasets.

Redundancy and R-factors

The selenium substructure of ELIC was determined based on the anomalous differences of the incorporated selenium atoms. To obtain sufficient anomalous signal to determine the coordinates of the selenium atoms for a low symmetry space group it was necessary to collect a very redundant dataset. By increasing the redundancy the statistics for the anomalous differences were significantly improved over a broad resolution range (figure 2.7). The high redundancy proved to be essential to accurately measure the small differences between a reflection and its Friedel mate. The collection of highly redundant data for the accurate measurement of the anomalous scattering has previously been reported by Hendrickson and Teeter for the structure determination of crambin[142] and has ever since been used as a standard procedure for the collection of anomalous data[143,144].

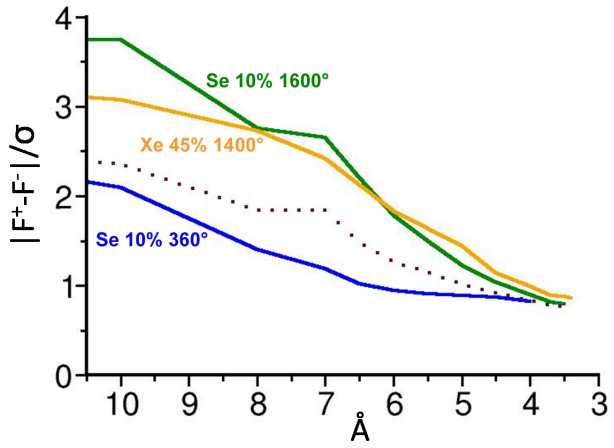

Figure 2.7.: **Anomalous signal-to-noise ratio plotted vs. resolution.** The y-axis shows the ratio of the anomalous signal to the noise with $\frac{\sum |F^+ - F^-|}{\sigma(F)}$ in dependence on resolution (x-axis). The indicated values give information about the beam intensity and the degree collected for each dataset. The dotted line corresponds to the theoretical dataset estimated from 360° at 10% beam intensity of the selenium crystal.

The quality of the anomalous data can be estimated by the resolution dependence of the ratio of the anomalous signal to the background, which can be either calculated on the intensities or the structure factor amplitudes according to the following equation:

$$\frac{\sum |F^+ - F^-|}{\sigma(F)}$$

This relationship can be used to estimate the extend for meaningful anomalous differences[145]. The data used for the anomalous substructure search is usually truncated at a resolution where this value drops below 1.3. Due to difficulties in predicting σ(F), particularly at low resolution or low redundancy, other factors have been proposed (e.g. the ratio of R_{anom} to $R_{p.i.m.}$[146,147] or the Bijvoet ratio[142]). Overall there is no reliable factor predicting the phasing power of an anomalous dataset and the final criterion for the quality of the anomalous signal is a successful structure solution[148].

The graph in figure 2.7 shows the resolution dependence in the ratio of the anomalous signal to the background of the selenium dataset. By combining 360° of data collected at a low beam intensity of 10% to avoid radiation damage, the anomalous differences are only measurable to a resolution up to 8–9 Å. The collection of 1600°, in contrast, extends the phase information to about 5 Å resolution and allowed the substructure solution of all selenium sites and the calculation of SAD phases. Similarly the anomalous data obtained from the xenon dataset also extends to a resolution of about 5 Å.

Table 2.1 gives an overview about the statistics of data collection. The selenium and the xenon datasets both were refined to a resolution of 3.3 Å and show a high completeness and a signal-to-noise ratio (I/σI) over 2.5. The high redundancy of the data gives rise to elevated R_{merge} (also

	Se (Native)	Xe
Data collection		
Space group	$P2_1$	$P2_1$
Cell dimensions		
a, b, c (Å)	105.5, 266.2, 110.8	106.3, 269.5, 112.1
α, β, γ (°)	90.0, 109.5, 90.0	90.0, 109.3, 90.0
Resolution (Å)*	30–3.3 (3.4–3.3)	30–3.3 (3.4–3.3)
R_{merge}	13.9 (116.7)	12.4 (83.0)
$R_{mrged\text{-}F}$	9.0 (50.4)	13.2 (53.5)
$I/\sigma I$	17.4 (2.7)	11.9 (2.5)
Completeness (%)	99.7 (99.9)	99.5 (99.9)
Redundancy	21.2 (15.2)	6.8 (6.8)
Refinement		
Resolution (Å)	30–3.3	
No. reflections	86081	
R_{work} / R_{free}	26.3 / 27.4	
No. atoms		
Protein	25020	
Ligand / ion	–	–
Water	–	
B-factors		
Protein	123.7	
Ligand / ion	–	–
Water	–	
R.m.s. deviations		
Bond lengths (Å)	0.007	
Bond angles (%)	1.4	

Values in parentheses are for highest-resolution shell.

Table 2.1.: **Data collection and refinement statistics**

called R_{sym}) values[149,150]. R_{merge} has been originally proposed by Blundell and Johnson[151] as statistical indicator for the quality of a dataset as:

$$R_{merge}(I) = \frac{\sum_{hkl} \sum_{i} |I_i(hkl) - \overline{I(hkl)}|}{\sum_{hkl} \sum_{i} I_i(hkl)}$$

It has been observed earlier that R_{merge} correlates inversely with the redundancy of the measured data[152,153] and because of this it is not an accurate statistical property, particularly when

considering redundant datasets. Redundancy independent R-factors have thus been proposed by different groups. Weiss and colleagues proposed the use of a redundancy-independent merging R-factor, $R_{r.i.m.}$ [154], which was described by Diederichs and Karplus as R_{meas} [150]. It describes the precision of the individual measurement, independent of how often a reflection has been measured:

$$R_{r.i.m.} = \frac{\sum_{hkl} \sqrt{\left[\frac{N}{(N-1)}\right]} \sum_{i} |I_i(hkl) - \overline{I(hkl)}|}{\sum_{hkl} \sum_{i} I_i(hkl)}$$

Diederichs and Karplus proposed $R_{mrgd\text{-}I}$ as an estimation of the precision of the averaged measurements:

$$R_{mrgd-I} = \frac{\sum_{hkl} |\overline{I_1(hkl)} - \overline{I_2(hkl)}|}{0.5 \sum_{hkl} [\overline{I_1(hkl)} + \overline{I_2(hkl)}]}$$

The total set of reflections is divided into two parts (I_1 and I_2). Each part is merged and averaged separately and finally an R-factor is calculated upon comparison of the two subsets. It is commonly used as $R_{mrgd\text{-}F}$, using the amplitudes instead of the intensities.

In the data in table 2.1 I report the classical $R_{merge}$and the $R_{mrgd\text{-}F}$. As mentioned before R_{merge} correlates with redundancy, therefore showing an elevated value of 116.7% in the highest resolution shell. If only a subset of the data is used (360°) R_{merge} in the highest shell drops to 73.7% . The redundancy independent R-factor $R_{mrgd\text{-}F}$ of 50.4% illustrates that the resolution cutoff at 3.3 Å resolution is cautiously chosen.

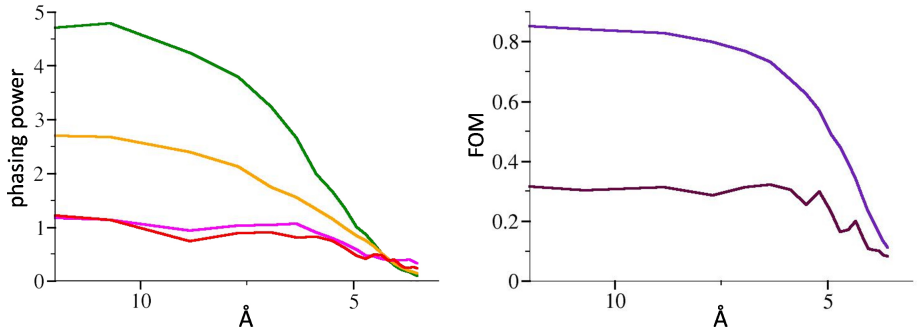

Figure 2.8.: **Phasing power and figure of merit in dependence of resolution.** The phasing power is shown of different contributions: anomalous data in acentric reflections of the selenium and xenon dataset (green and orange, respectively), isomorphous data in acentric and centric reflections of the xenon dataset (magenta and red, respectively). The figure of merit (FOM) is shown for acentric and centric reflections (indigo and brown, respectively).

Experimental phase information in a SAD experiment is based on the measurement of differences between Friedel symmetry-related reflections. The quality of the phase information is defined as the phasing power:

$$\text{phasing power} = \sqrt{\frac{\sum_n |F_{(H)calc}|^2}{\sum_n |\epsilon|^2}}$$

In this equation ϵ is the lack of closure error with $\epsilon = (F_{H(calc)} + F_P) - F_{PH}$. The phasing power is resolution dependent and it defines the limit, where the data still contributes meaningful phase information. A phasing power bigger than 1.5 indicates that the data contains valuable information, whereas a value substantially below 1 indicates unusable data. Figure 2.8 shows the phasing power of different datasets in dependence on resolution. The phasing power of the anomalous data of both the selenium and the xenon dataset indicates that both datasets contribute meaningful phase information to about 4 Å resolution, whereas the isomorphous contribution from the xenon dataset drops below 1 around 7 Å.

Any errors in the phase introduces noise in the electron density map. Thus the phase of each reflection is allocated a weighting factor, the figure of merit, m (FOM). It is calculated from the probability distribution for the phase of each reflection and for each reflection (hkl) it is defined as

$$m = \frac{|F(hkl)_{best}|}{|F(hkl)_{observed}|}$$

where $F(hkl)_{best}$ is chosen as the weighted average of the phase distribution of the reflection (hkl). The FOM reduces the magnitude assigned to a structure factor depending how accurately its phase is known. Figure 2.8 shows the dependence of the FOM on the resolution. It is relatively high to a resolution of 5.5 Å, indicating good phase probabilities up to this resolution.

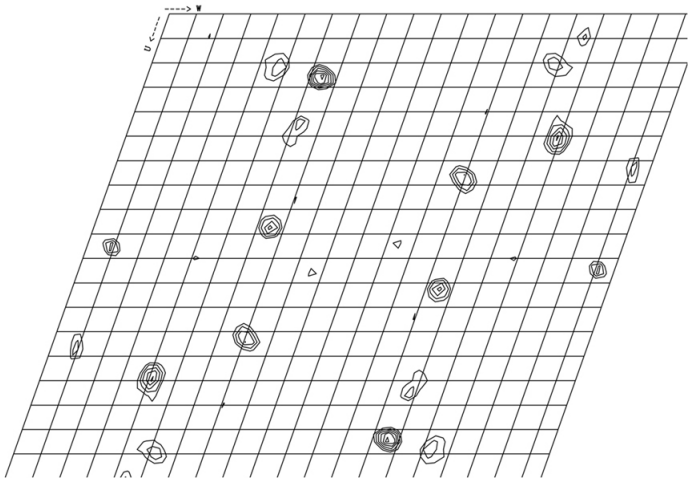

Figure 2.9.: **Patterson map.** Peaks of the selenium sites in the patterson map of ELIC. Shown is the harker section of the $P2_1$ space group. Contour levels start at 3σ in steps of 1σ.

Figure 2.9 shows the peaks in the anomalous difference patterson map of the selenium dataset (calculated at 5 Å). Several strong peaks at the Harker section of the $P2_1$ dataset indicate the presence of symmetry equivalent selenium atoms. The selenium sites were identified using the program SHELX C and D and were subsequently used to calculate initial phases for identifying the xenon sites by difference fourier methods. The initial sites in the Se-Met and Xe-datasets were refined and MIRAS (multiple isomorphous replacement, anomalous scattering) phases were calculated with SHARP. An electron density map calculated from MIRAS phases is shown in figure 2.10 in section **a**. While overall noisy the electron density shows a near continuous trace of the backbone, whereas electron density for the side chains is only occasionally visible.

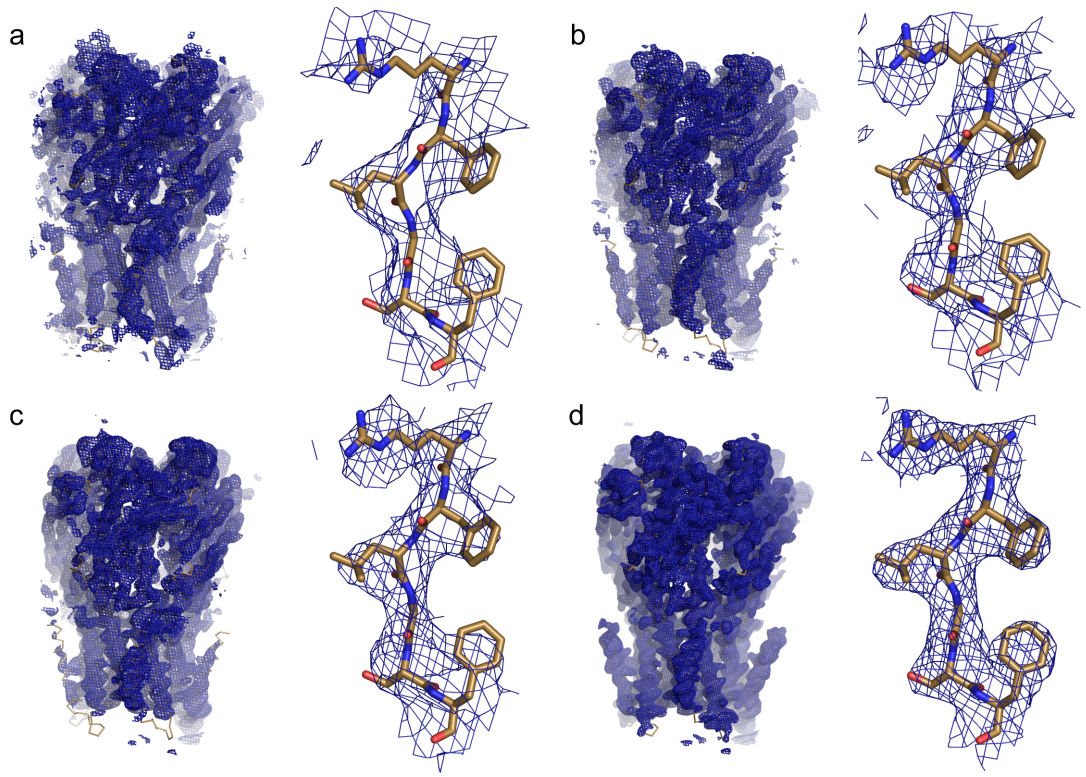

Figure 2.10.: **Refinement of ELIC.** Electron density after different steps of the refinement shown on the overall structure and at a section within the β6 strand of the extracellular domain. **a** after refinement of the sites in sharp. **b** after solvent flipping in SOLOMON[155]. **c** after 10-fold cyclic NCS averaging. **d** model phases. Section of this map are shown in figure 2.21.

Solvent flipping was used for initial stages of density modification as a powerful tool to reduce the phase error. The effect on the density can be seen in part **b** in figure 2.10. The main improvement is visible in the reduced overall noise of the map. The most powerful density modification procedure was taking advantage of the 10-fold non-crystallographic symmetry (NCS) due to the two pentamers in the asymmetric unit. The 10-fold NCS was used for cyclic symmetry averaging and phase extension. The resulting map is shown in part **c** of figure 2.10. The model was

built in O and initially refined by maintaining strict 10-fold NCS constraints in CNS. In later stages, the strict constraints were loosened and restraint individual B-factors were refined. During the individual refinement the 10 subunits maintained their very similar conformations with overall rmsd between the different subunits of <1.5 Å. The map (3.1 Å resolution, contoured at 1 σ) was calculated using the native amplitudes and model phases that were improved by cyclic 10-fold NCS averaging. The quality of the final $2F_o$-F_c electron density map that was calculated with refined model phases is shown in part **d** of figure 2.10. The high quality of the electron density with accurately defined side chains is apparent. Figure 2.11 displays selected regions of this final $2F_o$-F_c electron density as it was illustrated in the publication.

2.2.2. Structure of ELIC

The structure of ELIC was determined at 3.3 Å resolution. It represents the first high-resolution structure of any member of the pLGIC family and was published in 2008[156]. The paper (Hilf RJC. & Dutzler R. *X-ray structure of a prokaryotic pentameric ligand-gated ion channel*. **Nature**. 2008 Mar 20; 452(7185): 375-9) and accessory information is reprinted in the following part.

Figure 2.11.: **Electron density. a** Stereo view of experimental electron density map contoured at 1 σ superimposed on a Cα trace of the ELIC pentamer. Anomalous difference density of Se and Xe datasets is contoured at 5 σ and shown in red and green respectively. **b** Final electron density contoured at 1 σ superimposed on the refined model. Sections of this electron density are shown in **c–e**. **c** Stereo view of electron density in the interface between the extracellular (top) and the transmembrane domain. **d** View of the pore region, the front subunit is removed for clarity. **e** Electron density in the putative ligand-binding site. Figure **S3**

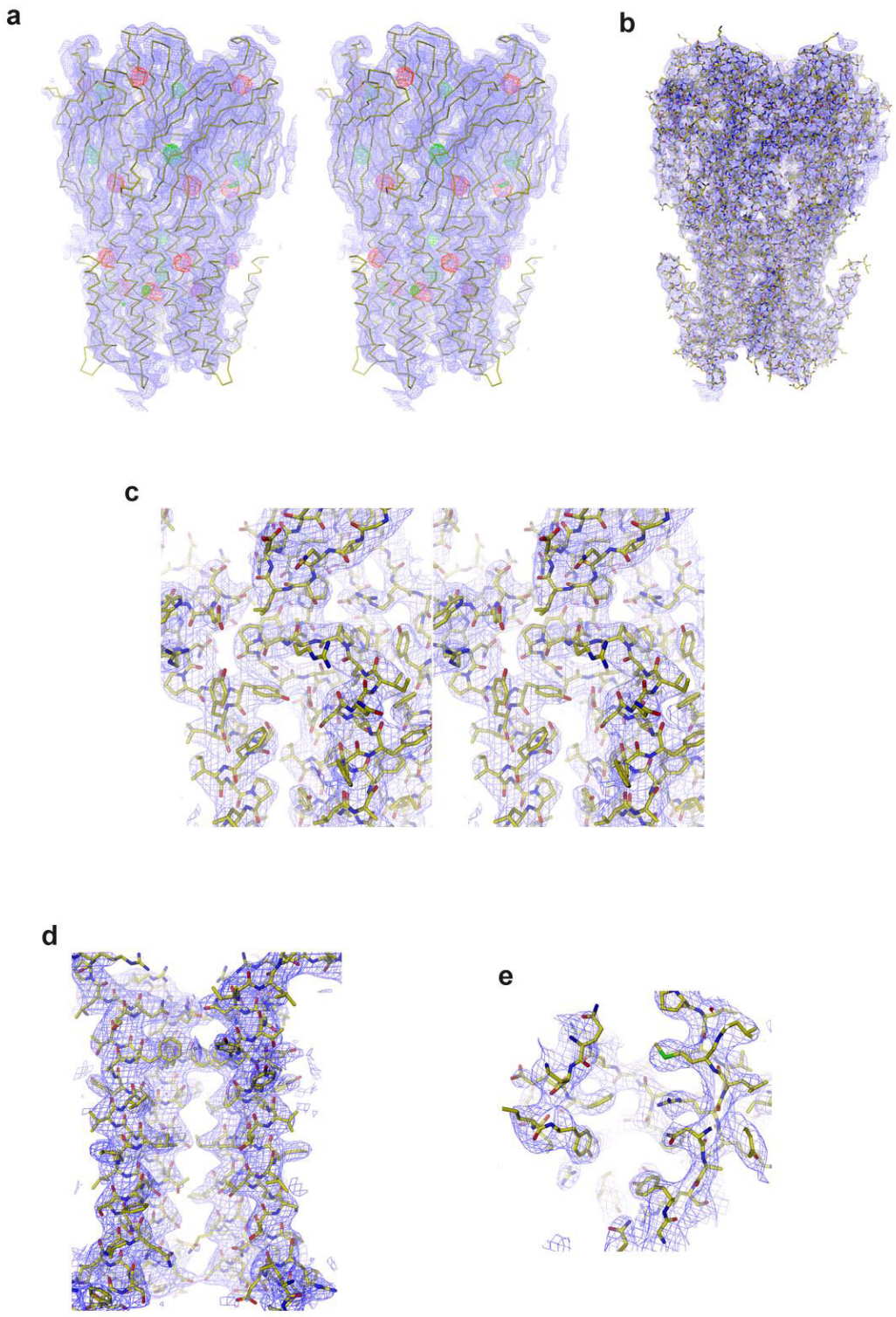
a
b
c
d
e

LETTERS

X-ray structure of a prokaryotic pentameric ligand-gated ion channel

Ricarda J. C. Hilf[1] & Raimund Dutzler[1]

Pentameric ligand-gated ion channels (pLGICs) are key players in the early events of electrical signal transduction at chemical synapses. The family codes for a structurally conserved scaffold of channel proteins that open in response to the binding of neurotransmitter molecules. All proteins share a pentameric organization of identical or related subunits that consist of an extracellular ligand-binding domain followed by a transmembrane channel domain. The nicotinic acetylcholine receptor (nAChR) is the most thoroughly studied member of the pLGIC family (for recent reviews see refs 1–3). Two sources of structural information provided an architectural framework for the family. The structure of the soluble acetylcholine-binding protein (AChBP) defined the organization of the extracellular domain and revealed the chemical basis of ligand interaction[4–6]. Electron microscopy studies of the nAChR from *Torpedo* electric ray have yielded a picture of the full-length protein and have recently led to the interpretation of an electron density map at 4.0 Å resolution[7–9]. Despite the wealth of experimental information, high-resolution structures of any family member have so far not been available. Until recently, the pLGICs were believed to be only expressed in multicellular eukaryotic organisms. The abundance of prokaryotic genome sequences, however, allowed the identification of several homologous proteins in bacterial sources[10,11]. Here we present the X-ray structure of a prokaryotic pLGIC from the bacterium *Erwinia chrysanthemi* (ELIC) at 3.3 Å resolution. Our study reveals the first structure of a pLGIC at high resolution and provides an important model system for the investigation of the general mechanisms of ion permeation and gating within the family.

ELIC is similar in length and sequence to its orthologue from the cyanobacterium *Gloebacter violaceous* (sharing 18% of identical amino acids) and it shows considerable homology to eukaryotic family members (with 16% sequence identity to nAChRα, Supplementary Fig. 1). When investigated in artificial lipid bilayers, the protein mediates cation-selective currents but it does not discriminate between different monovalent cations such as Na^+, K^+ and Cs^+, a functional behaviour that closely resembles the selectivity of acetylcholine and serotonin receptors[12] (Supplementary Fig. 2). The crystal structure of ELIC has been determined at 3.3 Å resolution by the SIRAS (single isomorphous replacement anomalous scattering) method (Supplementary Table 1, and Supplementary Figs 3 and 4). The pentameric protein is shown in Fig. 1. The five subunits are arranged like the staves of a barrel around a symmetry axis that defines the ion permeation path. The overall dimensions of the protein (95 Å × 110 Å) closely resemble the acetylcholine receptor ion channel, not including the cytoplasmic region, which is absent in ELIC. The subunits are tightly interacting in both, their extracellular and their membrane embedded part with adjacent subunits burying more than 5,000 $Å^2$ of the combined molecular surface. On the extracellular side, the protein subunits enclose a wide, aqueous, cylindrical vestibule with a diameter of about 16 Å that is lined by charged and hydrophilic residues. This vestibule narrows down at the membrane interface to a discontinuous, partly hydrophobic pore with a maximum diameter of about 7 Å that probably defines a closed conformation of the channel.

Each protein subunit is organized in two halves: the amino-terminal half that constitutes the extracellular domain and a carboxy-terminal half that makes up the pore domain (Fig. 1c). Both termini of the protein chain are located on the extracellular side. The extracellular domain consists of ten β-strands that are organized in two sheets to form a β-sandwich and a short α-helix. The topological organization of the extracellular domain of ELIC is very similar to its eukaryotic counterparts and to AChBP, except for an N-terminal α-helix that is abundant in eukaryotic proteins and missing in bacterial pLGICs. The regions of conserved sequence include the central part of the 'Cys-loop' that connects β6 and β7 but does not extend to the flanking disulphide-bridged cysteinse residues that are strictly conserved among eukaryotic pLGICs (Supplementary Fig. 1a). The transmembrane region consists of four α-helices that are connected by short loops. These four helices (named α1–α4) are equivalent to the previously described transmembrane regions M1–M4 of the acetylcholine receptor[8]. Three helices (α1–α3) span the membrane with small tilts with respect to its plane and form a tightly interacting bundle. In the pentameric protein, these helices are arranged in two concentric layers around the pore axis: an inner circle that is formed by helix α2 and an outer circle defined by the helices α1 and α3. Only residues of α2 contribute to the pore lining, whereas α1 and α3 appear to shield and stabilize the pore. All three segments are involved in interactions at subunit interfaces, whereas the fourth helix, α4, is located at the periphery of this barrel-like arrangement; it only loosely interacts with α1 and α3 and is not involved in subunit–subunit interactions (Fig. 1a). In an attempt to study the interaction of monovalent cations with ELIC, we soaked our crystals in solutions that only contain the respective cation, and we identified the bound ions by anomalous and isomorphous difference Fourier techniques (Supplementary Table 2). In that way, we studied the binding of Rb^+, Cs^+ and Tl^+ ions to the protein, which have been shown to permeate through ELIC and the related nAChR channels[12] (Supplementary Fig. 2c, d). Although this approach did not allow the identification of specific binding sites in the pore region, it revealed ordered binding of ions to sites in the extracellular ligand-binding domain (Supplementary Fig. 5).

The conservation in the extracellular part of ELIC becomes evident when comparing its structure with the structure of the homopentameric AChBP, which has proved to be a valuable representative for the ligand-binding domain[4]. A superposition of the two domains is shown in Fig. 2a. Three hundred and fifty Cα positions at the N-terminal half of the ligand-binding domain of the five subunits superimpose with a root mean square deviation of less than 1.5 Å. The largest differences are found in loop regions that interact with the transmembrane channel

[1]Department of Biochemistry, University of Zürich, Winterthurer Strasse 190, CH-8057 Zürich, Switzerland.

and which are naturally absent in the soluble binding protein. The ligand-binding site of AChBP that is also conserved among acetylcholine receptors is located in a pocket of the protein at the interface between two adjacent subunits (Fig. 2a). This pocket is covered on one side by an extended loop region connecting β9 and β10. In ELIC, the tip of this loop is mobile and thus only weakly defined in its electron density, which is consistent with the increased mobility of this region that has been reported for AChBP in the absence of bound ligand[6]. Although the ligands that trigger pore opening in ELIC have not yet been identified, it is interesting to compare the structures of the equivalent regions. The acetylcholine-binding site contains conserved aromatic amino acids from dispersed regions of the protein, which contribute to an aromatic-binding pocket for quaternary ammonium compounds that are stabilized by so-called 'cation–π' interactions[5,13] (Supplementary Fig. 6a). Although the ligand-promoting channel opening in ELIC could be as small as a proton, as has been suggested for the homologous GIvi channel[11], it is remarkable to find several of these aromatic residues conserved in the ELIC structure (Fig. 2b and Supplementary Fig. 6b). Ordered binding of Cs^+ and Tl^+ ions emphasizes the electrostatic attraction for cations in this region and underscores its role as a potential ligand-binding site that could promote channel opening like in eukaryotic pLGICs.

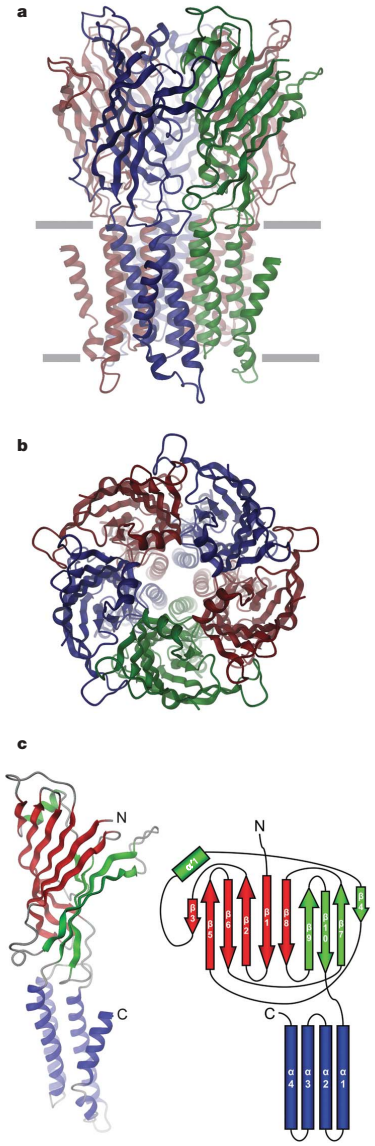

Figure 1 | ELIC structure. **a**, Ribbon representation of ELIC viewed from within the membrane with the extracellular solution above. The approximate membrane boundaries are indicated. **b**, Structure of the pentameric channel viewed from the extracellular side. **c**, Structure and topology of the ELIC subunit. The subunit is viewed from within the membrane. Secondary structure elements constituting the two sheets of the β-sandwich of the extracellular domain are coloured in red and green, respectively. The four helices of the pore region are coloured in blue. Figures 1–3 were prepared with DINO (http://www.dino3d.org).

Ligand-dependent gating involves the transduction of conformational rearrangements from the ligand-binding domain to the pore[2,14]. This process is mediated through interfacial contacts between the two domains[9]. The interface between the extracellular and pore domains is well defined in the ELIC structure and it involves, next to the covalent connection between β10 and α1, residues of three loop regions in the extracellular domain that contact the α2–α3 loop of the pore domain (Fig. 2c and Supplementary Fig. 6c). These interactions include conserved residues of the β6–β7 loop (the 'Cys' loop) and contacts to the β1–β2 turn and the β8–β9 loop of the neighbouring subunit. Several of those regions have previously been identified as influencing gating in different family members[2,15–17].

The wide and hydrophilic extracellular vestibule of ELIC leads into a narrow pore at the membrane boundary. The lumen of this pore is lined by residues of helix α2 that spans the membrane in a nearly perpendicular orientation. On its extracellular half, the pore is interrupted by bulky side chains that occlude a hydrophobic cavity that extends towards the centre of the membrane (Fig. 3a). This cavity is confined by Phe 246 on the extracellular side and by Leu 239 towards the cytoplasm. Below the constriction, a hydrophilic channel of width 6 Å leads from the membrane centre to the intracellular exit. The bulky hydrophobic side chains of Phe 246 and Leu 239 would prevent the diffusion of ions and thus probably serve as physical gates in the closed conformation of the channel. Unlike other ion-channel proteins that specifically bind the transported ions in narrow selectivity filters[18,19], we did not identify ordered binding of permeant ions in the pore of ELIC. However, we did observe binding of apolar Xe atoms in the hydrophobic cavity and at the extracellular side of Phe 246, thus underlining the hydrophobic nature of this region (Fig. 3a). When comparing the pore of ELIC with the structure of the equivalent region of nAChR, interesting differences become apparent. Unlike our structure, nAChR shows a continuous channel with a diameter of about 6 Å (ref. 9) (Fig. 3b and Supplementary Fig. 7). The difference in the pore size is most pronounced at the extracellular entry where the helices of nAChR are bent away from the channel axis, thus providing an aqueous funnel-shaped path in a region where the ELIC pore is occluded. On the intracellular side, the pore radius in both proteins is similar. This observation is in contrast to electrophysiological experiments on nAChR, which predicted a constriction towards the cytoplasm[20,21]. Apart from differences in the diameter, other features of the pore, such as the predominantly hydrophobic region at the membrane centre and the presence of acidic residues on both sides of the membrane boundary appear preserved.

An investigation of the electrostatic potential along the ion permeation path of ELIC reveals insight into the cation selectivity of the channel (Fig. 3b). The predominant negative potential throughout the channel results from the excess of acidic residues in the protein, which provide an attractive environment for cations despite the

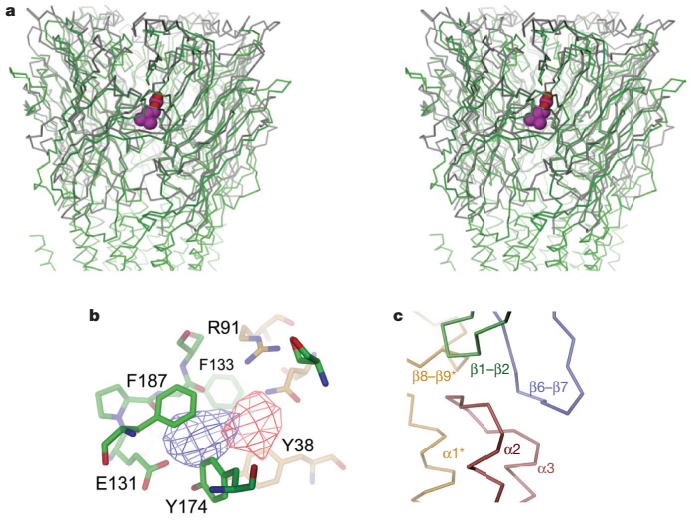

Figure 2 | Structure of the extracellular domain. **a**, Stereo view of AChBP (PDB code 1UV6) superimposed on the extracellular domain of ELIC. Proteins are shown as Cα representation and coloured in grey (AChBP) and green (ELIC). Carbamylcholine that is specifically bound to the acetylcholine-binding site of AChBP is shown as spacefilling model (carbon atoms in magenta). **b**, View of the putative ligand-binding site in ELIC. Carbon atoms of residues from the two subunits are coloured in green and orange, respectively. Selected residues are labelled. Anomalous difference electron density of bound Tl^+ and Cs^+ ions is contoured at 4σ and shown in blue and red, respectively. **c**, Cα representation of the interface region between the extracellular domain and the pore. The different elements are shown in unique colours, the 'Cys loop' (β6–β7) is coloured in blue. Residues of the neighbouring subunit are coloured in orange.

presence of positively charged residues in the extracellular vestibule, some of which are found close to the channel entrance. The electrostatic potential in the narrow pore region is dominated by acidic residues at the membrane boundary (for example, Glu 229 at the intracellular entrance). Because of the long-range nature of coulombic interactions and the low-dielectric environment of the membrane, the

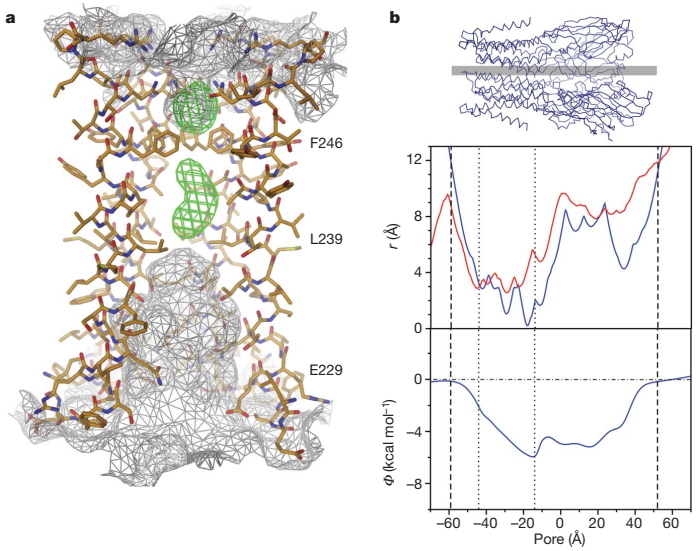

Figure 3 | ELIC pore. **a**, View of the α2 helices defining the pore region. The front subunit is removed for clarity. The molecular surface is shown as white mesh. Anomalous difference density of Xe atoms is contoured at 4σ and shown as green mesh. The positions of selected residues are indicated. **b**, Pore radius and electrostatic potential in the ELIC pore. Orientation of the ELIC channel is shown above. Molecular boundaries (dashed line) and transmembrane region (dotted line) are indicated. Top: pore radius of ELIC (blue) and nAChR (red) are shown. Bottom: electrostatic potential along the pore axis of ELIC as calculated from a numerical solution of the linearized Poisson–Boltzmann equation.

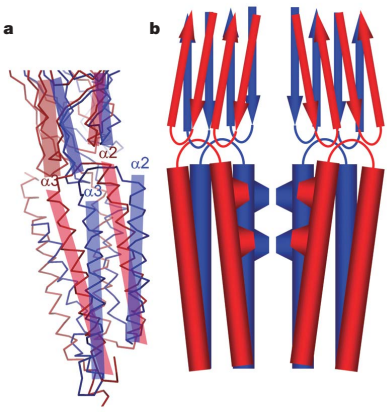

Figure 4 | Schematic model of pore opening. a, Superposition of selected regions from a single subunit of ELIC (blue) and the α-subunit of nAChR (red) close to the pore region. Differences in the helix tilt and the conformation of contacting groups from the extracellular region are highlighted. **b**, Schematic representation of two subunits, indicating a possible pore opening mechanism by a tilt of the helix at the extracellular side away from the pore axis in response to changes in the extracellular domain.

electrostatic potential in the channel is negative even though hydrophobic residues line the central pore region. This mechanism of electrostatic screening does not require the strict conservation of amino acids and may account for the fact that, although the pore regions of different family members are only weakly conserved, there is a common overall organization of hydrophobic residues in the centre and of charged residues at the periphery of the channel[22]. These charged residues have indeed been shown to confer ion selectivity to nAChR and other members of the family[23–27]. Although such a channel architecture allows for a discrimination of ions based on their charge, it does not allow for exquisite selectivity between two similar ions as found in K^+ channels[18].

Large hydrophobic residues in the centre of the pore have previously been shown to play an important role in channel closing in nAChR[8,20,28]. It has been proposed that these hydrophobic residues would impede ion permeation by a process called 'hydrophobic gating' as long as the channel does not exceed a certain size[29]. Unlike in the structure of nAChR, which shows a narrow but continuous pore, in ELIC these residues physically obstruct the channel. It will thus be interesting to see the conformational rearrangements leading to channel opening.

Different mechanisms of gating of pLGICs have been proposed in previous studies[8,21,30]. Although we do not want to engage in speculation about gating in the absence of additional data, it is interesting to compare the different conformations of the pore helices in ELIC and nAChR (Fig. 4). Both structures are believed to represent closed conformations of the respective proteins. If, however, the nAChR structure were to show a conformation that is closer to the structure of a conducting state, the difference might hint at a possible opening mechanism by an outward tilt of the pore helices on the extracellular side away from the channel axis (Fig. 4). This movement would be triggered by ligand binding to the extracellular domain and would be transmitted through the domain–domain interface.

The structure of ELIC shows the pore of a pLGIC in a non-conducting conformation. The protein shares many conserved features with its eukaryotic counterparts, which suggests that the basic mechanisms of ion permeation and gating are preserved across the prokaryotic–eukaryotic species boundary. Future studies will have to identify the ligands that promote channel opening and show the structure of a conducting conformation.

METHODS SUMMARY

ELIC was expressed in *Escherichia coli* with its N terminus fused to maltose-binding protein (MBP) preceded by a signal sequence (PelB). The protein was purified from isolated membranes in the detergent *n*-undecyl-β-D-maltoside. MBP was cleaved during purification by proteolytic digestion at a specific protease cleavage site located between MBP and the channel protein. Crystals were grown at pH 6.5 with addition of 13% PEG 4000, 200 mM ammonium sulphate and 0.5 mg ml^{-1} *E. coli* lipids. Data were collected at the X06-SA beamline at the Swiss Light Source of the Paul Scherrer Institute on a Pilatus detector (Dectris) (Supplementary Tables 1 and 2). The crystals were of space group $P2_1$ with two homo-pentameric channels in the asymmetric unit (Supplementary Fig. 4). The structure was determined by the SIRAS method, and phases were extended by cyclic tenfold non-crystallographic symmetry (NCS) averaging (Supplementary Fig. 3). All subunits were structurally very similar and were refined by maintaining strong constraints throughout (Supplementary Table 1). The final structure encompassing residues 11–316 was well refined, with good stereochemistry and no outliers in disallowed regions of the Ramachandran plot. For electrophysiological characterization in artificial lipid bilayers, the protein was reconstituted into liposomes and studied in a bilayer system.

Full Methods and any associated references are available in the online version of the paper at www.nature.com/nature.

Received 17 October 2007; accepted 15 January 2008.
Published online 5 March 2008.

1. Karlin, A. Emerging structure of the nicotinic acetylcholine receptors. *Nature Rev. Neurosci.* **3,** 102–114 (2002).
2. Lester, H. A., Dibas, M. I., Dahan, D. S., Leite, J. F. & Dougherty, D. A. Cys-loop receptors: new twists and turns. *Trends Neurosci.* **27,** 329–336 (2004).
3. Sine, S. M. & Engel, A. G. Recent advances in Cys-loop receptor structure and function. *Nature* **440,** 448–455 (2006).
4. Brejc, K. *et al.* Crystal structure of an ACh-binding protein reveals the ligand-binding domain of nicotinic receptors. *Nature* **411,** 269–276 (2001).
5. Celie, P. H. *et al.* Nicotine and carbamylcholine binding to nicotinic acetylcholine receptors as studied in AChBP crystal structures. *Neuron* **41,** 907–914 (2004).
6. Hansen, S. B. *et al.* Structures of *Aplysia* AChBP complexes with nicotinic agonists and antagonists reveal distinctive binding interfaces and conformations. *EMBO J.* **24,** 3635–3646 (2005).
7. Unwin, N. Structure and action of the nicotinic acetylcholine receptor explored by electron microscopy. *FEBS Lett.* **555,** 91–95 (2003).
8. Miyazawa, A., Fujiyoshi, Y. & Unwin, N. Structure and gating mechanism of the acetylcholine receptor pore. *Nature* **423,** 949–955 (2003).
9. Unwin, N. Refined structure of the nicotinic acetylcholine receptor at 4 Å resolution. *J. Mol. Biol.* **346,** 967–989 (2005).
10. Tasneem, A., Iyer, L. M., Jakobsson, E. & Aravind, L. Identification of the prokaryotic ligand-gated ion channels and their implications for the mechanisms and origins of animal Cys-loop ion channels. *Genome Biol.* **6,** R4 (2005).
11. Bocquet, N. *et al.* A prokaryotic proton-gated ion channel from the nicotinic acetylcholine receptor family. *Nature* **445,** 116–119 (2007).
12. Adams, D. J., Dwyer, T. M. & Hille, B. The permeability of endplate channels to monovalent and divalent metal cations. *J. Gen. Physiol.* **75,** 493–510 (1980).
13. Gallivan, J. P. & Dougherty, D. A. Cation–pi interactions in structural biology. *Proc. Natl Acad. Sci. USA* **96,** 9459–9464 (1999).
14. Purohit, P., Mitra, A. & Auerbach, A. A stepwise mechanism for acetylcholine receptor channel gating. *Nature* **446,** 930–933 (2007).
15. Campos-Caro, A. *et al.* A single residue in the M2–M3 loop is a major determinant of coupling between binding and gating in neuronal nicotinic receptors. *Proc. Natl Acad. Sci. USA* **93,** 6118–6123 (1996).
16. Grosman, C., Salamone, F. N., Sine, S. M. & Auerbach, A. The extracellular linker of muscle acetylcholine receptor channels is a gating control element. *J. Gen. Physiol.* **116,** 327–340 (2000).
17. Kash, T. L., Jenkins, A., Kelley, J. C., Trudell, J. R. & Harrison, N. L. Coupling of agonist binding to channel gating in the $GABA_A$ receptor. *Nature* **421,** 272–275 (2003).
18. Zhou, Y., Morais-Cabral, J. H., Kaufman, A. & MacKinnon, R. Chemistry of ion coordination and hydration revealed by a K^+ channel–Fab complex at 2.0 Å resolution. *Nature* **414,** 43–48 (2001).
19. Dutzler, R., Campbell, E. B. & MacKinnon, R. Gating the selectivity filter in ClC chloride channels. *Science* **300,** 108–112 (2003).
20. Wilson, G. & Karlin, A. Acetylcholine receptor channel structure in the resting, open, and desensitized states probed with the substituted-cysteine-accessibility method. *Proc. Natl Acad. Sci. USA* **98,** 1241–1248 (2001).
21. Paas, Y. *et al.* Pore conformations and gating mechanism of a Cys-loop receptor. *Proc. Natl Acad. Sci. USA* **102,** 15877–15882 (2005).
22. Le Novere, N. & Changeux, J. P. LGICdb: the ligand-gated ion channel database. *Nucleic Acids Res.* **29,** 294–295 (2001).
23. Konno, T. *et al.* Rings of anionic amino acids as structural determinants of ion selectivity in the acetylcholine receptor channel. *Proc R. Soc. Lond. B* **244,** 69–79 (1991).

24. Cohen, B. N., Labarca, C., Davidson, N. & Lester, H. A. Mutations in M2 alter the selectivity of the mouse nicotinic acetylcholine receptor for organic and alkali metal cations. *J. Gen. Physiol.* **100,** 373–400 (1992).
25. Corringer, P. J. *et al.* Mutational analysis of the charge selectivity filter of the alpha7 nicotinic acetylcholine receptor. *Neuron* **22,** 831–843 (1999).
26. Gunthorpe, M. J. & Lummis, S. C. Conversion of the ion selectivity of the 5-HT(3a) receptor from cationic to anionic reveals a conserved feature of the ligand-gated ion channel superfamily. *J. Biol. Chem.* **276,** 10977–10983 (2001).
27. Imoto, K. *et al.* Rings of negatively charged amino acids determine the acetylcholine receptor channel conductance. *Nature* **335,** 645–648 (1988).
28. Revah, F. *et al.* Mutations in the channel domain alter desensitization of a neuronal nicotinic receptor. *Nature* **353,** 846–849 (1991).
29. Beckstein, O. & Sansom, M. S. A hydrophobic gate in an ion channel: the closed state of the nicotinic acetylcholine receptor. *Phys. Biol.* **3,** 147–159 (2006).
30. Cymes, G. D., Ni, Y. & Grosman, C. Probing ion-channel pores one proton at a time. *Nature* **438,** 975–980 (2005).

Supplementary Information is linked to the online version of the paper at www.nature.com/nature.

Acknowledgements We thank I. Toth from the Scottish Crop Research Institute for providing g-DNA of *E. chrysanthemi*, B. Blattmann and A. Haisch for assistance with crystal screening, D. Sargent for help with Xe derivatization, C. Schulze-Briese and the staff of the X06SA beamline for support during data collection, the Protein Analysis Group at the Functional Genomics Center of the University of Zürich for help with mass spectrometry, R. MacKinnon for comments on the manuscript and members of the Dutzler laboratory for help in all stages of the project. Data collection was performed at the Swiss Light Source of the Paul Scherrer Institute. This work was supported by a grant from the National Center for Competence in Research in Structural Biology and the EMBO Young Investigator Program to R.D. R.J.C.H. is affiliated with the Molecular Life Sciences Ph.D. Program of the University/ETH Zürich.

Author Contributions R.D. and R.J.C.H. designed the project. R.J.C.H. performed all experiments. R.D. assisted in data collection, structure determination and electrostatic calculations. R.D. and R.J.C.H. jointly wrote the manuscript.

Author Information Coordinates have been deposited in the Protein Data Bank under code 2vl0. Reprints and permissions information is available at www.nature.com/reprints. Correspondence and requests for materials should be addressed to R.D. (dutzler@bioc.uzh.ch).

2.2.3. Supplementary Material

	Cs^+	Tl^+	Rb^+
Data collection			
Space group	$P2_1$	$P2_1$	$P2_1$
Cell dimensions			
a, b, c (Å)	104.9, 266.8, 110.7	105.0, 265.5, 110.3	105.2, 265.3, 110.6
α, β, γ (°)	90.0, 111.5, 90.0	90.0, 109.2, 90.0	90.0, 111.3, 90.0
Resolution (Å)*	30–4.4 (4.6–4.4)	30–4.5 (4.7–4.5)	30–4.2 (4.4–4.2)
R_{sym} or R_{merge}	16.3 (52.7)	13.8 (57.6)	14.3 (52.0)
$I / \sigma I$	8.8 (3.5)	7.9 (2.8)	9.6 (4.0)
Completeness (%)	99.1 (99.3)	98.6 (99.3)	99.1 (98.6)
Redundancy	6.6 (5.1)	3.5 (3.4)	6.7 (6.4)

* Values in parentheses are for highest-resolution shell.

Table 2.2.: **Data collection statistics for ion soaks.**

Ion selectivity filters have been observed in other ion channels as narrow regions of the ion conduction pore where partially dehydrated ions are coordinated by polar protein atoms (see section 1.5.5). To detect ion-binding sites within ELIC, the crystals were soaked in solutions containing different cations, which could easily be detected in electron densities by their anomalous (cesium and thallium) or isomorphous (rubidium) differences. Table 2.2 gives an overview of the data collection statistics for the best cesium, thallium and rubidium datasets. Figure 2.12 shows the anomalous or isomorphous difference electron density from the different datasets superimposed on the structure of ELIC. Additionally the anomalous difference electron density of xenon atoms bound to the protein is shown. Several binding sites for each of the ions were identified. However, no ion-binding sites were found within the pore region of ELIC, whereas apolar xenon atoms are localized within the hydrophobic region of the pore. The location of xenon within the pore of ELIC is interesting, since it is used as an anesthetic that binds to the closed state of the nAChR[157], although the site conferring sensitivity to xenon was located within the β subunit of the nAChR at a position closer to the intracellular site[158]. Figure 2.14 compares the pore regions of ELIC and the nAChR.

Ion-binding sites for cesium and thallium were identified within the LBP of the extracellular domain. The coordination of cations by aromatic and negatively charged residues lining the LBP hints at a positively charged ligand for ELIC. The potential ligand is restricted by the pocket size and its chemical properties. The geometry and energetic restriction allows a potential identification of a ligand by a computational docking approach[159].

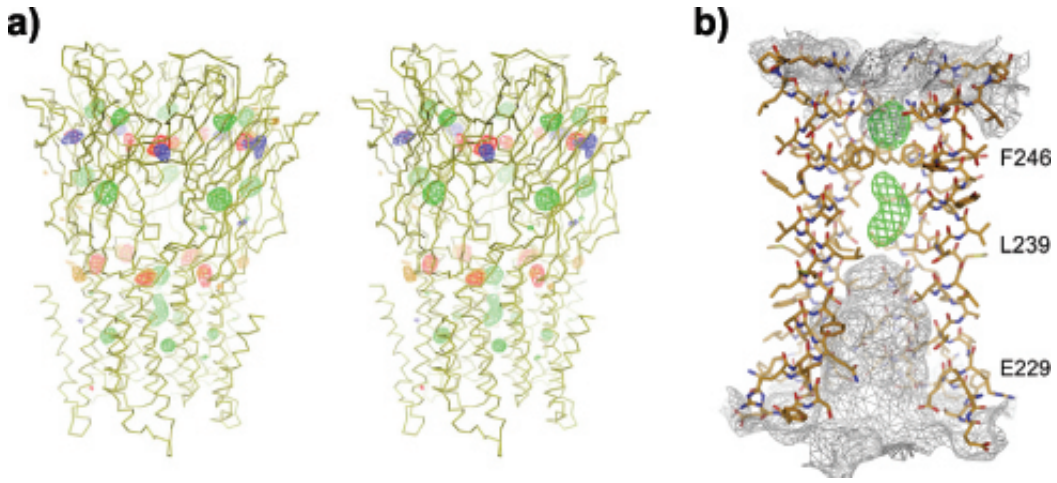

Figure 2.12.: **Cation-binding sites in ELIC. a** Stereo view of ELIC in a Cα representation. Difference electron density from crystals soaked in solutions of different cations (contoured at 4 σ) is shown superimposed. Anomalous difference electron density of crystals soaked in Tl^+, Cs^+ and xenon is shown in blue, red and green, respectively. Isomorphous difference electron density of crystals soaked in Rb^+ is shown in orange. **b** View of the α2-helices defining the pore region. The front subunit is removed for clarity. The molecular surface is shown as white mesh. Anomalous difference density of Xe atoms is contoured at 4σ and shown as green mesh. The positions of selected residues are indicated. Figure **S5**

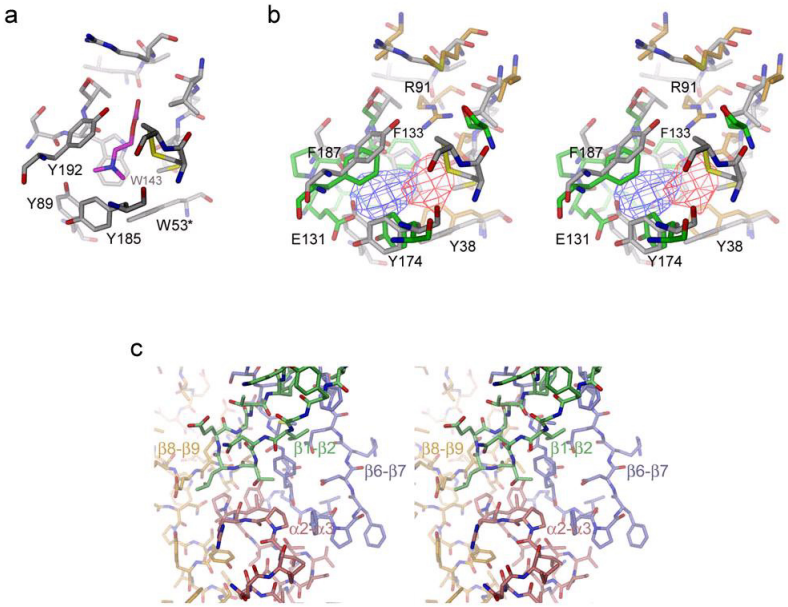

Figure 2.13.: **Ligand-binding region and domain interface. a** Acetylcholine-binding site of AChBP. C atoms of residues surrounding the carbamylcholine ligand (C atoms colored in magenta) are shown in grey. Conserved aromatic residues are labeled. $\star$ Indicates residues contributed from the neighboring subunit. **b** Stereo view of the acetylcholine-binding site of AChBP (grey) superimposed on residues of the equivalent region of ELIC. C-atoms of residues from the two subunits of ELIC are colored in green and orange respectively. Selected residues of ELIC are labeled. Anomalous difference electron density of Tl^+ and Cs^+ ions bound to ELIC is contoured at 4 σ and shown in blue and red respectively. **c** Stereo view of an all atom representation of the domain interface with a color coding as in Fig. 2c in the paper. Figure **S6**

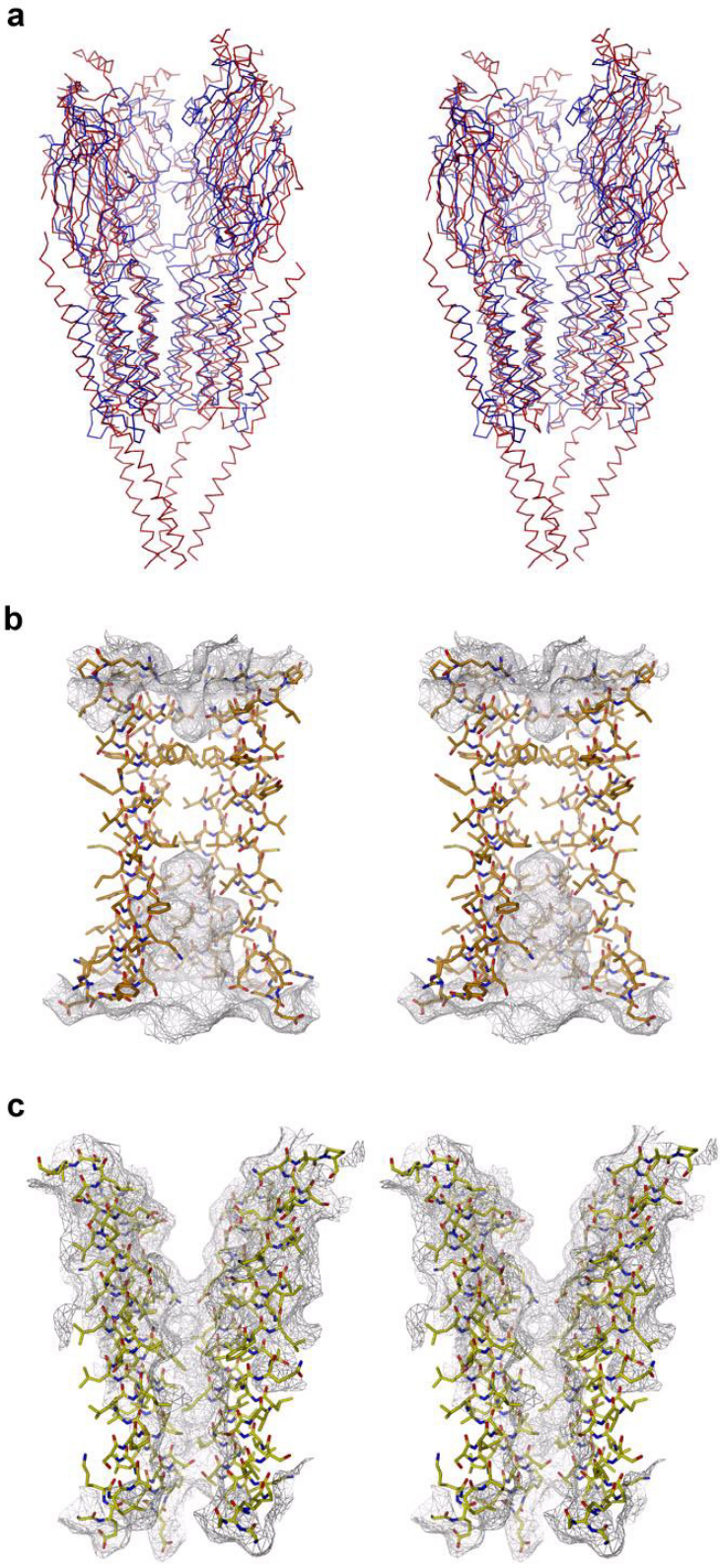
a
b
c

Figure 2.14.: **Comparison of the pore regions of ELIC and nAChR. a** Stereo view of a superposition of ELIC (blue) and nAChR (red, PDB code 2BG9) with the front subunit removed for clarity. The superposition was generated using 222 Cα positions in the cytoplasmic domain of the β, γ and δ subunits of nAChR and their corresponding positions in ELIC. **b** Stereo view of the α2-helices defining the pore region of ELIC. The front subunit is removed for clarity. Molecular surface is shown as white mesh. **c** Stereo view of the pore region of nAChR. The molecular surface of the channel region is shown superimposed on the αM2-helices. The front subunit is removed for clarity. Figure **S7**

2.3. The *Gloebacter violaceus* pentameric ligand-gated ion channel

A mechanistic understanding of ion channel function requires structural knowledge of conducting and non-conducting conformations of the protein. ELIC was shown to represent a non-conducting conformation of a pLGIC pore. Since the ligand, which promotes pore opening, is still unknown, ELIC has so far not permitted to study the mechanism of gating and ion permeation. The bacterial homologue from *Gloebacter violaceus* (GLIC), in contrast, was shown to be opened by a drop in the extracellular pH[137]. I have therefore chosen GLIC to investigate a conducting state of a pLGIC. GLIC was expressed and purified analogously to ELIC. Its X-ray structure was determined from a crystal form growing at low pH, where the open probability of the channel is high. The structure shows a distinct conformation that is different from ELIC and likely represents a conducting conformation[160]. To investigate its functional properties GLIC was in parallel expressed in *Xenopus* oocytes and studied by two-electrode voltage-clamp and patch-clamp techniques.

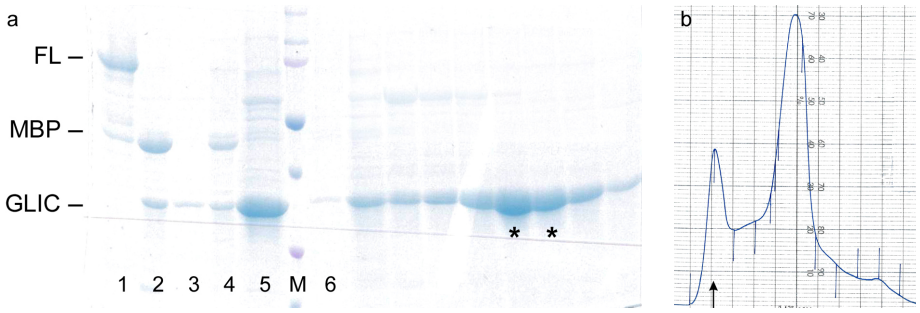

Figure 2.15.: **Purification of GLIC. a** Samples from different steps of the purification. The size of the fusion protein (FL), the MBP and GLIC are indicated. **1** sample eluted from the Ni-NTA column. **2** sample after 2h incubation with HRV 3C protease. **3** digested protein after removal of the MBP and the 3C protease, **4** rebound MBP. **5** sample injected on a SEC column. **6** fractions from SEC. Fractions indicated with ∗ were pooled for crystallization. **M** standard molecular weight marker (BioRad) with 75 (red), 50, 37 and 25 (red) kDa. **b** Gelfiltration profile on a Superdex S200 column. The void volume is indicated (arrow).

GLIC was cloned in the same way as ELIC, as shown in figure 2.2 on page 29. The fusion protein includes a pelB signal sequence, followed by a His_{10}-Tag and MBP. The purification of GLIC was straightforward and is documented in figure 2.15. The ratio of MBP to GLIC after cutting of the fusion protein was more unfavorable compared to ELIC as can be seen in lane **2** in part **a** of figure 2.15, which indicates partial proteolysis during expression and purification. Since the overall expression of GLIC was lower and the protein seemed to be less stable than ELIC, bigger expression cultures had to be used (i.e. 20 l TB cultures for GLIC compared to 10 l for ELIC). The gelfiltration profile of GLIC figure 2.15 **b** indicates a more favorable ratio of the aggregation peak to the pentamer. However, this ratio varied between different purifications and detergents.

Like ELIC, GLIC was stable in a broad range of maltoside detergents (C_8 – C_{14}), whereas detergents from other classes led to aggregation of the protein. GLIC purified in different mal-

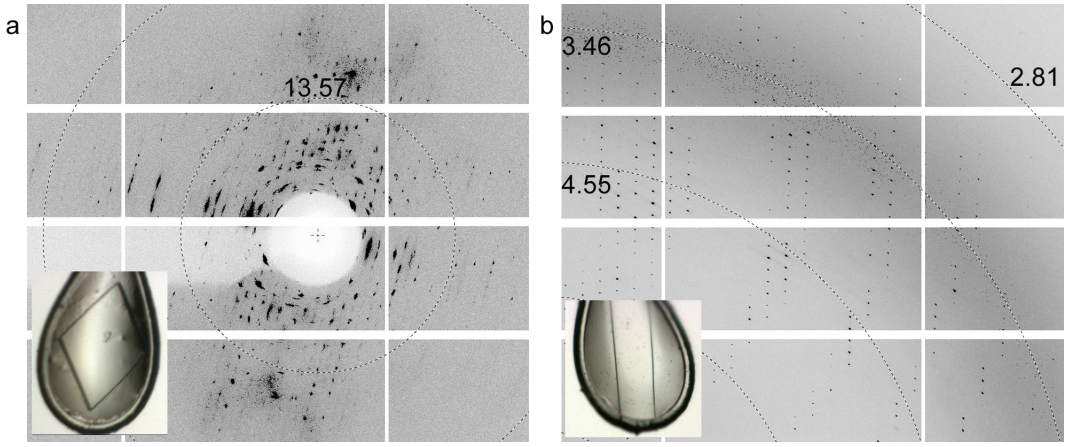

Figure 2.16.: **Diffraction patterns of GLIC crystals.** Shown are the crystals as mounted in the loop with the respective diffraction pattern. Resolution rings are indicated. **a** Crystal grown in 500 mM KCl, 9 % PEG 4000, pH 9.5. **b** 225 mM $(NH_4)SO_4$, 9 % PEG 4000, pH 4.0.

toside detergents crystallized in many different conditions. However, as frequently observed for membrane proteins, most of these crystals did not diffract sufficiently to be suited for structure determination. Figure 2.16 shows two examples of crystals and their diffraction patterns. In general, crystals grown at high pH did not diffract well, whereas several conditions were found at low pH, where the crystals diffracted significantly better. Crystals grown from 200–250 mM $(NH_4)SO_4$ in 9–13% PEG 4000 at pH 4.0 had the best diffraction properties, they allowed the collection of a complete dataset at 3.1 Å resolution and were used for structure determination. These crystals were of space group C2 with one pentamer in the asymmetric unit which is apparent from a pronounced peak in a self rotation function originating from the pentameric symmetry of the molecule (see figure 2.17.

The data collection and refinement statistics are shown in table 2.3 on page 56 and the crystal packing is shown in figure 2.18. The protein forms tail-to-tail interactions between the intracellular loops of two interacting pentamers and contacts between the extracellular domains.

Initial phases to determine the GLIC structure were obtained by molecular replacement using the structure of ELIC as a search model. The phases were subsequently improved and extended by cyclic five-fold NCS averaging. By using different truncated structures of ELIC model bias could be avoided. While all search models provided correct solutions in the rotation translation functions an incorrect trace of the pore region in phases originating from the full-length structure of ELIC was observed due to model bias. This bias in the phases is apparent in the side chain electron density of Phe-246 in the ELIC structure, which is replaced by an isoleucine in GLIC. A section of the electron density calculated with molecular replacement phases from the full-length structure of ELIC is shown in figure 2.19 **a**. The electron density of the helix pair clearly superimposes on the ELIC structure. With truncated models of ELIC, where the loops of the LBD facing the TMD and the α2-helix were removed, the new position of helix α2 started to emerge (figure 2.19 **b**), which indicates a different conformation for GLIC. Thus, the truncated

search model resulted in less biased initial phases which were improved and extended making use of the five-fold NCS of GLIC in the C_2 cell.

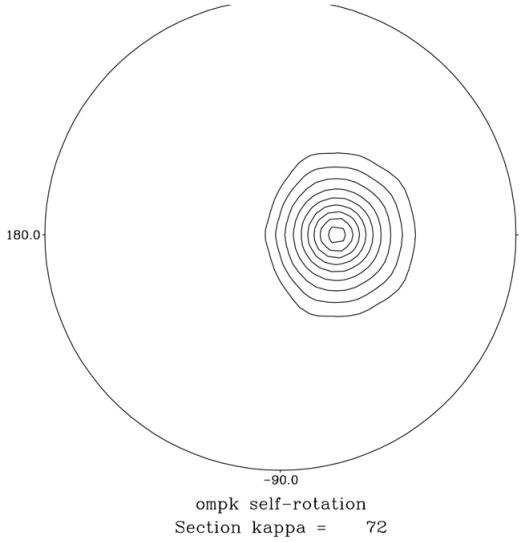

Figure 2.17.: **Self-rotation function of GLIC.** Shown is the kappa section at 72°. Contour levels are $10\,\sigma$.

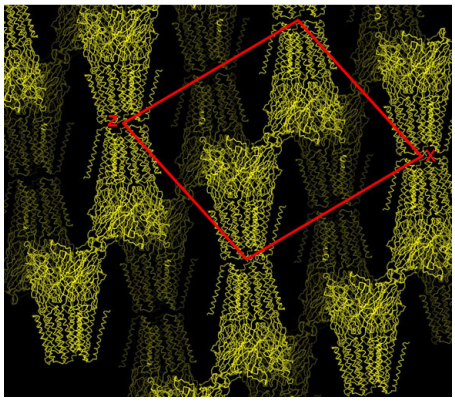

Figure 2.18.: **Crystal packing of GLIC in the C2 crystal form.** The view is along Y, the unit-cell axes are indicated. Figure **S2**

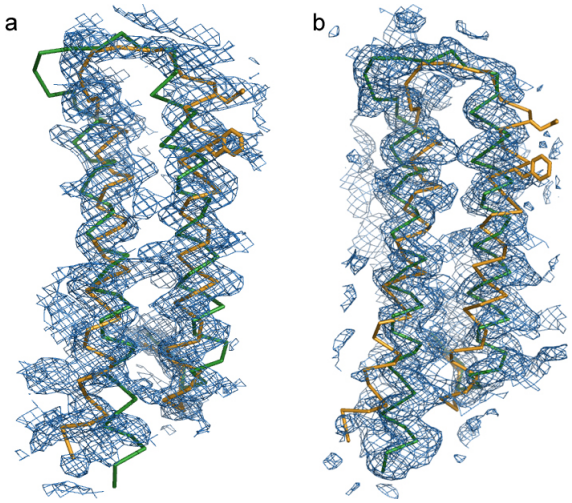

Figure 2.19.: **Model bias in molecular replacement.** Shown are the α2-α3-helix pairs of the final ELIC (orange) and GLIC (green) structures. Residues 246 and 250 of ELIC are shown as sticks. Electron densities of different molecular replacement runs are shown. **a** The full-length ELIC structure was used as a search model. **b** ELIC was truncated as described in the text. Helix α2 was removed from the search model.

	WT	E221A
Data collection		
Space group	C2	C2
Cell dimensions		
a, b, c (Å)	178.5, 133.5, 160.5	180.3, 133.7, 161.8
α, β, γ (°)	90.0, 101.6, 90.0	90.0, 102.3, 90.0
Resolution (Å)*	40–3.1 (3.27–3.1)	40–3.5 (3.7–3.5)
R_{sym} or R_{merge}	9.2 (60.7)	13.1 (54.4)
$I/\sigma I$	23.1 (2.6)	16.1 (2.6)
Completeness (%)	99.6 (99.9)	99.1 (99.5)
Redundancy	6.3 (6.5)	6.3 (6.5)
Refinement		
Resolution (Å)	20–3.1	20–3.5
No. reflections	66589	46690
R_{work} / R_{free}	23.8 / 26.6	25.5 / 27.6
No. atoms		
Protein	12605	12585
Ligand / ion	–	–
Water	47	
B-factors		
Protein	87.1	107.0
Ligand / ion	–	–
Water	59.5	
R.m.s. deviations		
Bond lengths (Å)	0.01	0.01
Bond angles (%)	1.4	1.5

* Values in parentheses are for highest-resolution shell.

Table 2.3.: **Data collection statistics and refinement for wild type and E221A mutant.**

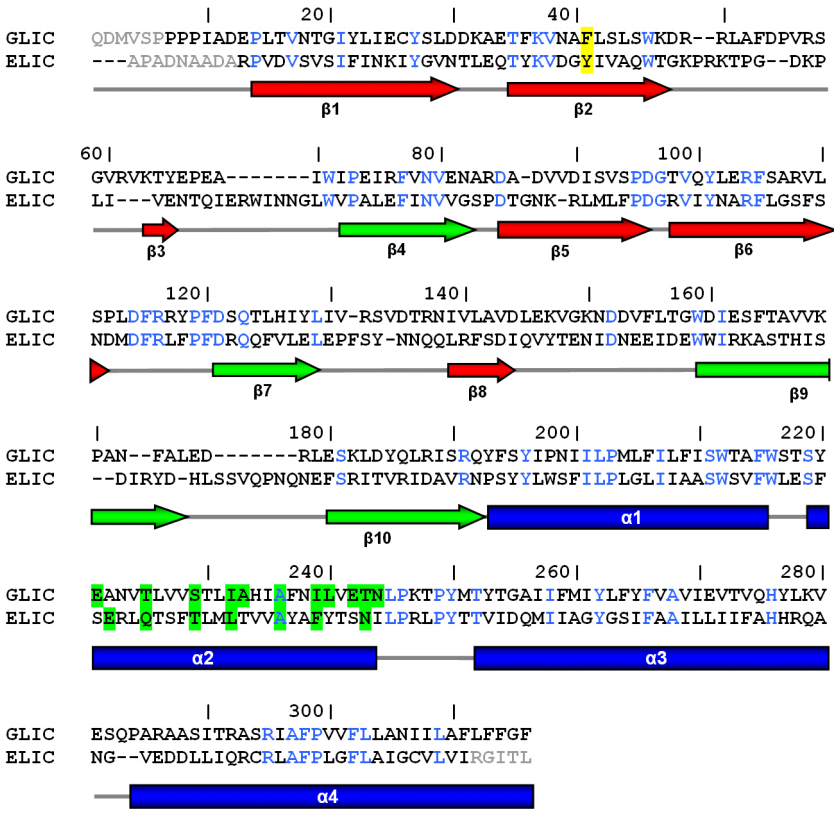

Figure 2.20.: **Sequence alignment.** Structure-based alignment of the pLGICs of *G. violaceus* (GLIC, PDB-ID 3EHZ) and *E. chrysanthemi* (ELIC, PDB-ID 2VL0). Secondary structure and numbering of GLIC are indicated below and above the sequences. Secondary structure elements contributing to the two sheets in the β-sandwich of the extracellular domain are colored in red and green, respectively. α-Helices of the pore domain are colored in blue. Strictly conserved residues between GLIC and ELIC are colored in blue. Residues that are not defined in the electron density are colored grey. Residues contributing to the pore lining in GLIC and ELIC are highlighted in green. Figure **S4**

The final electron density in different regions of GLIC is shown in figure 2.21. The phases are completely devoid of model bias and show well defined electron density for all residues. Residual electron density is found in the pore region and was interpreted as water molecules (figure 2.26 on page 69).

While the sequence conservation between ELIC and GLIC is moderate, both proteins share a very similar structural organization. Figure 2.20 displays a structure-based alignment of ELIC and GLIC. It differs with respect to the sequence-based alignment in figure 2.4 in the region of

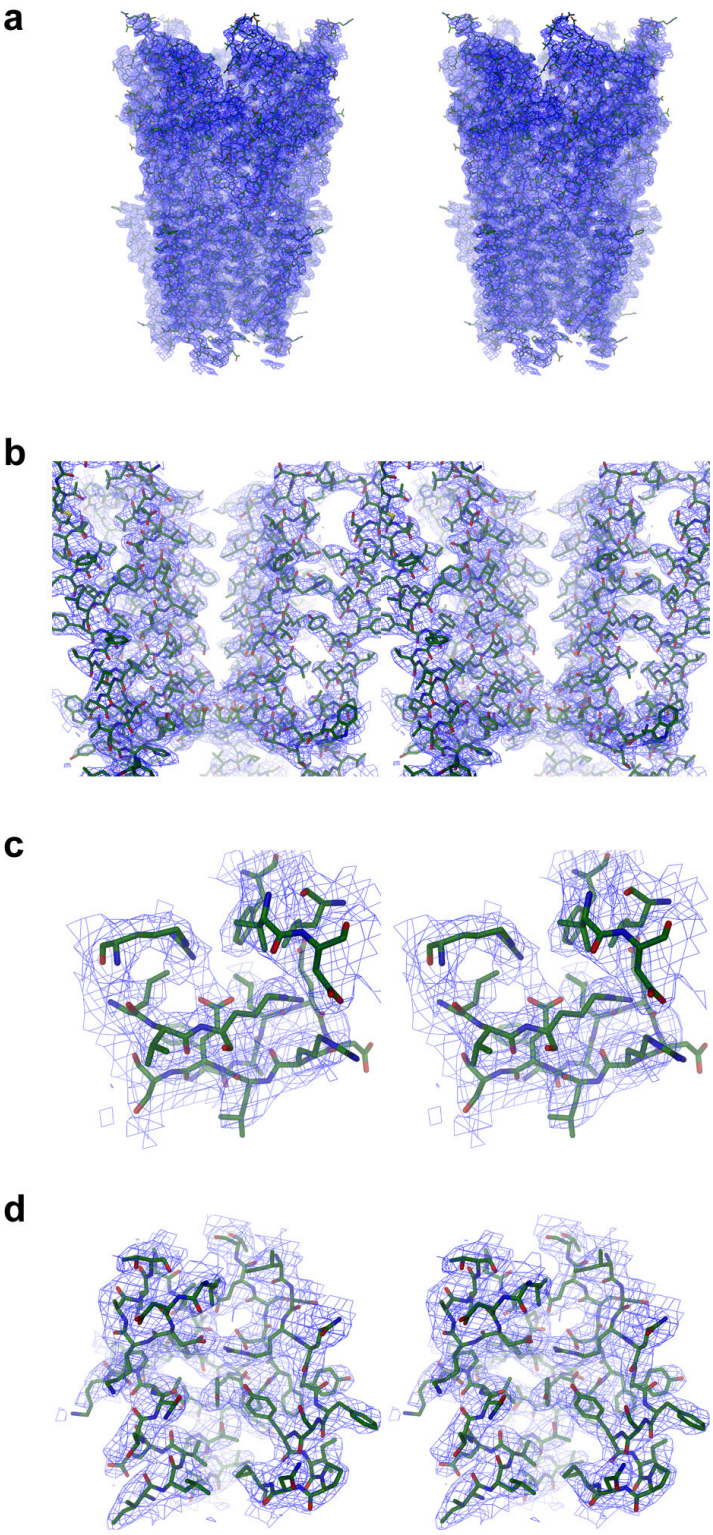
a
b
c
d

the $\beta 2$–$\beta 3$ loop in the extracellular domain, a poorly conserved region located at the extracellular end of the LBD.

The structure of GLIC was published and described in the paper (Hilf RJC. & Dutzler R. *Structure of a potentially open state of a proton-activated pentameric ligand-gated ion channel.* **Nature.** 2009 Jan 1; 457(7225): 115-8), which is reprinted on the following pages including several supplementary figures not mentioned in the text (figure 2.27 and 2.28 on pages 69 and 70, respectively).

Figure 2.21.: **Stereo view of electron density. a** Averaged electron density superimposed on the GLIC pentamer. The map (3.1 Å resolution, contoured at 1 σ) was calculated using the native amplitudes and model phases that were improved by cyclic fivefold NCS averaging. The view is from within the membrane. Sections of the electron density are displayed in **b**–**d**. **b** Pore region. The view is as in **a**. **c** Putative ligand-binding region viewed from the extracellular side. **d** Interface between the extracellular domain and the pore. The view is as in **a**. Figure **S3**

LETTERS

Structure of a potentially open state of a proton-activated pentameric ligand-gated ion channel

Ricarda J. C. Hilf[1] & Raimund Dutzler[1]

The X-ray structure of a pentameric ligand-gated ion channel from *Erwinia chrysanthemi* (ELIC) has recently provided structural insight into this family of ion channels at high resolution[1]. The structure shows a homo-pentameric protein with a barrel-stave architecture that defines an ion-conduction pore located on the fivefold axis of symmetry. In this structure, the wide aqueous vestibule that is encircled by the extracellular ligand-binding domains of the five subunits narrows to a discontinuous pore that spans the lipid bilayer. The pore is constricted by bulky hydrophobic residues towards the extracellular side, which probably serve as barriers that prevent the diffusion of ions. This interrupted pore architecture in ELIC thus depicts a non-conducting conformation of a pentameric ligand-gated ion channel, the thermodynamically stable state in the absence of bound ligand. As ligand binding promotes pore opening in these ion channels and the specific ligand for ELIC has not yet been identified, we have turned our attention towards a homologous protein from the cyanobacterium *Gloebacter violaceus* (GLIC). GLIC was shown to form proton-gated channels that are activated by a pH decrease on the extracellular side and that do not desensitize after activation[2]. Both prokaryotic proteins, ELIC and GLIC form ion channels that are selective for cations over anions with poor discrimination among monovalent cations[1,2], characteristics that resemble the conduction properties of the cation-selective branch of the family that includes acetylcholine and serotonin receptors[3,4]. Here we present the X-ray structure of GLIC at 3.1 Å resolution. The structure reveals a conformation of the channel that is distinct from ELIC and that probably resembles the open state. In combination, both structures suggest a novel gating mechanism for pentameric ligand-gated ion channels where channel opening proceeds by a change in the tilt of the pore-forming helices.

GLIC was crystallized at pH 4, a condition where the open probability of the channel is high, and its structure was determined by molecular replacement followed by cyclic non-crystallographic symmetry averaging (Supplementary Figs 1–3, Supplementary Table 1). In its overall organization, the structure of GLIC closely resembles that of ELIC (Fig. 1): the extracellular domain encompasses 10 β-strands that are organized as a sandwich of two tightly interacting β-sheets, while the transmembrane domain folds into a bundle of four α-helices. As for other pLGICs of prokaryotic origin, an extended region between helices α3 and α4 is absent and replaced by a short loop[5]. The close correspondence between the ELIC and GLIC structures is emphasized in a superposition of their Cα positions (Fig. 1c). Despite the moderate sequence conservation (20% identical residues, Supplementary Fig. 4), both proteins are very similar on a structural level. Whereas the elements of secondary structure are highly conserved, spatial differences in the ligand-binding and the transmembrane domain indicate that the two

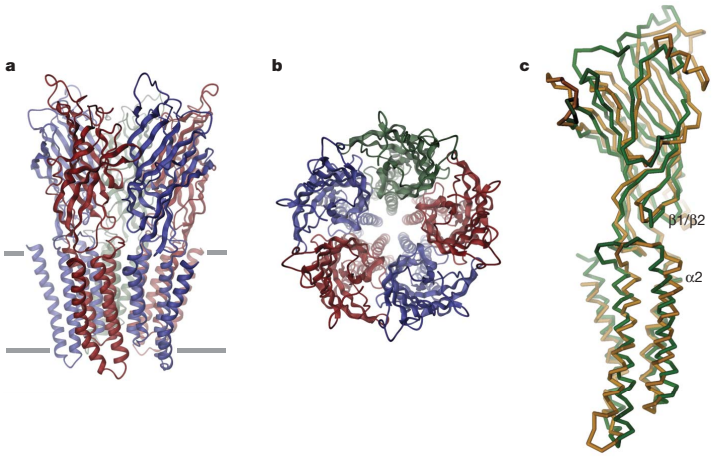

Figure 1 | GLIC structure. **a**, Ribbon representation of GLIC viewed from within the membrane with the extracellular solution above. The approximate membrane boundaries are indicated. **b**, Structure of the pentameric channel viewed from the extracellular side. **c**, Superposition of GLIC (green) and ELIC (orange, PDB 2vl0) subunits. The protein is shown as a Cα trace, the subunit is viewed from within the membrane. The superposition was generated by a least squares fit of the Cα positions of the respective α1 helices of the five subunits of the pentameric channel. Figures 1–4 were prepared with DINO (http://www.dino3d.org).

[1]Department of Biochemistry, University of Zürich, Winterthurerstrasse 190, CH-8057 Zürich, Switzerland.

proteins adopt two distinct conformations of the ion conduction pore (Fig. 2, Supplementary Fig. 5).

The conformational differences between the two ion channels are manifested in their pore geometry: whereas the transmembrane pore of ELIC is constricted on its extracellular side, the equivalent region of GLIC shows a funnel-shaped opening with a linearly decreasing diameter that places its narrowest part at the intracellular entry of the channel (Fig. 2c). At this constricted position of GLIC, the ELIC pore is dilated to a water-filled cavity of about 6 Å in diameter. The mismatch in the pore geometry results from differences in the orientation of the α2 and α3 helices. With respect to ELIC, both helices in GLIC have rotated as rigid unit by about 9° around an axis that intersects with residue Val 267 and that runs parallel to the membrane (Fig. 2a). This rotation results in an outward movement of the helix pair away from the pore axis on the extracellular side and an inward movement towards the axis at the intracellular entry of the channel. In contrast to the large differences in the position of the α2 and α3 helices, the location of helix α1 that connects the transmembrane pore to the extracellular domain is virtually unchanged (Fig. 1c, Supplementary Fig. 5).

A comparison of the pore region of the nicotinic acetylcholine receptor (nAChR)—which was modelled into electron density at 4 Å resolution—with the corresponding region in the two bacterial channels reveals interesting similarities: the extracellular part of the nAChR pore resembles the funnel-shaped structure of GLIC, whereas the diameter in the intracellular half is closer to ELIC (Supplementary Fig. 6). Although the nAChR structure has been proposed to represent a non-conducting conformation[6,7], as it was obtained in the absence of ligands, its relation to the two conformations of bacterial pentameric ligand-gated ion channels (pLGICs) at high resolution remains ambiguous.

Although the shape of the transmembrane channel in GLIC differs, the chemical features that are common to members of this branch of the family are preserved (Fig. 3)[3]. As in other cation-selective pLGICs, the extracellular half of the pore is dominated by hydrophobic residues, some of which carry bulky side chains. In contrast to the outer half, the intracellular part is lined by polar side chains of serine and threonine residues that provide a hydrophilic character to this region. Both ends of the transmembrane channel are framed by rings of acidic residues that are located at the membrane boundary and that contribute to the overall negative electrostatic environment in the pore (Fig. 2c). Residual electron density in the water-filled channel indicates the presence of partially ordered solvent molecules (Supplementary Fig. 7). A ring of glutamate residues on the intracellular pore entry is remarkable. Equivalent residues in the nAChR, termed the 'intermediate ring of charges', have previously been identified as major determinants of conductance and cation selectivity[8,9]. In GLIC, the side chains of the five glutamate residues that are well defined in the electron density project into the lumen of the pore and form a ring of interacting ionizable groups (Fig. 3a, Supplementary Fig. 3b). They define the narrowest part of the channel and resemble a narrow selectivity filter, akin to other selective ion channels[10], that might directly interact with ions which have stripped part of their hydration shell. When investigating crystals that were soaked in solutions containing the permeant cations Rb^+, Cs^+ and the divalent cation Zn^{2+}, we were able to locate electron density of bound ions in the region intra- and extracellular to the constriction, thus emphasizing its potential role for conductance and ion selectivity in GLIC (Fig. 3b, Supplementary Table 1).

The tight interactions of the five glutamate side chains defining the pore constriction might impede the free diffusion of ions. Because in a cellular context the intracellular part of the open channel faces the physiological pH of the cytoplasm, it is possible that the protonation state of these residues is shifted at low pH and that the interactions observed in the electron density are a consequence of the crystallization conditions. When investigated by excised inside-out patch-clamp recording, the current passed by the channel decreases upon lowering the intracellular pH, as expected when the net charge of the protein becomes more positive (Supplementary Fig. 1c). To investigate the extent to which the observed pore structure might be influenced by local interactions, we have determined the structure of the mutant E221A at 3.5 Å. The decreased cation selectivity of the mutant emphasizes the critical role of this residue for ion conduction (Supplementary Fig. 1d). The structure of the mutant, which

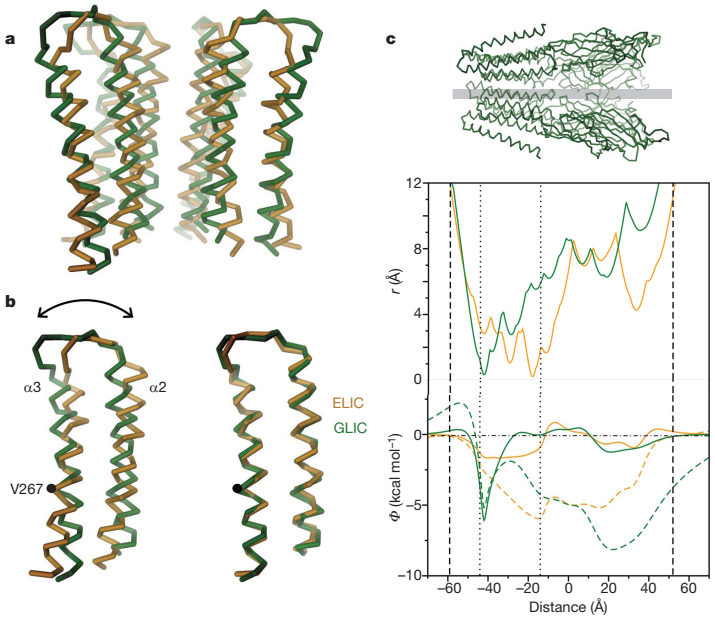

Figure 2 | Comparison of the pore region. **a**, View of the Cα trace of the α2–α3 helices. The respective regions of the superimposed structures of GLIC (green) and ELIC (orange) are shown. The front subunit is removed for clarity. The view is from within the membrane. **b**, Conformation of the α2–α3 helix pair of a single subunit as observed in the structures (left) and after a least squares fit of the Cα positions of the respective helix pair of ELIC onto GLIC (right). The rotation axis is indicated. **c**, Pore radius (r) and electrostatic potential (Φ) in GLIC and ELIC. Orientation of GLIC is shown above; vertical dashed lines, molecular boundaries; vertical dotted lines, transmembrane region. Top plot, r of GLIC (green) and ELIC (orange). Bottom plot, Φ along the pore axis of GLIC (green) and ELIC (orange), as calculated from a numerical solution of the linearized Poisson–Boltzmann equation at 0 and 150 mM monovalent salt concentration (respectively dashed and solid lines).

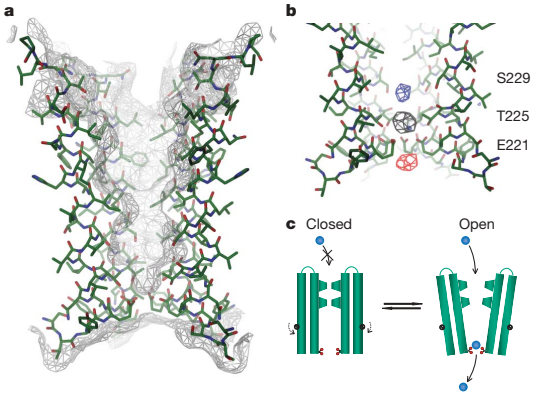

Figure 3 | Pore structure and ion binding. a, View of the α2 helices of GLIC defining the pore region. The front subunit is removed for clarity. The molecular surface is shown as grey mesh. **b**, Intracellular part of the pore region. Shown are the isomorphous difference electron density of Cs^+ (grey, contoured at 4.5σ) and Rb^+ (blue, contoured at 3.5σ), and the anomalous difference electron density of Zn^{2+} (red, contoured at 4.5σ). The position of selected residues is indicated. **c**, Schematic representation of the pore opening mechanism. The α2/α3 helices of two subunits in the closed (left) and open (right) conformation are shown. The ion-coordinating glutamate residues are shown in red, the permeating ions in blue. The axis of rotation (black) in each subunit is indicated.

crystallized in similar conditions as wild type, showed an unaltered overall conformation of the protein backbone with a pore where the intracellular constriction is removed (Supplementary Fig. 8). A similar pore structure would be obtained in a case where the glutamate side chains change their conformation (Supplementary Fig. 8b, c). Our results thus suggest that the overall conformation of the pore-forming helices is not perturbed by local interactions of the partly protonated residues at low pH, and that minor changes in the side-chain conformation are sufficient to increase the pore radius. The conical aqueous pore structure and the ability to bind ions at the narrow intracellular constriction thus suggest that the structure of GLIC either depicts a conducting state of a pLGIC or a conformation that is very close to a conducting state (Fig. 3c).

Although GLIC shares the hallmarks of pLGICs, the ligand that triggers its channel opening is unusual. GLIC has been shown to be activated by a decrease in the extracellular pH (ref. 2). It is thus conceivable that the titration of a group in the consensus ligand-binding region causes conformational transitions in the extracellular domain that are similar to those induced in response to the binding of neurotransmitters in other members of the family[11]. The ligand-binding site of pLGICs is located at the interface between two subunits, and is covered by the strands β9 and β10 (Fig. 4). When compared to ELIC and acetylcholine-binding protein (AChBP) this site shows distinctive features. The structure around β9 is only weakly conserved, particularly in the loop region connecting β9 and β10 (which is seven residues shorter than in ELIC) (Fig. 4a, Supplementary Fig. 4). Whereas in ELIC the loop is mobile and thus only poorly defined in the electron density, its conformation in GLIC is well defined with residues being involved in a variety of interactions, some of which involve ionizable residues (Fig. 4b, Supplementary Fig. 3c). Several of these interactions are unique to GLIC, such as a salt bridge between Arg 76 and Glu 180 at the position where the quaternary ammonium is bound in AChBP[12,13]. The tight interactions in the loop region of GLIC resemble the conformation that has been observed in AChBP in the presence of its substrate analogue carbamylcholine[13], except that the pocket for the ligand found in AChBP and in the respective position in ELIC is filled with protein side chains (Supplementary Fig. 9). The structural features of the ligand-binding region are thus in accordance with an activated ligand-occupied state of the domain.

Conformational differences in the conserved regions of the ligand-binding domain hint towards transitions that lead to channel opening. When compared to ELIC, parts of the ligand-binding domain in GLIC have undergone considerable structural rearrangements. The movements are most pronounced for residues in one of the two β-sheets constituting the extracellular domain that was previously termed the 'inner sheet', part of which has tilted by about 5° towards the membrane plane (Fig. 4a). The structural differences between ELIC and GLIC also affect the loop regions connecting the strands β1/β2 and β6/β7 at the boundary between the cytoplasmic domain and the pore. Both regions contact the α2/α3 loop in the transmembrane domain and have previously been identified to play a critical role in channel opening[14,15]. Yet, the extent of the movement in the extracellular domain is small compared to the large conformational difference in the adjacent region of the pore domain, as if the breaking of a critical interaction in the interface would have allowed the relaxation of a strained conformation of the channel (Fig. 1c, Supplementary Figs 3d, 10). Within the extracellular domain, the GLIC structure shows the relationship between conserved residues that are critical for channel opening. These residues include Arg 191 at the end of β10 that forms a pair of salt bridges with Asp 31 in the β1/β2 turn and Asp 121 in the β6/β7 loop (which is part of the Cys-loop signature sequence, Fig. 4c). Mutations that remove either of the two interactions in the nAChR and other pLGICs drastically decrease the open probability of the channel, thus emphasizing the importance of the respective loop regions for the transduction of conformational signals from the ligand-binding site to the pore domain[14–17].

The pore structure of GLIC is in striking accordance with electrophysiological investigations on the conducting conformation of the nAChR. Different studies have previously predicted a funnel-shaped channel with a short constriction on the intracellular side that harbours a single ion-binding site at the narrowest part of the pore[18,19]. Whereas the structure of ELIC in a non-conducting conformation showed a pore that was constricted on the outside and lacked binding sites for ions in the pore, the structure of GLIC now displays the predicted features. The structure also allows a potential explanation

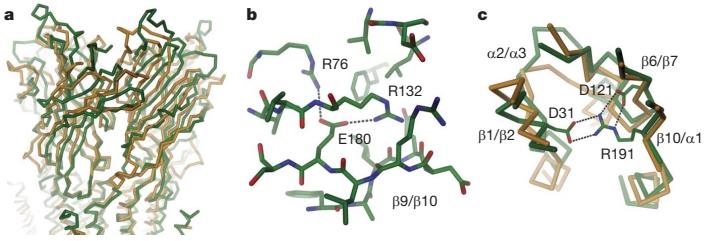

Figure 4 | Extracellular domain. a, View of the ligand-binding domains in the superimposed structures of GLIC (green) and ELIC (orange). Proteins are shown as Cα representation. **b**, Ligand-binding region of GLIC. Residues in the vicinity of the β9/β10 loop are shown. The view is from the extracellular side. Selected residues and their interactions are indicated. **c**, Cα representation of the interface region between the extracellular domain and the pore in GLIC (green) and ELIC (orange) viewed from the extracellular side. Selected residues in GLIC are shown as sticks, ionic interactions are indicated by dotted lines.

for the dominant role of the residues constituting the 'intermediate ring of charges' in channel function[8,9]. These residues, which correspond to the ion-coordinating glutamates in GLIC, and that are in the same position in the homopentameric α-7 nAChR and one helix turn towards the cytoplasm in the muscle nAChR, have been identified to exert a prevailing influence on ion conduction and cation selectivity[20–22]. The GLIC structure now suggests that the negatively charged side-chains directly interact with the partly desolvated permeant cations, rather than merely contributing to the overall negative electrostatics in the intracellular part of the pore. The analysis of the electrostatic potential of GLIC shows a pronounced energy minimum near the intracellular entry of the open channel that is decreased in the closed channel and that was previously observed in a functional study that investigated the binding of positive charged MTS (methanethiosulphonate) reagents to the nAChR (Fig. 2c)[23,24].

The comparison of the two high resolution structures of pLGICs gives structural insight into the mechanisms underlying pore opening. These mechanisms have been ambiguous so far, and have mainly been derived from electron microscopy images at low resolution[25]. Although previous studies have proposed that channel opening proceeds by a rotation of the pore-lining helices around their helix axis[6], the results of our study suggest a different mechanism. Assuming that the structures of ELIC and GLIC depict the closed and open conformations of a pLGIC pore, opening occurs by a change in the tilt of the helices α2 and α3 that move as a rigid body around an axis that runs parallel to the membrane and that intersects with a residue in α3 about two-thirds across the transmembrane channel (Fig. 3c). This mechanism is in accordance with previously recorded functional data[26–28]. Our study thus provides a first structural view at high resolution into how a pLGIC may open and selectively conduct ions.

METHODS SUMMARY

GLIC was expressed in *Escherichia coli* with its amino terminus fused to maltose-binding protein (MPB) that was preceded by a signal sequence (PelB). The protein was purified from isolated membranes in the detergents n-dodecyl-β-D-maltoside or n-tridecyl-β-D-maltoside. MPB was cleaved during purification by proteolytic digestion at a specific site located between MBP and the channel protein. Crystals were grown at pH 4.0 with addition of 9% PEG 4000, 225 mM $(NH_4)_2SO_4$ and 0.5 mg ml^{-1} *E. coli* lipids. Data at 3.1 Å resolution were collected at the X06-SA beamline at the Swiss Light Source (SLS) of the Paul Scherrer Institute (PSI) on a Pilatus detector (Dectris) (Supplementary Table 1). The crystals were of space group *C*2 with one homo-pentameric channel in the asymmetric unit (Supplementary Fig. 2). The structure was determined by molecular replacement using as search model a modified structure of ELIC, with all side chains truncated and helix α2 and loop regions at the interface between the ligand-binding domain and the channel removed. Phases were improved and extended by cyclic fivefold NCS averaging. The final electron density was of very high quality and devoid of model bias (Supplementary Fig. 3). All subunits are structurally very similar and were refined maintaining strong constraints throughout (Supplementary Table 1). The final structure that encompasses residues 7–316 is well refined with good stereochemistry and with no outliers in disallowed regions of the Ramachandran plot.

Full Methods and any associated references are available in the online version of the paper at www.nature.com/nature.

Received 23 June; accepted 26 September 2008.
Published online 5 November 2008.

1. Hilf, R. J. & Dutzler, R. X-ray structure of a prokaryotic pentameric ligand-gated ion channel. *Nature* **452,** 375–379 (2008).
2. Bocquet, N. *et al.* A prokaryotic proton-gated ion channel from the nicotinic acetylcholine receptor family. *Nature* **445,** 116–119 (2007).
3. Karlin, A. Emerging structure of the nicotinic acetylcholine receptors. *Nature Rev. Neurosci.* **3,** 102–114 (2002).
4. Adams, D. J., Dwyer, T. M. & Hille, B. The permeability of endplate channels to monovalent and divalent metal cations. *J. Gen. Physiol.* **75,** 493–510 (1980).
5. Tasneem, A., Iyer, L. M., Jakobsson, E. & Aravind, L. Identification of the prokaryotic ligand-gated ion channels and their implications for the mechanisms and origins of animal Cys-loop ion channels. *Genome Biol.* **6,** R4 (2004).
6. Miyazawa, A., Fujiyoshi, Y. & Unwin, N. Structure and gating mechanism of the acetylcholine receptor pore. *Nature* **423,** 949–955 (2003).
7. Unwin, N. Refined structure of the nicotinic acetylcholine receptor at 4Å resolution. *J. Mol. Biol.* **346,** 967–989 (2005).
8. Imoto, K. *et al.* Rings of negatively charged amino acids determine the acetylcholine receptor channel conductance. *Nature* **335,** 645–648 (1988).
9. Konno, T. *et al.* Rings of anionic amino acids as structural determinants of ion selectivity in the acetylcholine receptor channel. *Proc. R. Soc. Lond. B* **244,** 69–79 (1991).
10. Zhou, Y., Morais-Cabral, J. H., Kaufman, A. & MacKinnon, R. Chemistry of ion coordination and hydration revealed by a K^+ channel-Fab complex at 2.0 Å resolution. *Nature* **414,** 43–48 (2001).
11. Sine, S. M. & Engel, A. G. Recent advances in Cys-loop receptor structure and function. *Nature* **440,** 448–455 (2006).
12. Brejc, K. *et al.* Crystal structure of an ACh-binding protein reveals the ligand-binding domain of nicotinic receptors. *Nature* **411,** 269–276 (2001).
13. Celie, P. H. *et al.* Nicotine and carbamylcholine binding to nicotinic acetylcholine receptors as studied in AChBP crystal structures. *Neuron* **41,** 907–914 (2004).
14. Lee, W. Y. & Sine, S. M. Principal pathway coupling agonist binding to channel gating in nicotinic receptors. *Nature* **438,** 243–247 (2005).
15. Sala, F., Mulet, J., Sala, S., Gerber, S. & Criado, M. Charged amino acids of the N-terminal domain are involved in coupling binding and gating in alpha7 nicotinic receptors. *J. Biol. Chem.* **280,** 6642–6647 (2005).
16. Schofield, C. M., Jenkins, A. & Harrison, N. L. A highly conserved aspartic acid residue in the signature disulfide loop of the alpha 1 subunit is a determinant of gating in the glycine receptor. *J. Biol. Chem.* **278,** 34079–34083 (2003).
17. Jha, A., Cadugan, D. J., Purohit, P. & Auerbach, A. Acetylcholine receptor gating at extracellular transmembrane domain interface: The cys-loop and M2–M3 linker. *J. Gen. Physiol.* **130,** 547–558 (2007).
18. Dani, J. A. Open channel structure and ion binding sites of the nicotinic acetylcholine receptor channel. *J. Neurosci.* **9,** 884–892 (1989).
19. Dani, J. A. & Eisenman, G. Monovalent and divalent cation permeation in acetylcholine receptor channels. Ion transport related to structure. *J. Gen. Physiol.* **89,** 959–983 (1987).
20. Galzi, J. L. *et al.* Mutations in the channel domain of a neuronal nicotinic receptor convert ion selectivity from cationic to anionic. *Nature* **359,** 500–505 (1992).
21. Corringer, P. J. *et al.* Mutational analysis of the charge selectivity filter of the alpha$_7$ nicotinic acetylcholine receptor. *Neuron* **22,** 831–843 (1999).
22. Gunthorpe, M. J. & Lummis, S. C. Conversion of the ion selectivity of the 5-HT(3a) receptor from cationic to anionic reveals a conserved feature of the ligand-gated ion channel superfamily. *J. Biol. Chem.* **276,** 10977–10983 (2001).
23. Pascual, J. M. & Karlin, A. State-dependent accessibility and electrostatic potential in the channel of the acetylcholine receptor. Inferences from rates of reaction of thiosulfonates with substituted cysteines in the M2 segment of the alpha subunit. *J. Gen. Physiol.* **111,** 717–739 (1998).
24. Wilson, G. G., Pascual, J. M., Brooijmans, N., Murray, D. & Karlin, A. The intrinsic electrostatic potential and the intermediate ring of charge in the acetylcholine receptor channel. *J. Gen. Physiol.* **115,** 93–106 (2000).
25. Unwin, N. Acetylcholine receptor channel imaged in the open state. *Nature* **373,** 37–43 (1995).
26. Paas, Y. *et al.* Pore conformations and gating mechanism of a Cys-loop receptor. *Proc. Natl Acad. Sci. USA* **102,** 15877–15882 (2005).
27. Cymes, G. D., Ni, Y. & Grosman, C. Probing ion-channel pores one proton at a time. *Nature* **438,** 975–980 (2005).
28. Cymes, G. D. & Grosman, C. Pore-opening mechanism of the nicotinic acetylcholine receptor evinced by proton transfer. *Nature Struct. Mol. Biol.* **15,** 389–396 (2008).

Supplementary Information is linked to the online version of the paper at www.nature.com/nature.

Acknowledgements We thank B. Blattmann and C. Stutz-Duocommun for assistance with crystal screening, C. Schulze-Briese and the staff of the X06SA beamline for support during data collection, the protein analysis group at the functional genomics centre of the University of Zurich for help with mass spectrometry, R. MacKinnon for comments on the manuscript and members of the Dutzler laboratory for help in all stages of the project. Data collection was performed at the Swiss Light Source of the Paul Scherrer Institute. The research leading to these results was supported by a grant from the National Center for Competence in Research (NCCR) in Structural Biology and by an EC FP7 grant for the EDICT consortium (HEALTH-201924). R.J.C.H. is affiliated with the Molecular Life Sciences Ph.D. programme of the University/ETH Zurich.

Author Contributions R.D. and R.J.C.H. designed the project. R.J.C.H. carried out all experiments. R.D. assisted in data collection and structure determination. R.D. and R.J.C.H. jointly wrote the manuscript.

Author Information Coordinates of GLIC have been deposited in the Protein Data Bank under accession number 3EHZ (WT), and 3EI0 (E221A). Reprints and permissions information is available at www.nature.com/reprints.
Correspondence and requests for materials should be addressed to R.D. (dutzler@bioc.uzh.ch).

2.3.1. Supplementary Material

To confirm the proton-dependent activation of GLIC, the protein was expressed in *Xenopus laevis* oocytes and currents were recorded by the two-electrode voltage-clamp technique. Figure

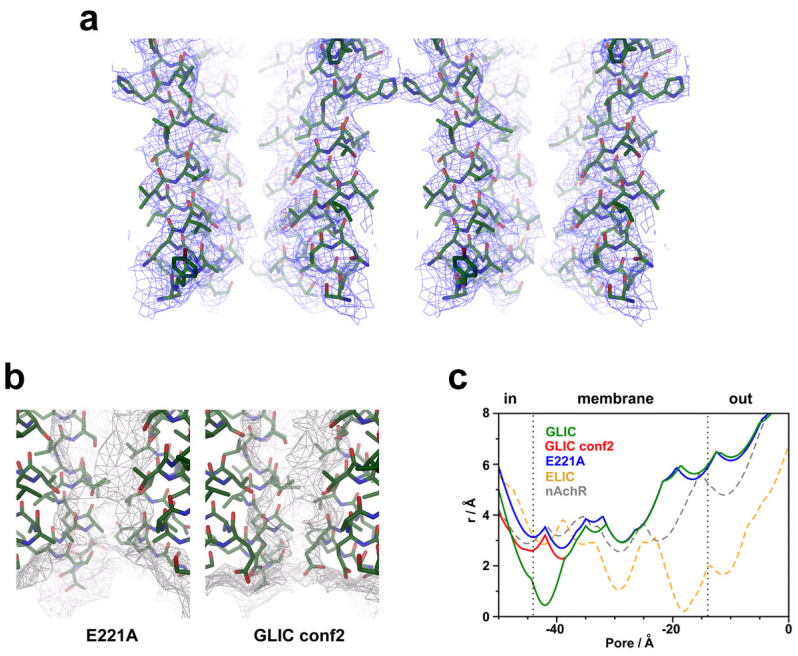

Figure 2.22.: **E221A structure.** **a** $2F_o$-F_c electron density at 3.6 Å(contoured at 1 σ) is shown superimposed on the pore helices of the refined E221A mutant. **b** Intracellular pore entry of mutant E221A (left) and the WT structure with a changed conformation of the Glu-221 side chain (GLIC conf2, right). The molecular surface is shown as white mesh. **c** Pore radii of GLIC (green), the mutant E221A (blue) and GLIC conf2 (red). Pore radii of ELIC (orange) and nAChR (grey) are shown as dashed lines for comparison. Figure **S8**

Figure 2.23.: **Electrophysiology.** **a** pH-activation of GLIC. Two-electrode voltage-clamp recordings of *Xenopus* oocytes expressing GLIC in comparison to water-injected oocytes. Currents were recorded at 40 mV. The pH of the solution is indicated. **b** Block of currents mediated by GLIC in response to the addition of 5 mM TBA. Currents were recorded at -20 mV. **c** GLIC mediated macroscopic currents recorded by the inside-out patch-clamp technique at 60 mV. The pH of the intracellular solution is indicated, the pipette solution was at pH 4.0. **d** Reversal potential of currents mediated by the WT protein and by the mutant E221A as measured from whole-cell currents (pH 4.0) at two different salt concentrations of the extracellular solution (high salt: 130 mM NaCl, low salt: 30 mM NaCl). Figure **S1**

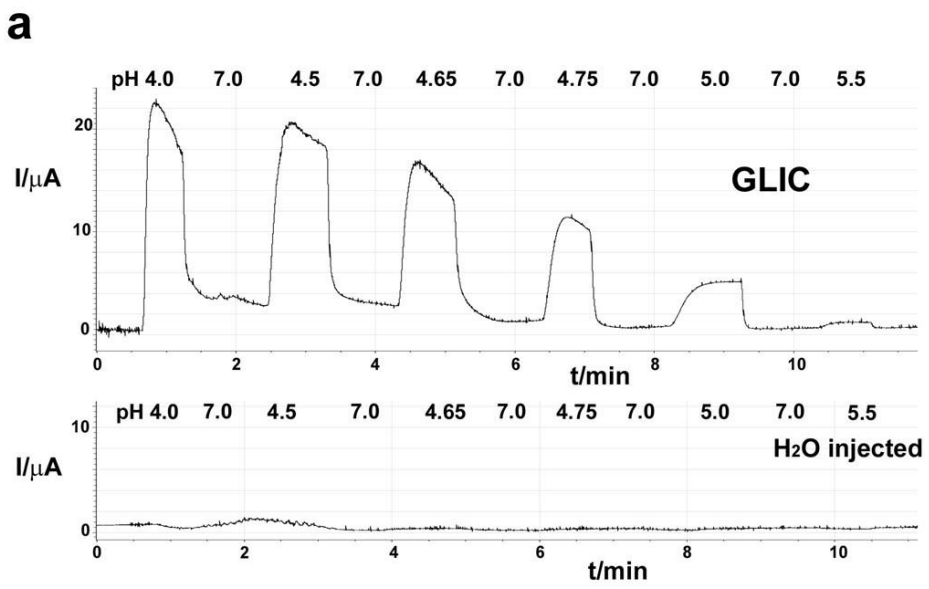
a
pH 4.0 7.0 4.5 7.0 4.65 7.0 4.75 7.0 5.0 7.0 5.5
I/μA
GLIC
t/min
H2O injected

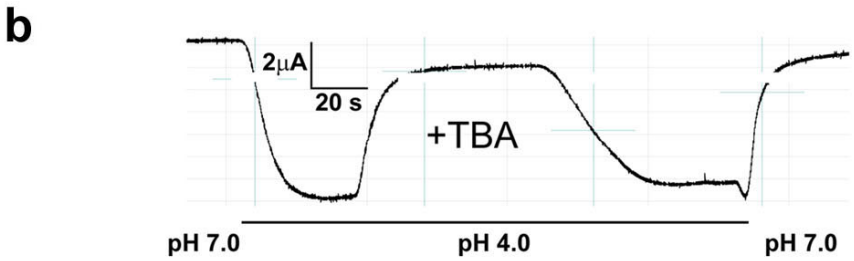
b
2μA
20 s
+TBA
pH 7.0
pH 4.0
pH 7.0

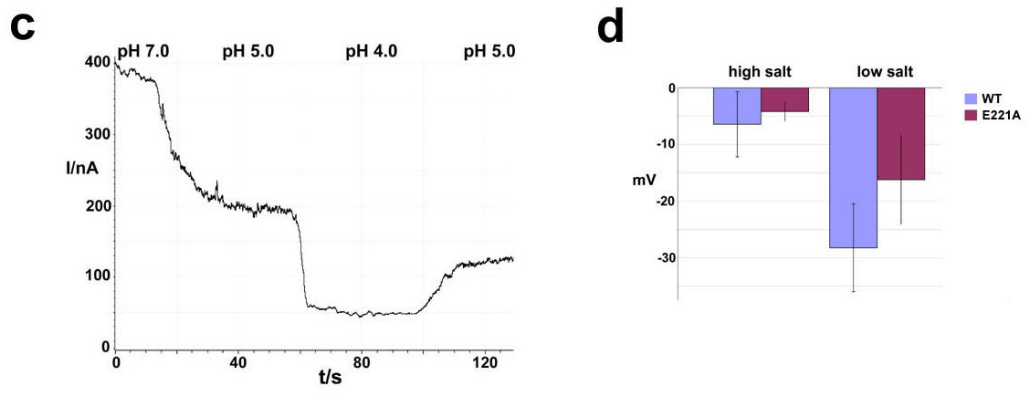
c
pH 7.0
pH 5.0
pH 4.0
pH 5.0
I/nA
t/s
d
high salt
low salt
WT
E221A
mV

2.23 **a** shows a representative trace showing the activation of GLIC. Upon lowering the pH of the outside solution from pH 7 to pH 4 a steep increase in currents can be observed. The currents remain high indicating that the channels do not desensitize. In this way the channel can be repetitively opened and closed. The midpoint of activation lies at around pH 4.8 and a maximum open probability is reached at pH 4.0. The voltage response of water-injected oocytes upon lowering of the pH is comparably small and confirms that the observed currents originate from the GLIC protein. GLIC mediates cation selective currents that can be reversible blocked by tetrabutylammonium (TBA), a typical cation channel blocker (figure 2.23 **b**,**d**).

Part **c** of figure 2.23 shows GLIC mediated macroscopic currents in excised inside-out patches with an extracellular solution of pH 4.0 within the patch pipette activating the channel. A bath solution of pH 7.0 resembles the cellular environment, with the intracellular side facing the neutral pH of the cytoplasm. A decrease of the intracellular pH to pH 5.0 and subsequently to pH 4.0 reversibly reduces the current. The switch to pH 4.0 reflects a state which is close to the crystallization condition with low pH on both sides of the membrane. The observed decrease in the channel conductance can be caused by two different factors: A decrease of pH could either lead to the protonation of distant residues affecting channel conductance, or specifically protonate single side chains of the intracellular ring of glutamate residues (E221, corresponding to 'intermediate ring of charges'), which could lead to a local change in the side chain conformation. In this case a ring of partially charged interacting residues, similar as observed in the crystal structure of GLIC, could restrict ion flow. To verify that a potential protonation of E221 does not perturb the backbone structure of the pore region, I have determined the crystal structure of the E221A mutant (see figure 2.22). This structure shows the same overall orientation of the backbone as WT. The truncated side chains remove the intracellular constriction thus leading to a minimal pore radius of 3 Å. A similar pore radius is found at the intracellular entry of ELIC and the nAChR or in the WT structure of GLIC if the E221 side chains adopt an alternative conformation facing towards the cytoplasm (figure 2.22 **b** and **c**). A pore radius of about 3 Å would also allow the passage of ions. The structure of GLIC at low pH thus probably overall shows the structure of a conducting state (opposed to the non-conducting state in ELIC, see figure 2.24) with minor changes in the local conformation in the region of E221 that can be attributed to the low pH of the crystallization conditions.

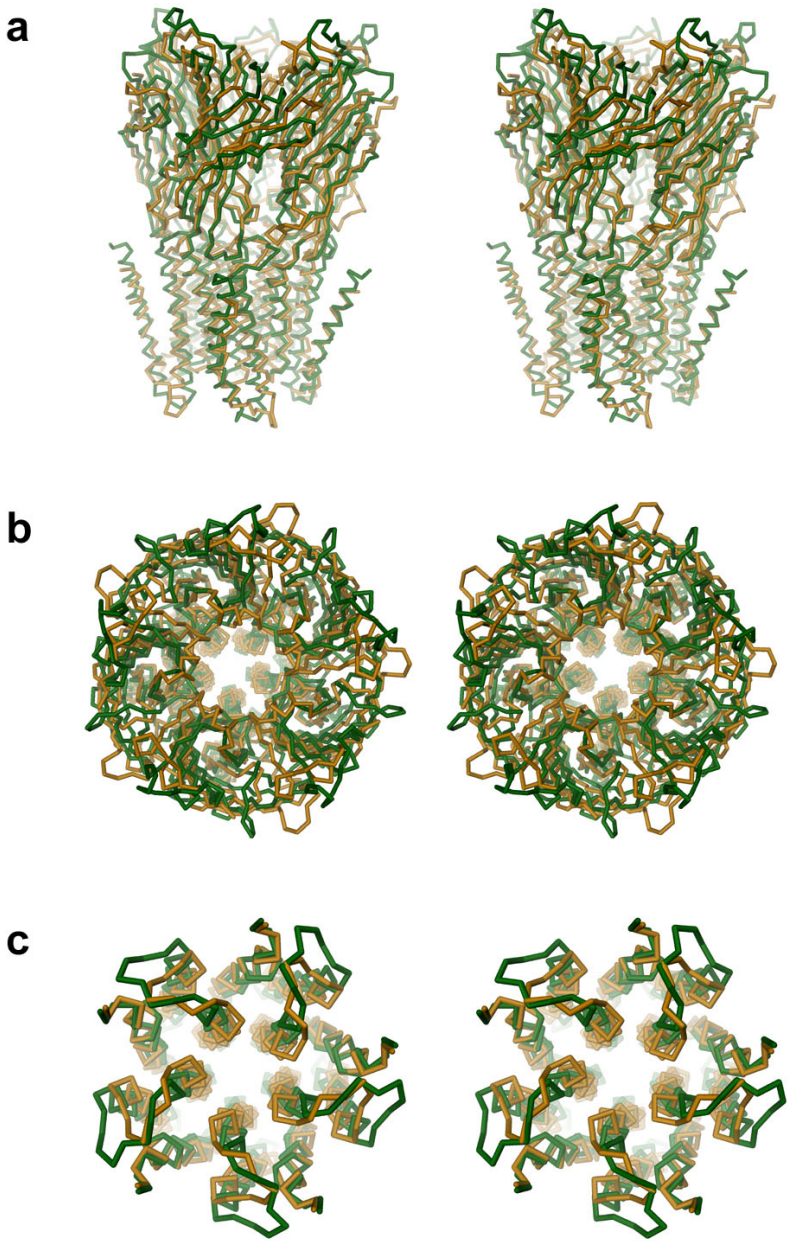

Figure 2.24.: **Superposition of GLIC and ELIC. a** Stereo view of a superposition of the ELIC (green) and GLIC (orange) pentamers. The proteins are shown as Cα traces. The view is from within the membrane. **b** Stereo view of a superposition of the two proteins viewed from the extracellular side. **c** Stereo view of the pore region. The view is as in **b**. The helices α1, α2, α3 and the connecting loops are shown. Figure **S5**

	Cs^+	Tl^+	Zn^{2+}
Space group	C2	C2	C2
Cell dimensions			
a, b, c (Å)	176.0, 133.2, 158.1	179.4, 133.0, 161.1	182.1, 132.5, 161.8
α, β, γ (°)	90.0, 101.1, 90.0	90.0, 102.3, 90.0	90.0, 102.7, 90.0
Resolution (Å)*	40–4.5 (4.6–4.4)	40–4.0 (4.1–4.0)	40–3.5 (3.7–3.5)
R_{sym} or R_{merge}	11.5 (33.0)	12.8 (77.8)	13 (56.7)
$I / \sigma I$	8.19 (3.6)	12.3 (2.6)	15.5 (3.0)
Completeness (%)	98.2 (98.0)	100.0 (99.7)	99.0 (100.0)
Redundancy	3.5 (3.4)	6.9 (7.0)	6.3 (6.0)

* Values in parentheses are for highest-resolution shell.

Table 2.4.: **Data collection statistics for ion soaks.**

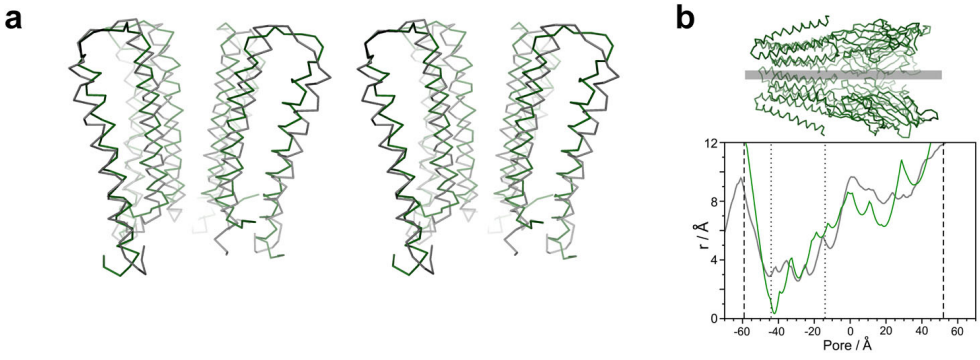

Figure 2.25.: **GLIC and nAChR pore. a** Stereo view of a Cα trace of the α2–α3-helices. The respective regions of the superimposed structures of GLIC (green) and nAChR (grey, PDB-ID 2BG9) are shown. The front subunit is removed for clarity. The view is from within the membrane. **b** Pore radius in GLIC and nAChR. Orientation of GLIC is shown above. Molecular boundaries (- - - - -) and transmembrane region ($\cdot\cdot\cdot\cdot\cdot\cdot$) are indicated. Pore radius of GLIC (green) and nAChR (grey) are shown. Figure **S6**

Figure 2.25 compares the ion pore of GLIC and the nAChR. The α2–α3-helix backbones forming the pore region show similar overall orientations. The differences in the pore diameter are partly due to side chain conformations that are not defined in the 4 Å density of the nAChR. Since the nAChR was proposed to depict a closed state of a receptor while GLIC is in an open state, the relationship between the two structures is still ambiguous.

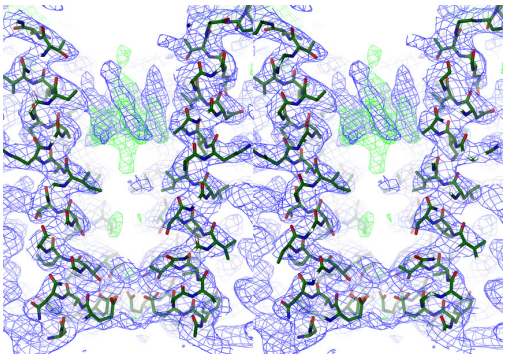

Figure 2.26.: **Stereo view of the pore region.** Residual electron density in the aqueous channel indicates the presence of ordered solvent molecules. The view is from within the membrane. The front subunit is removed for clarity. Residues of helix $\alpha 2$ are shown as sticks. Cyclic averaged electron density is contoured at 1 σ and shown as blue mesh. F_o–F_c difference electron density is contoured at 3.5 σ and shown as green mesh. Figure **S7**

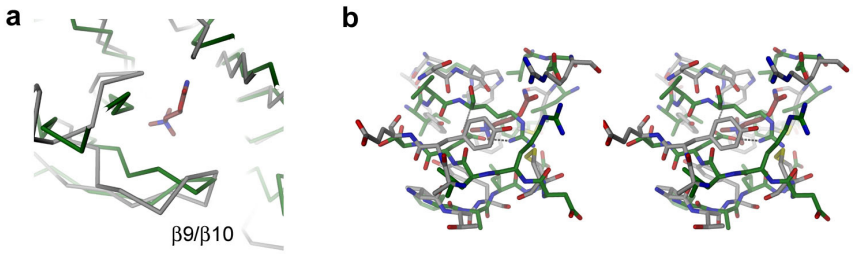

Figure 2.27.: **Ligand-binding region.** **a** Section of the superimposed ligand-binding region of GLIC (green) and AChBP (grey, PDB code 1UV6) shown as Cα traces. Carbamylcholine bound to the AChBP is shown as sticks (C atoms colored brown). The view is from the extracellular side. **b** Stereo view of residues surrounding the bound carbamylcholine. Color-coding and view are as in **a**. Ionic interactions in GLIC are indicated. Figure **S9**

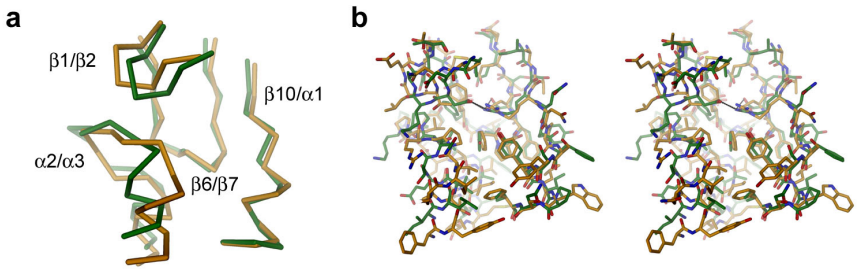

Figure 2.28.: **Interface between extracellular domain and the pore.** **a** Cα representation of the interface between the two domains of the GLIC (green) and ELIC (orange) subunit. The view is from within the membrane. **b** Stereo view of residues in the interface region. The view and color-coding is as in **a**. Interactions between selected residues in GLIC are indicated (- - -). Figure **S10**

CHAPTER 3

DISCUSSION AND OUTLOOK

3.1. A Prokaryotic Perspective on pLGIC Structure

pLGICs have been studied for decades and a wealth of information has accumulated over the years. However, structural information was scarce. The crystal structures of ELIC and GLIC have provided first insight into the family at high resolution. The direct comparison of the two structures provides valuable insights into the overall architecture, the determinants for ion selectivity, and since the two structures of ELIC and GLIC clearly show two different conformations of the channel, into a potential gating mechanism of pLGICs. A review discussing the impact of both structures on the understanding of pLGIC function is included on the following pages[161].

In the same issue of the journal containing a manuscript on the structure of GLIC from our laboratory, a second publication on the GLIC structure by Bocquet and coworkers was published back-to-back with our manuscript[162]. Both proteins were crystallized in similar conditions at low pH. The differences between these two structures are thus overall small with a total root mean square deviation of 2.03 Å for all atoms and a root mean square deviation of 1.45 Å for the Cα positions only.

Available online at www.sciencedirect.com
ScienceDirect
Current Opinion in Structural Biology
ELSEVIER

A prokaryotic perspective on pentameric ligand-gated ion channel structure

Ricarda JC Hilf and Raimund Dutzler

The X-ray structures of two prokaryotic pentameric ligand-gated ion channels have recently provided detailed insight into this important family of neurotransmitter receptors. These prokaryotic homologs share the overall architecture of their eukaryotic counterparts with conservation in functionally important residues. Although both structures are similar they show distinct conformations of the ion conduction pore. One structure depicts a nonconducting state of the channel with a narrow transmembrane pore that is interrupted by conserved hydrophobic residues. The second structure reveals a conducting conformation where the hydrophobic constriction has opened to an aqueous funnel-shaped channel. The two structures thus suggest a novel gating mechanism for the family, where pore opening proceeds by a change of the tilt of the pore-forming helices.

Address
Department of Biochemistry, University of Zurich, Winterthurerstrasse 190, CH-8057 Zürich, Switzerland

Corresponding author: Dutzler, Raimund (dutzler@bioc.uzh.ch)

Current Opinion in Structural Biology 2009, **19**:1–7

This review comes from a themed issue on
Membranes
Edited by Declan Doyle and Graham Shipley

0959-440X/$ – see front matter
Published by Elsevier Ltd.

DOI 10.1016/j.sbi.2009.07.006

The pentameric ligand-gated ion channels (pLGICs) constitute a large family of neurotransmitter receptors that includes cation selective acetylcholine and serotonin receptors and anion selective GABA and glycine receptors [1]. The channels are closed in the absence of ligands and open upon binding of neurotransmitters to a specific site in the extracellular domain that protrudes into the synaptic cleft. Ligand binding induces a conformational change in this part of the protein, which is transmitted to the transmembrane pore and which promotes channel opening [2–5]. In eukaryotic pLGICs this open conformation is only transient and leads to a stable desensitized state upon prolonged exposure to neurotransmitters. Despite the differences in their conduction properties all family members share a conserved architecture [6,7]. The proteins form pentameric complexes of either identical or homologous subunits. Each subunit contains an extracellular ligand-binding domain followed by a transmembrane pore region that is composed of four hydrophobic membrane spanning helices and an intracellular loop that is located between the last two transmembrane helices.

Owing to their large physiological importance different members of the pLGIC family have been subject to investigations over the last decades [6]. Two sources of information have provided insight into their structural organization. Several structures of the acetylcholine binding protein (AChBP), a homopentameric soluble protein that closely resembles the ligand-binding domain, have revealed the organization of the extracellular part and have shed light on the chemical basis of ligand binding [8–10]. The structural organization of the full-length receptor at 4 Å resolution was disclosed from electron microscopy studies of the nicotinic acetylcholine receptor (nAChR) from *Torpedo* electric ray [11,12]. However, despite the large efforts, high-resolution structures of different conformations of the protein that are a prerequisite for a mechanistic comprehension of channel function were for a long time not available.

Although pLGICs were previously believed to be expressed only in multicellular eukaryotic organisms, the abundance of genomic information has allowed the identification of few prokaryotic family members [13•]. The X-ray structures of two channels from the bacteria *Erwinia chrysanthemi* (ELIC) [14••] and *Gloebacter violaceus* (GLIC) [15••,16••] have recently provided first insight into the family at high resolution. The discussion of their structural and functional properties is the focus of this review. Both proteins are selective for cations over anions but do not discriminate between different monovalent cations [17••], similar to the cation selective branch of the family [18,19]. Although their overall structures are similar they show different conformations of the ion conduction pore and thus provide insight into potential mechanisms of pore opening and selective ion conduction.

The structure of prokaryotic pLGICs

Prokaryotic pLGICs share the most important structural features of the family. They consist of an extracellular domain followed by a transmembrane pore but they lack the extended intracellular region of eukaryotic channels that provides interaction sites with scaffolding proteins but is not essential for channel function [20]. The prokaryotic proteins form homo-pentamers and show a

Figure 1

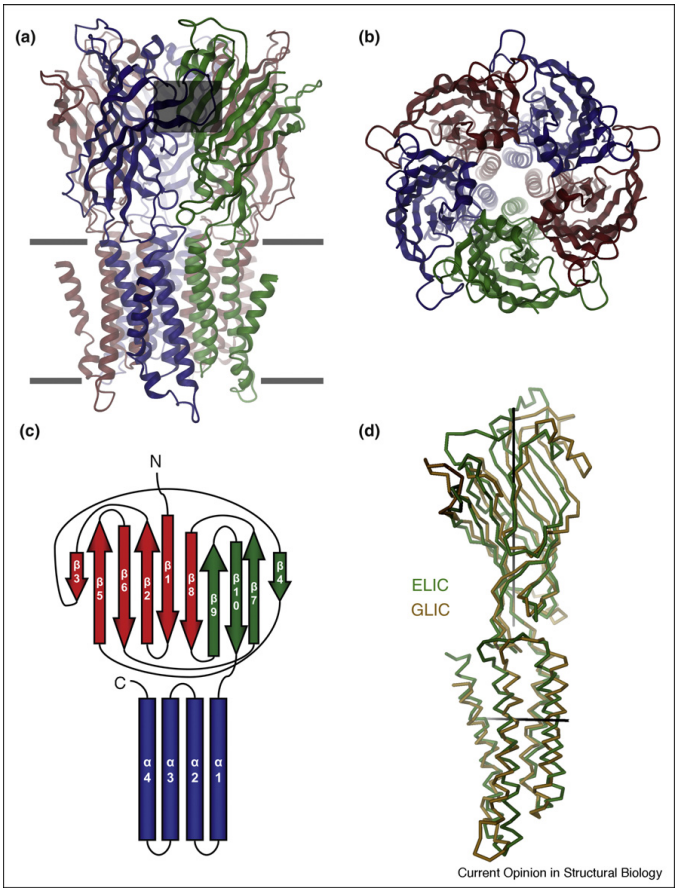

PLGIC structure. **(a)** Ribbon representation of ELIC viewed from within the membrane with the extracellular solution above. The approximate membrane boundaries and the location of the ligand-binding pocket are indicated. **(b)** View of ELIC from the extracellular side along the pore axis. **(c)** Topology of bacterial pLGICs. The secondary structure elements of the extracellular domain forming the 'inner sheet' and 'outer sheet' are colored in red and green, respectively. The four helices of the pore region are colored in blue. **(d)** Superposition of ELIC (orange) and GLIC (green) subunits. The proteins are shown as Cα trace. The superposition is viewed from within the membrane. The rotation axes approximating the movements in the extracellular domain and pore domain are indicated. Figures 1–3 were prepared with DINO (http://www.dino3d.org).

comparably simpler functional behavior [17••]. Yet, the conservation of important sequence elements suggests a close mechanistic relationship between the prokaryotic and eukaryotic branch.

The structure of ELIC has provided first insight into the architecture of pLGICs at high resolution [14••]. The pentameric molecule is composed of structurally identical subunits arranged around a fivefold axis of symmetry that defines the ion conduction path (Figure 1). The subunits are tightly interacting and enclose a wide aqueous vestibule in the extracellular part that narrows to a confined pore in the transmembrane region. Each subunit consists of two separate parts, an extracellular domain that is predominantly composed of β-strands and the transmembrane domain that consists of four consecutive α-helical membrane spanning segments (α1–α4) that are equivalent to the regions M1–M4 of the nAChR (Figure 1c). Overall, the extracellular domain closely resembles the AChBP [8]. It consists of 10 β-strands that are organized as sandwich of two interacting sheets, which were previously termed 'inner

sheet' and 'outer sheet'. The conservation extends to the ligand-binding region that is located at the interface between two adjacent subunits. In the AChBP the quaternary ammonium group of acetylcholine is surrounded by aromatic residues that bind the ligand by so-called cation–π interactions [21–23]. While in ELIC this site is structurally similar and bound cations hint at a positively charged ligand, its chemical identity is still unknown [14••].

The transmembrane domain of ELIC matches the same region of the nAChR [11]. Four helices are arranged in two concentric circles around the ion conduction pore. The inner circle is formed by α-helix 2. This helix exclusively contributes to the pore lining, while the outer circle composed of α-helices 1 and 3 appears to stabilize the pore. α-Helix 4, in contrast, is located at the periphery of the transmembrane domain and is not involved in intersubunit interactions. In the absence of ligands pLGICs adopt a stable nonconducting conformation. Such a conformation is observed in the structure of ELIC, whereas GLIC reveals a conducting state of the pore. GLIC forms cation selective channels that are opened upon an increase of the proton concentration at the extracellular side and that do not inactivate after prolonged exposure to the ligand [17••]. Two structures of GLIC were determined independently at low pH, a condition where the open probability of the channel is high, and show a very similar view of this protein [15••,16••]. Although the sequence identity to ELIC is only about 20% both proteins are similar in length and in their overall structure. Conformational differences between the two channels thus provide direct insight into structural transitions that can be approximated by independent movements in the extracellular domain and the pore region (Figure 1d).

The pore region

The conformational differences between ELIC and GLIC are most pronounced in the transmembrane domain that defines the ion conduction pore (Figure 2). The physicochemical character of the pore is conserved within the cation selective branch of the family. It is lined by the side chains of residues that, because of the pentameric symmetry of the channel, form rings with distinct properties (Figure 2b). On the intracellular entry a ring of glutamate residues (that was previously named the 'intermediate ring of charge') places negatively charged groups at the boundary between the cytoplasm and the narrow channel. In the acetylcholine receptor these residues play a dominating role for ion selectivity and conductance [24–26]. The following two layers of polar residues provide a hydrophilic character to the intracellular half of the pore. On the extracellular part, in contrast, three rings of apolar residues render this region predominantly hydrophobic. Two of the hydrophobic rings carry bulky side chains and have been found in ELIC to interrupt the water-filled channel. Similar to the previous prediction for the nAChR these residues thus probably serve as gates that prevent ion conduction in the closed conformation of the protein [11,27]. With respect to ELIC, in GLIC part of the transmembrane domain encompassing α-helices 2 and 3 have tilted much like a rigid-unit by about 12° around an axis that is located half-way across the membrane and runs parallel to its plane [15••] (Figure 2a). α1, in contrast, which connects the extracellular domain to the transmembrane part, remains comparatively rigid. The movement of the α2–α3 helix pair changes the shape of the ion permeation path. Whereas in ELIC this path is constricted on its extracellular part, it is funnel-shaped in GLIC where the hydrophobic outside has opened to a large water-filled cavity whose diameter decreases toward the hydrophilic intracellular entry (Figure 2b). The difference in the two channel conformations is emphasized in their ability to bind ions to specific sites in the pore. Whereas in the closed structure of ELIC no ions were located in this region, a crystal derivatized with Xenon showed binding of this noble gas to the extracellular hydrophobic part of the channel [14••]. The localization of Xenon atoms is interesting in light of its role as an anesthetic that blocks the closed conformation of the acetylcholine receptor [28]. In the open channel conformation of GLIC, in contrast, different monovalent and divalent ions were localized in the narrow intracellular part of the channel in direct contact to the side chains of polar protein residues that may act akin to a selectivity filter found in other selective ion channel proteins [15••] (Figure 2b). The comparison of the bacterial channels with the EM structure of the nAChR reveals interesting features. Although the nAChR structure was attributed to represent a closed state of the channel, since it was obtained in the absence of ligands, it shows a continuous aqueous pore with an overall conformation of the α2–α3 helices that resembles the respective orientation in GLIC. Its exact relationship with the two prokaryotic structures at higher resolution is thus still unclear. Overall the GLIC structure is in striking correspondence with the predicted shape of the open state of the nAChR as revealed from electrophysiological studies [29,30] while the ELIC structure differs from models of its closed state that have put the pore constriction at the intracellular entry [30,31], whereas ELIC is constricted on its extracellular side.

The extracellular domain

A second large conformational rearrangement that distinguishes the structures of ELIC from GLIC is found in the extracellular domain (Figure 3) [16••]. This rearrangement can be approximated by a 12° rotation around an axis that runs between both sheets with an about 60° inclination with respect to the membrane plane (Figure 3a). The movement does, however, not extend to the loop regions at the domain boundary that either remain comparably rigid or undergo changes that diverge

Figure 2

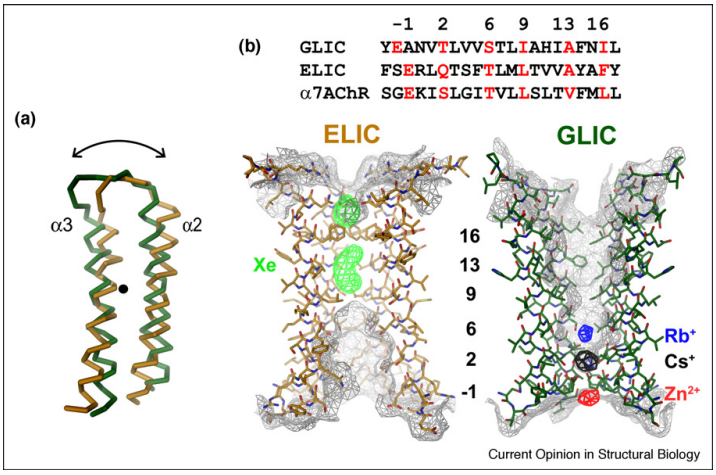

Pore region. **(a)** Conformation of the α2–α3 helix pair of a single subunit. The respective region of the superimposed structures of GLIC (green) and ELIC (orange) is shown as Cα trace. The rotation axis is indicated. **(b)** View of the α2 helices defining the pore regions in ELIC (left) and GLIC (right). The front subunit has been removed for clarity. The molecular surface is shown as white mesh. Electron density of Xe atoms bound to the pore of ELIC is shown as green mesh. Electron density of ions bound to the pore of GLIC is shown in blue (Rb^+) black (Cs^+), and red (Zn^{2+}). A sequence alignment of α2 highlights the conservation in the pore region. The numbering was previously established for the pore of the nAChR and is shown above.

from the described rotational motion. In its overall conformation the extracellular domain of ELIC closely resembles the structure of the AChBP while GLIC significantly differs. It is also remarkable that the diversity seen in ELIC and GLIC resembles the distinct conformations observed in the structure of the nAChR [32]. While ELIC is closer to the α-subunits of the nAChR, GLIC is closer to the three remaining subunits. This resemblance hints at similar conformational transitions upon channel activation, but the detailed relationship is currently unclear, particularly since it was hypothesized that the GLIC-like α-conformation might change into the ELIC-like conformation upon ligand-induced channel activation [12], while in the bacterial proteins GLIC represents the activated state.

In line with the differences in the activating ligand, the conservation in the extracellular domain does not extend toward the ligand-binding pocket. Unlike in ELIC where the β9–β10 loop covering the empty ligand-binding site is mobile, in GLIC this region is filled with predominantly charged protein sidechains that are involved in a tight network of interactions [15••]. It is currently still unknown whether the pH sensor that controls pore opening is found among these residues.

The interface

The independent movements in both domains are coupled at the domain–domain interface [33,34]. This highly conserved region includes besides the covalent connection between β10 and α1 contacts between the β1–β2 turn and the β5–β6 loop of the extracellular domain with the α2–α3 loop of the pore. In GLIC the side chains of negatively charged residues in β1–β2 turn and the β6–β7 loop (the cys-loop) form salt bridges with a conserved Arg residue at the end of β10 [15••] (Figure 3c). Since neither the end of β10 nor the cys-loop shows pronounced differences between ELIC and GLIC, this interaction might stabilize the local structure in both conformations of the channel. The adjacent β1–β2 turn, in contrast, differs in both structures. This turn makes the main contacts to the pore by interactions with the α2–α3 loop. While in GLIC the position of the loop is stabilized by a salt bridge, in ELIC this interaction is not formed and the loop has changed its position. The conformational changes in the β1–β2 turn are accompanied by comparably larger movements in the pore domain, as if the release of a critical interaction would have allowed the relaxation of a strained conformation in the pore. These movements cause a change in the interdomain interactions. While in GLIC the tip of the β1–β2 turn packs against a conserved Pro residue in the α2–α3 linker, both residues have moved apart in ELIC (Figure 3d). A similar interaction pattern, termed the 'principle pathway of coupling', has previously been identified in the acetylcholine receptor to be a key element for channel activation [35].

Figure 3

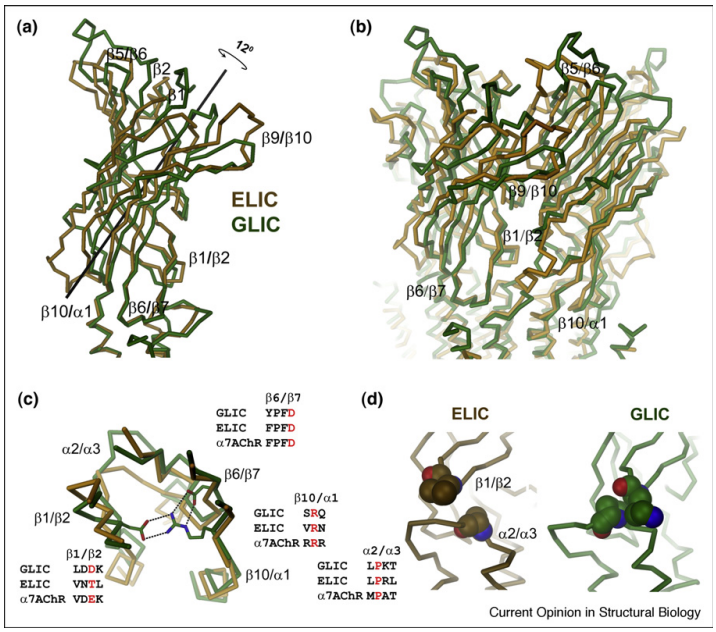

Extracellular domain. **(a)** Cα representation of single domains of the superimposed structures of GLIC (green) and ELIC (orange). The rotation axis describing the relationship between the two domains is shown. **(b)** Structure of the superimposed pentamers. Selected regions are labeled. **(c)** Cα representation of the interface region between the extracellular domain and the pore. Color scheme is as in a, the view is from the extracellular side. Conserved residues in GLIC are displayed as sticks, ionic interactions are indicated as dashed lines. A sequence alignment of selected regions emphasizes the conservation within the pLGIC family. **(d)** Section of the interface region viewed from within the membrane of ELIC (left, orange) and GLIC (right, green). Selected residues at the tip of the β1–β2 turn and the α2–α3 linker are shown as space-filling models.

Discussion

The high-resolution structures of two prokaryotic pLGICs have provided a first detailed view of this family of ion channels in different conformations. The similarity between the two proteins and the conservation of important sequence elements between prokaryotic and eukaryotic channels suggest that the two structures are representative for conducting and nonconducting states. Under this assumption channel opening could follow a hypothetical sequence of events (Figure 4). In the closed conformation, as represented by the structure of ELIC, the aqueous ion translocation path is occluded by bulky hydrophobic residues. Pore opening is initiated by ligand binding to a specific site located in the extracellular domain at the interface between two neighboring subunits. The binding of the ligand provides the energy to change the conformation of the extracellular domain, which in turn triggers a local change in the β1–β2 turn that makes the main contacts to the moving elements of the pore domain via interactions to the α2–α3 loop. In the closed conformation these interactions are weak, while they are tightening upon pore opening by contact formation with a conserved Pro residue. The conformational change of the β1–β2 turn is probably stabilized by a salt bridge between conserved residues on the turn and at the end of the last β-strand of the extracellular domain. The formation of novel interactions promotes channel opening that proceeds by a tilt of the α2–α3 helix pair that moves like a rigid-unit to open the extracellular hydrophobic part of the transmembrane pore to a water-filled funnel-shaped pore and that brings polar and charged residues at the intracellular entry into proximity to coordinate the partly desolvated cations.

This potential pore opening mechanism differs from the current view of gating in pLGICs that was based on electron microscopy data of the nAChR at low resolution [11,36], but it is in accordance with functional data [37–39]. We now need to determine structures of different states of the pore in the same protein to follow the trajectory of the individual atoms and to see whether the two known structures are indeed representative for main channel conformations. It will also have to be shown how far the properties of prokaryotic pLGICs can be extended to

Figure 4

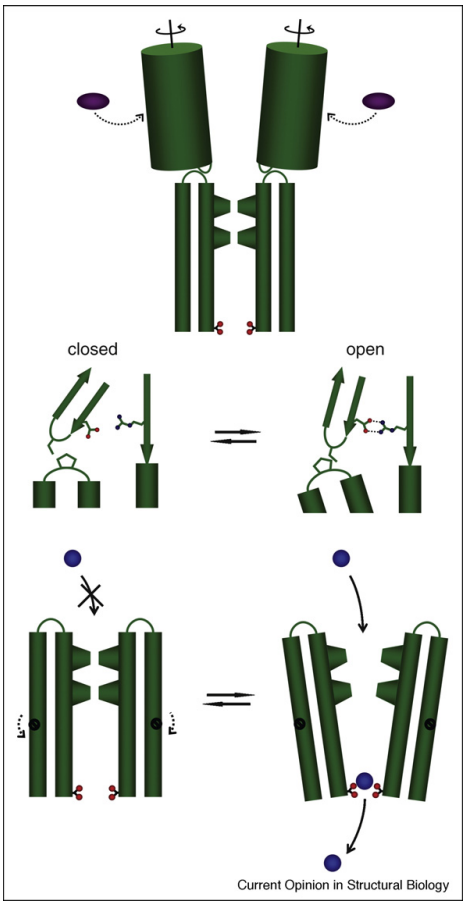

Potential mechanism of gating. **(Top)** Schematic representation of two subunits of the channel. The extracellular domains are represented as cylinders. The conformational transitions upon ligand binding are indicated. **(Center)** Model of the interface region in a single subunit in the closed (left) and open state (right). Selected residues and their interactions are shown. **(Bottom)** Model of the pore region. The α2–α3 helices of two subunits in the closed (left) and open states (right) are shown. Conserved glutamate residues at the intracellular entry are indicated, the ions are drawn as blue spheres.

eukaryotic family members that exhibit a more complex functional behavior. The conservation of critical elements suggests that key mechanisms might be essentially conserved. Since the prokaryotic proteins, like some of their eukaryotic counterparts, are homo-pentamers that obey strict fivefold symmetry, it will also be necessary to explore the relationship with hetero-pentameric pLGICs like the muscle-type nAChR whose structure indicates a break in the symmetry of its subunits [12]. Although the pLGICs have been in the center of attention for the last decades the field is with respect to a structural understanding of channel function still at an early stage.

Acknowledgements

This work was supported by the Swiss National Science Foundation (SNSF) and the National Center for Competence in Research (NCCR) Structural Biology.

References and recommended reading

Papers of particular interest, published within the period of review, have been highlighted as:

- • of special interest
- •• of outstanding interest

1. Hille B: *Ion Channels of Excitable Membranes*. edn 3. Sunderland, MA: Sinauer Associates Inc.; 2001.

2. Changeux J, Edelstein SJ: **Allosteric mechanisms in normal and pathological nicotinic acetylcholine receptors**. *Curr Opin Neurobiol* 2001, **11**:369-377.

3. Purohit P, Mitra A, Auerbach A: **A stepwise mechanism for acetylcholine receptor channel gating**. *Nature* 2007, **446**:930-933.

4. Lape R, Colquhoun D, Sivilotti LG: **On the nature of partial agonism in the nicotinic receptor superfamily**. *Nature* 2008, **454**:722-727.

5. Mukhtasimova N, Lee WY, Wang HL, Sine SM: **Detection and trapping of intermediate states priming nicotinic receptor channel opening**. *Nature* 2009.

6. Sine SM, Engel AG: **Recent advances in Cys-loop receptor structure and function**. *Nature* 2006, **440**:448-455.

7. Zouridakis M, Zisimopoulou P, Poulas K, Tzartos SJ: **Recent advances in understanding the structure of nicotinic acetylcholine receptors**. *IUBMB Life* 2009, **61**:407-423.

8. Brejc K, van Dijk WJ, Klaassen RV, Schuurmans M, van Der Oost J, Smit AB, Sixma TK: **Crystal structure of an ACh-binding protein reveals the ligand-binding domain of nicotinic receptors**. *Nature* 2001, **411**:269-276.

9. Celie PH, Klaassen RV, van Rossum-Fikkert SE, van Elk R, van Nierop P, Smit AB, Sixma TK: **Crystal structure of acetylcholine-binding protein from *Bulinus truncatus* reveals the conserved structural scaffold and sites of variation in nicotinic acetylcholine receptors**. *J Biol Chem* 2005, **280**:26457-26466.

10. Hansen SB, Sulzenbacher G, Huxford T, Marchot P, Taylor P, Bourne Y: **Structures of Aplysia AChBP complexes with nicotinic agonists and antagonists reveal distinctive binding interfaces and conformations**. *EMBO J* 2005, **24**:3635-3646.

11. Miyazawa A, Fujiyoshi Y, Unwin N: **Structure and gating mechanism of the acetylcholine receptor pore**. *Nature* 2003, **423**:949-955.

12. Unwin N: **Refined structure of the nicotinic acetylcholine receptor at 4 Å resolution**. *J Mol Biol* 2005, **346**:967-989.

13. • Tasneem A, Iyer LM, Jakobsson E, Aravind L: **Identification of the prokaryotic ligand-gated ion channels and their implications for the mechanisms and origins of animal Cys-loop ion channels**. *Genome Biol* 2005, **6**:R4.
First description of prokaryotic pLGICs. This bioinformatics study contains the first report of prokaryotic pLGICs. The article provides an exhaustive overview of different genes identified in the sequenced genomes of prokaryotic organisms and it discusses their topological organizations and putative functional properties.

14. •• Hilf RJ, Dutzler R: **X-ray structure of a prokaryotic pentameric ligand-gated ion channel**. *Nature* 2008, **452**:375-379.
First structure of a prokaryotic pLGIC. The article describes the structure of the pLGIC from the bacterium *Erwinia chrysanthemi* (ELIC). The ELIC structure provides the first detailed insight into the family at high resolution. The protein shows a closed conformation of the channel.

15. Hilf RJ, Dutzler R: **Structure of a potentially open state of a •• proton-activated pentameric ligand-gated ion channel**. *Nature* 2009, **457**:115-118.
One of two back-to-back publications, which describe the X-ray structure of the pLGIC from the bacterium *Gloebacter violaceous* (GLIC). The GLIC structure shows a conducting conformation of the channel. A comparison with the structure of ELIC reveals the conformational changes, which might lead to channel activation.

16. Bocquet N, Nury H, Baaden M, Le Poupon C, Changeux JP, •• Delarue M, Corringer PJ: **X-ray structure of a pentameric ligand-gated ion channel in an apparently open conformation**. *Nature* 2009, **457**:111-114.
The second publication describing the X-ray structure of GLIC. Both publications show similar structures of conducting conformations and come to similar conclusions.

17. Bocquet N, Prado de Carvalho L, Cartaud J, Neyton J, Le •• Poupon C, Taly A, Grutter T, Changeux JP, Corringer PJ: **A prokaryotic proton-gated ion channel from the nicotinic acetylcholine receptor family**. *Nature* 2007, **445**:116-119.
First functional characterization of a prokaryotic pLGIC. The article presents an electrophysiological study that describes GLIC as cation selective channel with a single channel conductance of 8pS, which is activated by a decrease in pH on the extracellular side.

18. Adams DJ, Dwyer TM, Hille B: **The permeability of endplate channels to monovalent and divalent metal cations**. *J Gen Physiol* 1980, **75**:493-510.

19. Jensen ML, Schousboe A, Ahring PK: **Charge selectivity of the Cys-loop family of ligand-gated ion channels**. *J Neurochem* 2005, **92**:217-225.

20. Jansen M, Bali M, Akabas MH: **Modular design of Cys-loop ligand-gated ion channels: functional 5-HT3 and GABA rho1 receptors lacking the large cytoplasmic M3M4 loop**. *J Gen Physiol* 2008, **131**:137-146.

21. Celie PH, van Rossum-Fikkert SE, van Dijk WJ, Brejc K, Smit AB, Sixma TK: **Nicotine and carbamylcholine binding to nicotinic acetylcholine receptors as studied in AChBP crystal structures**. *Neuron* 2004, **41**:907-914.

22. Gallivan JP, Dougherty DA: **Cation–pi interactions in structural biology**. *Proc Natl Acad Sci U S A* 1999, **96**:9459-9464.

23. Xiu X, Puskar NL, Shanata JA, Lester HA, Dougherty DA: **Nicotine binding to brain receptors requires a strong cation–pi interaction**. *Nature* 2009, **458**:534-537.

24. Imoto K, Busch C, Sakmann B, Mishina M, Konno T, Nakai J, Bujo H, Mori Y, Fukuda K, Numa S: **Rings of negatively charged amino acids determine the acetylcholine receptor channel conductance**. *Nature* 1988, **335**:645-648.

25. Konno T, Busch C, Von Kitzing E, Imoto K, Wang F, Nakai J, Mishina M, Numa S, Sakmann B: **Rings of anionic amino acids as structural determinants of ion selectivity in the acetylcholine receptor channel**. *Proc Biol Sci* 1991, **244**:69-79.

26. Wilson GG, Pascual JM, Brooijmans N, Murray D, Karlin A: **The intrinsic electrostatic potential and the intermediate ring of charge in the acetylcholine receptor channel**. *J Gen Physiol* 2000, **115**:93-106.

27. Beckstein O, Sansom MS: **A hydrophobic gate in an ion channel: the closed state of the nicotinic acetylcholine receptor**. *Phys Biol* 2006, **3**:147-159.

28. Yamakura T, Borghese C, Harris RA: **A transmembrane site determines sensitivity of neuronal nicotinic acetylcholine receptors to general anesthetics**. *J Biol Chem* 2000, **275**:40879-40886.

29. Dani JA: **Open channel structure and ion binding sites of the nicotinic acetylcholine receptor channel**. *J Neurosci* 1989, **9**:884-892.

30. Wilson G, Karlin A: **Acetylcholine receptor channel structure in the resting, open, and desensitized states probed with the substituted-cysteine-accessibility method**. *Proc Natl Acad Sci U S A* 2001, **98**:1241-1248.

31. Wilson GG, Karlin A: **The location of the gate in the acetylcholine receptor channel**. *Neuron* 1998, **20**:1269-1281.

32. Unwin N, Miyazawa A, Li J, Fujiyoshi Y: **Activation of the nicotinic acetylcholine receptor involves a switch in conformation of the alpha subunits**. *J Mol Biol* 2002, **319**:1165-1176.

33. Bouzat C, Bartos M, Corradi J, Sine SM: **The interface between extracellular and transmembrane domains of homomeric Cys-loop receptors governs open-channel lifetime and rate of desensitization**. *J Neurosci* 2008, **28**:7808-7819.

34. Bouzat C, Gumilar F, Spitzmaul G, Wang HL, Rayes D, Hansen SB, Taylor P, Sine SM: **Coupling of agonist binding to channel gating in an ACh-binding protein linked to an ion channel**. *Nature* 2004, **430**:896-900.

35. Lee WY, Sine SM: **Principal pathway coupling agonist binding to channel gating in nicotinic receptors**. *Nature* 2005, **438**:243-247.

36. Unwin N: **Acetylcholine receptor channel imaged in the open state**. *Nature* 1995, **373**:37-43.

37. Cymes GD, Ni Y, Grosman C: **Probing ion-channel pores one proton at a time**. *Nature* 2005, **438**:975-980.

38. Cymes GD, Grosman C: **Pore-opening mechanism of the nicotinic acetylcholine receptor evinced by proton transfer**. *Nat Struct Mol Biol* 2008, **15**:389-396.

39. Paas Y, Gibor G, Grailhe R, Savatier-Duclert N, Dufresne V, Sunesen M, de Carvalho LP, Changeux JP, Attali B: **Pore conformations and gating mechanism of a Cys-loop receptor**. *Proc Natl Acad Sci U S A* 2005, **102**:15877-15882.

3.2. Comparison to Previous Results and Response in Current Research

The review on the previous pages focuses on the direct comparison of ELIC and GLIC and relates some of their features to the AChBP and the nAChR. Although the sequences of both prokaryotic proteins have low homology compared to their eukaryotic counterparts, their overall size and topology corresponds well to the nAChR of *Torpedo*. Several key features of the family, such as the residues at the interface between the two domains of the protein that play an important role in gating and the chemical properties of the pore are conserved within the family. Still, despite the overall agreement there are discrepancies between the structural and functional results that have to be discussed in the context of previous research.

Ligand Binding and Conformational Changes in the LBD

Although the ligands activating ELIC have not yet been identified, its ligand-binding domain resembles the AChBP. Several residues of the putative ligand-binding pocket in ELIC are conserved compared to the same region of the AChBP or the nAChR. In the AChBP the arrangement of aromatic residues constitutes an environment for cation-π interactions. Contrary to the AChBP, the LBP of ELIC also contains two acidic residues, which increases the negative electrostatic character of this region and indicates that the ligand probably contains a positive charge. Bound cations that were identified to bind to the LBP additionally support this hypothesis. It appears thus likely that ELIC is opened by a ligand of the size of a typical neurotransmitter similar to eukaryotic members of the family[43]. Contrary to ELIC, the same region in GLIC does not contain any aromatic residues (see figure 2.27 on page 69). Instead, the region of the pocket is filled by protein side chains which are involved in a tight network of salt-bridges, which poten-

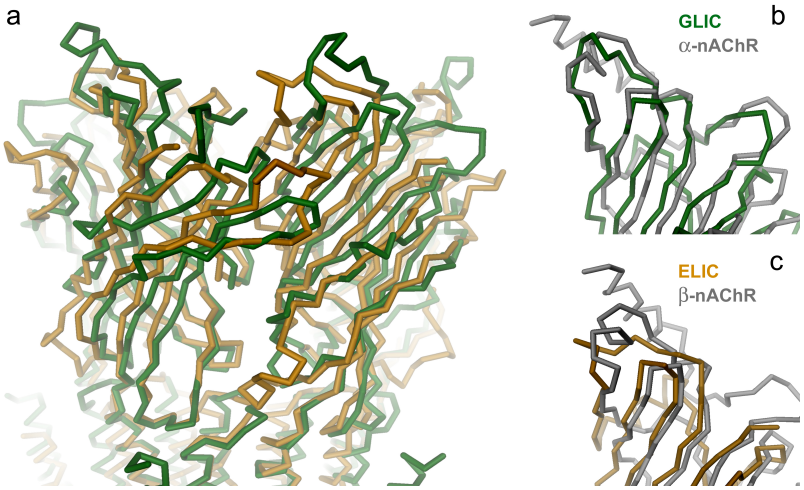

Figure 3.1.: **Comparison of the structure of ELIC, GLIC and the nAChR.** Ribbon representation of the structure of the LBD. **a** Superposition of the LBD of ELIC (orange) and GLIC (green). **b** Superposition of GLIC and the α subunit of the *Torpedo* nAChR (grey). **c** Superposition of ELIC and a non-α subunit of the *Torpedo* nAChR (grey).

tially include the residues responsible for proton binding and channel activation. The gating by a decrease of the pH is a unique feature within the family of pLGICs.

As GLIC was crystallized at low pH, where the open probability is high, the conformation seen in the extracellular domain likely corresponds to the 'ligand-bound' activated state. The difference between ELIC and GLIC thus provides information about possible conformational changes upon activation. The closure of the C-loop, which has already been observed in different crystal structures of AChBPs, is evident in GLIC, whereas in ELIC the loop is flexible and displaced from the protein core. Interestingly, in molecular dynamics simulations followed by a Poisson Boltzmann Monte Carlo calculation, the forced closure of this loop in the *Torpedo* nAChR leads to detectable single-channel conductance with similar selectivity properties as found in electrophysiological measurements[163].

A similar overall conformational change in the LBD as found upon comparison of the ELIC and GLIC structures was found in molecular dynamic simulations of a homology model of the human α7 LBD[164]. Remarkably this change is not observed in the transition from the unoccupied to the ligand-bound AChBP, which stays relatively rigid except for the movements of the C-loop. Still, the AChBP might not undergo these conformational changes since its role is to only bind acetylcholine and not to transmit information to a transmembrane domain. Apart from relations to computational studies it is clearly interesting to compare the two prokaryotic structures with the different subunit conformations observed in the *Torpedo* nAChR. While ELIC superimposes well with the conformations of non-α subunits, the structure of GLIC is closer to the conformation of the two α-subunits (see figure 3.1). Since contrary to the bacterial channels in the nAChR the non-α conformation has been attributed to the open state and the α conformation was supposed to represent the conformation in the closed state, it is still not clear how the different structures relate to each other.

Ion Selectivity

An important feature, which is conserved throughout the family, are the chemical properties of the residues facing the lumen of the ion conduction pore (section 1.5.5 on page 15). The polar and acidic residues in the lower half of the channel have been shown to be important for ion selectivity and conductance (see section 1.5.5)[99–102]. ELIC and GLIC both show the same chemical pattern of residues as their eukaryotic counterparts that also include a hydrophobic extracellular half of the pore. In the structure of GLIC the charged and polar residues were seen to be involved in direct coordination of ions similar to ion selectivity filters observed before in other ion channel families. Moreover, the mutant E221A, that removes conserved ionizable residues at the intracellular pore entry shows a decreased cation selectivity, which underlies the importance of this region in GLIC to select and conduct ions. Besides the pore region also the lumen of the extracellular domain has been shown to be important for prescreening of ions[108]. The residues which have been found to be important for ion selectivity within the extracellular domain have been identified in ELIC (see figure 3.2) and correspond to aspartate 86 (D89 in GLIC) and to glutamate 64 (E72 in GLIC). Both in distance and in geometry they fulfill the proposed requirements to function as selectivity screen in the extracellular lumen.

	Diameter Å	SD
Torpedo		
TM1 (1OED)	20.4	0.77
TM2	19.1	0.56
TM3	18.2	1.43
TM1(2BG9)	19.8	0.74
TM2	18.1	0.75
TM3	18.4	2.02
EC	30.3	1.54
EC (2QC1)	21	-
AChBP D97		
$SO4^{2-}$	19.3	0.18
Epibatidine	20.8	0.20
Conotoxin IMI	21.3	0.14
ELIC (2VL0)		
EC D86*	19.7	0.07
EC E64*	20.2	0.05
TM E229	16.3	0.17

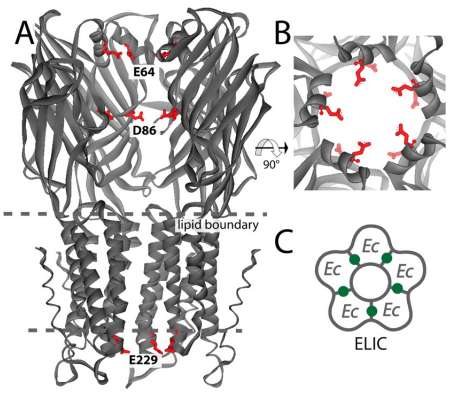

Figure 3.2.: **Ion selectivity in ELIC within the LBD.** Table of distances including SD values of residues important for ion selectivity in the nAChR, the AChBP and ELIC. **a** Ribbon representation of ELIC viewed from within the membrane with the front subunit removed. Residues predicted to be important for ion selectivity are shown in red. **b** Top view looking down the channel. Representation is as in **a**. **c** Scheme of binding sites shown in green within ELIC. Figure taken from Hansen et al.[108].

Pore Shape and Gating

Next to the selection of ions the transmembrane pore also functions as a gate that prevents the passage of ions in non-conducting conformations of the channel. To assess the conformational changes which occur during gating within the pLGICs the shape of the pore in different homologues has been studied by different methods including electrophysiological recordings, SCAM and structural analysis using electron microscopy. The electron microscopy structure of the *Torpedo* nAChR shows a continuously water-filled channel with a minimum diameter of 6 Å in two constricting regions at the center of the membrane and at the intracellular exit, respectively (see section 1.5.4)[13]. It was proposed that the central region is forming a gate by preventing the passage of hydrated ions by a mechanism called hydrophobic gating. While in the structure of the nAChR the gate was attributed to a narrow region in the center of the membrane, a study that investigated the accessibility of sites to MTS reagents has located the gate at the intracellular end of the pore[66,68] (see figure 1.6 on page 12). In contrast to both experimental investigations the structure of ELIC locates the pore constriction on the extracellular side in a region that ranges from the extracellular entrance to about halfway down the channel. This constriction is formed by two rings of bulky hydrophobic residues surrounding a hydrophobic cavity. The intracellular half of the pore is widening to a diameter of about 6 Å. Molecular dynamics simulations of ELIC have found the pore in a stable conformation, which does not permit any passage of ions[165]. Thus the conformation seen in ELIC is distinctly different from any previous results or predictions. The helices in the transmembrane region of ELIC are well packed and continue the five-fold symmetry of the protein. For these reasons it is unlikely that the structure shows the pore after a hydrophobic collapse due to extraction of the protein from the membrane. However, it is possible that the conformation observed in ELIC is more tightly closed than in the resting closed state of the nAChR. The nAChR is known for the fast kinetics of channel activation upon

ligand binding, which is indicative for small conformational changes between the resting closed and the open state. It is currently unknown whether the activation of ELIC would be comparably fast or whether it would follow the slow kinetics of opening observed for GLIC[137]. It was thus suggested that the conformation seen in ELIC might be closer to a desensitized state of the nAChR.

A unique feature in ELIC is a mutation in a conserved negatively charged amino acid in the $\beta1$–$\beta2$-loop of the extracellular domain that is of large functional importance. This residue is part of a group of residues called the 'principal pathway' that mediate the conformational changes upon gating from the extracellular domain to the pore[51](see section 1.5.4 and figure 1.6 on page 12). It is thus still possible that the ligand-induced opening of ELIC might have been lost in the course of evolution. It is remarkable though that selective currents mediated by ELIC could be observed in bilayer experiments, indicating that the ion conduction characteristics are not compromised.

In contrast to the pore shape of ELIC, the funnel-shaped pore of GLIC is in accordance with predictions for the open state based on accessibility measurements and physiological recordings[66,68,69]. It shows a wide opening in the extracellular half of the channel lined by hydrophobic residues. The intracellular half of the channel is formed by polar and charged residues which have been found in GLIC to coordinate ions that have shed most of their hydration shell.

The pore shape of ELIC, GLIC and the *Torpedo* nAChR has been compared extensively by Absalom and colleagues[166] in the light of the recent structures, but also in the context of SCAM data. Before comparing the structures they point out the drawback that the differences in packing of the $\alpha1$- and $\alpha3$-helices to helix $\alpha2$, which is tighter in ELIC and GLIC, might be due to the different methods used to determine the structures. However, the location of the selectivity filter as seen in GLIC is found to be in agreement with functional data and accessibility studies also including the anion selective branch of the family. Nevertheless, the location of the gate remains under debate pointing at positions $3'$ (in the mouse nAChR), $6'$ ($GABA_AR$), $9'$ (GlyR or *Torpedo* nAChR) or at the extracellular entrance to the pore (ELIC).

Using the different structures or models of the pore, two main gating models were predicted for the opening mechanism of the family of pLGIC. Based on the electron microscopy structures of N. Unwin and different computational studies, a rotational gating model was proposed. In this model the $\alpha2$-helices and parts of the extracellular domain rotate independently from the rest of the protein and in that way remove hydrophobic constrictions from the ion pore[71](see section 1.5.3). An alternative model is based on accessibility studies and electrophysiological recordings and denies any rotation of the helices[82]. This model proposes a tilt of the pore forming helices away from the channel axis in the intracellular end of the channel[68,164], which removes the constriction at the intracellular end of the pore.

The two high-resolution crystal structure of the two prokaryotic pLGICs allowed the proposal of an alternative gating model. Assuming that ELIC is representative of a non-conducting closed state and GLIC a representative of the open state, the conformational changes between these two proteins indicate the movements underlying pore opening. This mechanism is described in detail in[160] (see section 2.3 on page 52) and[161] (see section 3.1 on page 71). Common to the mechanisms proposed by Paas, Cymes and coworkers is the absence of a rotation within the $\alpha2$-helices and the involvement of a tilt of these helices to open the ion pore. While Paas and colleagues propose a tilt of the helices, it is in the opposite direction compared to the movement

relating ELIC to GLIC (see figure 1.7 on page 14). For a clarification of the gating mechanism of pLGICs, high-resolution structural data in the open and closed state from a single homologue are required. A way how this could be accomplished is outlined in the last section of this thesis.

3.3. Outlook

After having first structures of pLGIC in hand, a main goal of future investigations will be to determine different conformations for the same proteins (i. e. the structure of ELIC in the open or of GLIC in the closed state).

The stabilization of the open conformation of ELIC requires knowledge of its ligand. To identify this currently unknown agonist different approaches can be taken. Based on the structure of the LBP educated guesses of the chemical nature of potential ligands can be made. A more thorough strategy is using computational docking to screen the theoretical binding of small compounds from a library, preselected on certain criteria (e.g. size)[159]. However, since the ligand has to bind tighter to the unknown open state than to the closed state, this search presents a significant challenge. Promising candidates of a virtual screen can be tested in vitro with different methods. Since the protein is easily purified, it can be reconstituted in liposomes as described in section 4.2.4 on page 88. Subsequent radioactive uptake assays[167] or recordings in planar lipid bilayers offer screening possibilities. However, due to their fragility planar lipid bilayers are not suited for the exchange of solutions needed for ligand screening. Alternative methods for screening include the expression of ELIC in *Xenopus* oocytes or HEK293 cells. This approach seems promising, as both systems have been successfully used to express GLIC. Two-electrode voltage-clamp recordings in oocytes or attached whole-cell patch-clamp measurements offer a rapid way to screen for activating ligands. Since it cannot be excluded that the gating network in the 'principal pathway' is interrupted in ELIC it might be necessary to investigate whether it could be restored by introducing the conserved negative charge by a point mutation.

An alternative route for obtaining structural information of a second state of one of the two homologues would be investigations on the closed conformation of GLIC. The main challenge in this case will be to grow crystals at high pH, a condition where GLIC is closed. While GLIC was found to crystallize in different conditions at high pH (from 6.5–9.5), so far no well diffracting crystal could be obtained. A broader, more thorough screen, maybe including more recently developed methods like the lipidic cubic or lipidic sponge-phase[168], might permit to find a suitable crystallization condition at high pH. An alternative approach in a similar direction would include the selection of antibodies[83] or designed ankyrin-repeat proteins[169] against the closed state of GLIC, to stabilize this structure in crystallization and / or to add possible crystal contacts.

Besides the work on prokaryotic proteins a large challenge for the future will be the structure determination of eukaryotic homologues which are more difficult to express and crystallize but which show a more complex functional behavior.

CHAPTER 4

METHODS

4.1. Molecular Biology

4.1.1. Cloning

To identify prokaryotic homologues of the pLGIC family, the sequence of the human $\alpha 1$ subunit of the nicotinic acetylcholine receptor was used as template in BLAST searches. The database for the search included all available prokaryotic genomes[170]. As alternative method to identify distant prokaryotic homologues, the search was repeated with different bacterial pLGICs as templates. As result the genes encoding for twelve different bacterial pLGICs were identified in the genomes of *Crocosphaera watsonii* (NCBI Reference Sequence: ZP_00518157.1), *Cyanothece sp.* (ZP_01729418.1), *Cytophaga hutchinsonii* (NZ_AABD03000001.1), *Erwinia chrysanthemi* (ASAP ID ABF-0015453), *Francisella tularensis subsp.* (YP_170294.1), *Gloebacter violaceus* (NP_927143.1), *Lyngbya sp.* (ZP_01621-420), *Methanosarcina barkeri* (ZP_00541022.1), *Methanosarcina acetivorans* (NP_616554.1), *Nostoc punctiformis* (ZP_00112462.2), *Rhodopseudomonas palustris* (NP_948199.1) and *Synechococcus sp.* (NP_896686.1).

Bacterial cell pellets or the genomic DNA were obtained from different sources, and the respective genes were amplified and cloned into a modified pET28 expression vector (Novagen) using the restriction enzymes NdeI and EcoRI whenever possible. The modified pET28 vector places the genes under control of the T7 promoter with a C-terminal protease cleavage site (*Herpes simplex* (HRV) 3C (GE Healthcare)) followed by a His_6-Tag. All following constructs used the genes cloned in this vector as starting template. The native signal sequences were identified with the SignalP prediction server[138]. These signals were removed in constructs that included the *E. coli* periplasmic secretion signal sequence pelB (from the vector pET26b, Novagen) and the secreted fusion proteins DsbA and DsbB (from the vectors pET39b and pET40b, Novagen).

The final plasmids used in[156] and[160] were constructed by cloning the genes of the *Erwinia chrysanthemi* pLGIC (ELIC) and *Gloebacter violaceus* pLGIC (GLIC) including a C-terminal stop codon at the end of the gene into a version of the pETM44 vector (EMBL) containing an N-terminal His_{10}-Tag using the NcoI and XhoI cutting sites. The whole cassette was subsequently subcloned into the pET26b vector to add the pelB signal sequence at the N-terminus using the SacI and XhoI restriction sites. The final construct includes from the N-terminus the pelB signal sequence, a His_{10}-Tag, the MBP, the HRV 3C protease cleavage site and the pLGIC with its native stop codon (see figure 4.1).

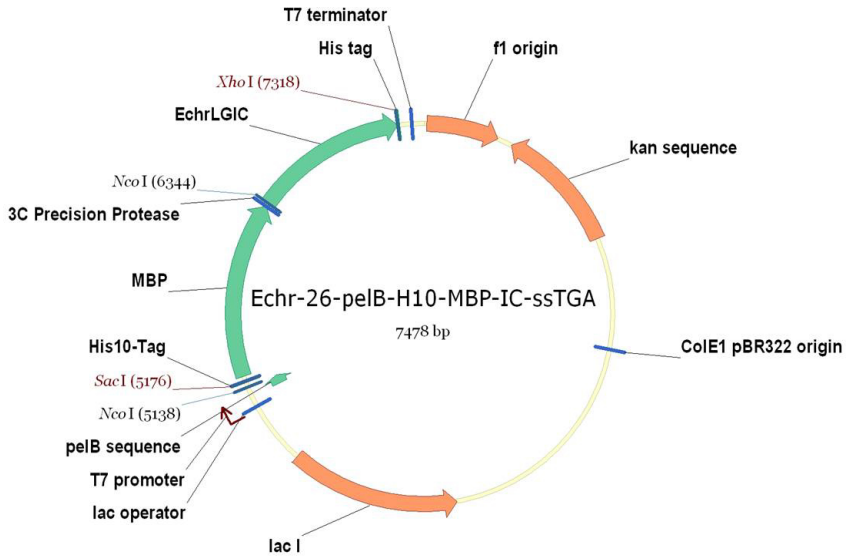

Figure 4.1.: **pLGIC construct in the pET26 vector.** Shown is the construct used for expression of the ELIC-fusion protein. Elements shown in green represent the final expressed protein including the pelB signal sequence, the His_{10}-Tag, the MBP and the pLGIC. Orange elements come from the backbone of the pET26 vector and include the origin, the antibiotic resistance and the lacI for induction. Promoter, terminator and origin of replication are indicated.

4.2. Biochemical Methods

4.2.1. Expression and Membrane Purification

The *Erwinia chrysanthemi* pLGIC (ELIC) and *Gloebacter violaceus* pLGIC (GLIC) were expressed in BL21 (DE3) cells in terrific broth (TB) medium (12 g peptone, 24 g tryptone, 4 ml glycerol, 50 mg kanamycin, 2.31 g KH_2PO_4 and 12.54 g K_2HPO_4 per liter). Cells were grown at 37°C until an OD_{600} of ~1.6 to 1.8, subsequently cooled to 19°C. Protein expression was induced with 0.2 mM IPTG for ~12–13 hours at 19°C. For protein purification ELIC was usually grown in 10 l and GLIC in 20 l batches, resulting in a yield of about 3 mg and 1.5 mg of purified protein, respectively. For reconstitution ELIC and GLIC were expressed in a porin-depleted *E. coli* strain[171].

Cells were harvested at 4.000 rpm (rotor: Sorvall H6000A) for 20 min or at 5.000 rpm (rotor: Sorvall SLC-6000) for 12 min and the cell pellet was resuspended in 50 mM K-Phosphate (pH 8.0), 150 mM NaCl (buffer A) with the addition of 1 mM phenylmethyl sulfonyl fluoride (PMSF), 20 μg/ml DNase I, 1 mg/ml lysozyme, 1 μg/ml pepstatin and 1 μg/ml leupeptin. Cells were lysed with an Emulsiflex high-pressure homogenizer (Avestin) with three to four passages at ~6000 psi and the lysate was cleared by low-spin centrifugation at 10.500 g for 25 min. Membranes were isolated by ultracentrifugation at 45.000 rpm (TI-70 rotor) for 1 h. For storage membranes were homogenized in 10% sucrose (w/v) in 1/10 of the extraction volume and flash-

Selenomethionin medium			
10 × Salt solution		Supplements	
K_2HPO_4	56 g	Vitamin B1	32 mg
KH_2PO_4	16 g	Thymine	32 mg
$(NH_4)SO_4$	8 g	Se-Met	50 mg
Na-citrate	1 g	Amino Acid (each)	40 mg
$MgSO_4 \cdot 7H_2O$	0.8 g	Glucose	5.76 g

Table 4.1.: Composition of the Se-Met medium. Amounts are given for a final volume of 1 l for both solutions. The final medium consists of supplements including 1 × salt solution.

frozen in liquid nitrogen and stored at -80 °C. For generating selenomethionine labeled protein cells were grown in minimal medium containing all amino acids and selenomethionine instead of methionine. The composition of this medium is listed in table 4.1.

4.2.2. Extraction

All steps were carried out at 4°C. Membranes were homogenized in buffer A (10 ml buffer / g of membrane) and extracted by addition of 1.2–1.5 % detergent. For crystallization setups ELIC was extracted with n-Undecyl-β-D-maltoside (UDM, Anatrace, Inc.) and purified in buffers containing 3 mM UDM, whereas GLIC was extracted with n-Dodecyl-β-D-maltoside (DDM, Anatrace, Inc.) and purified with 0.5 mM DDM in all following buffers. If ELIC and GLIC were used for reconstitution, the purification was carried out in 5 mM n-Decyl-β-D-maltoside (DM, Anatrace, Inc.), since its higher CMC (1.8 mM) makes it easier to remove the detergent by dialysis. Extraction was carried out for 1.5–2 h at 4°C and the solution subsequently centrifuged at 14.500 rpm (rotor: Heraeus 3335) for 25 min. The obtained supernatant was supplemented with 15 mM imidazole to reduce unspecific binding to the IMAC column.

4.2.3. Purification

ELIC and GLIC were purified by affinity-chromatography on a Ni-NTA column (Qiagen) with a column volume of ~10 ml. The protein was loaded on the column in a single pass, followed by two washing steps with buffer A containing 15 mM and 55 mM imidazole until OD_{280} reached baseline. The proteins were eluted with 300 mM imidazole in a final volume of ~15 ml. To remove the His_{10}-Tag and the MBP, the eluted fusion protein was digested for 2 h at 4°C by addition of 3C precision protease in a 1:20 w/w ratio of protease to fusion protein. During these 2 h the solution was dialyzed against a buffer containing 10 mM K-Phosphate (pH 8.0), 150 mM NaCl and detergent at a concentration of 1.2×CMC to remove the imidazole. After cutting, the solution was passed over the same Ni-NTA column used for purification to remove the MBP/His_{10}-Tag and the his-tagged 3C protease. The flow-through containing the pLGIC was collected and concentrated using an Amicon Centrifugal Filter Unit (Millipore) with a 30 kDa molecular weight cutoff to a volume of ~ 400 μl. The protein was subjected to gelfiltration on a Superdex S200 column (GE Healthcare) in a buffer containing 10 mM K-Phosphate (pH 8.0), 150 mM NaCl and either 3 mM UDM (for ELIC) or 0.5 mM DDM (for GLIC). The

chromatogram usually showed two peaks, one at the void volume of the column and a second peak corresponding to a pentameric channel (at 11.2 ml). The second peak was pooled and concentrated to 10 mg/ml.

For reconstitution into proteoliposomes the proteins were purified with an additional anion exchange step using a Poros 50 HQ column (Applied Biosystems) prior to gelfiltration. In this case the protein was dialyzed into a low salt (10 mM NaCl) buffer, containing the respective detergent and 50 mM TRIS (pH 8.0) to prevent interactions of the phosphate with the column material which would lead to local changes in pH. The protein was loaded on the anion exchange column (1.8 ml column volume) and eluted with a gradient from 10 mM to 0.6 M NaCl (in 55 ml). ELIC and GLIC start to elute at about 0.3 M NaCl. The peak fractions containing ELIC and GLIC were concentrated and subjected to gelfiltration as described before.

4.2.4. Reconstitution

ELIC and GLIC were reconstituted following the protocol which was previously used for the reconstitution of EcClC[171]. *E. coli* polar lipid extracts (Avanti, dissolved to 25 mg/ml in chloroform) were dried with argon, washed two times with the same volume of pentane and resuspended in reconstitution buffer (450 mM KCl, 25 mM citric acid, 25 mM phosphoric acid, pH 7.0) using a water bath sonifier. The lipids were solubilized with addition of 35 mM CHAPS and stored at room temperature for at least one hour. Afterwards the lipids were cooled to 4°C. All following steps were carried out at 4°C. Protein was added to the lipids in a protein-to-lipid ratio of 5–10 μg/ml with a final lipid concentration of 15 mg/ml. The detergent was removed by at least three dialysis steps each against a 2000fold excess volume over ~ 30–34 h. The liposomes were frozen in liquid nitrogen and stored at -80°C.

4.3. Crystallization and Crystallography

4.3.1. Crystallization

ELIC and GLIC were crystallized in sitting drops at 4°C. Crystals were obtained by mixing protein (10 mg/ml) containing additional 0.5 mg/ml *E. coli* polar lipids (Avanti Polar Lipids, Inc.) in a 1:1 ratio with the respective reservoir solution. The reservoir solution for ELIC is composed of 200 mM $(NH_4)SO_4$, 50 mM ADA (pH 6.5) and 10–15 % PEG 4000 (w/v). The reservoir solution for crystallization of GLIC contains 200–250 mM $(NH_4)SO_4$, 50 mM Na-acetate (pH 4.0) and 9–12 % PEG 4000 (w/v). The GLIC mutant E221A was crystallized in higher $(NH_4)SO_4$ concentration of 500 mM. In all cases crystals appeared within 3–4 days.

4.3.2. Crystal Freezing and Derivatization

For cryo-protection, the crystals of ELIC and GLIC were transferred into mother liquor containing initially 15 % and subsequently 30 % ethylene glycol and flash-frozen in liquid propane. For Xe derivatization, crystals were exposed to a Xe atmosphere at 20 bar for 10 min and flash-frozen as described above. For soaking of Cs^+-, Tl^+- and Rb^+-ions, crystals were incubated in mother liquor where $(NH_4)SO_4$ and NaCl were replaced by the respective sulphate salt for 5 min

to 1 h and flash frozen after addition of 30 % ethylene glycol. Zn^{2+} was soaked into the crystals with a solution containing 100 mM ZnCl instead of 100 mM NaCl and crystals were frozen as described above.

4.3.3. Data collection and structure determination

All datasets of ELIC and GLIC were collected on frozen crystals on the X06SA beamline at the Swiss Light Source of the Paul Scherrer Institute on a PILATUS detector (Dectris). The data were indexed, integrated and scaled with XDS[172] and further processed with CCP4 programs[155].

The structure of ELIC was determined by the SIRAS method using the anomalous and isomorphous contributions of a Se-Met derivative that also served as native dataset and a Xe derivative. Due to their long rod-like shape the ELIC crystals offered the possibility to collect data at several different spots of the crystal. In this way one Se-Met derivatized crystal could be used to collect 1600° of data.

For ELIC the Se sites in the Se-Met derivative were identified with SHELX C and D[145,173] and were used to calculate initial phases for the identification of the Xe sites by difference Fourier techniques. Se and Xe sites were refined in SHARP[174], phases were improved by solvent flattening and extended to 3.3 Å by tenfold NCS symmetry averaging in DM[175]. The model was built in O[176] and initially refined by maintaining strict tenfold NCS constraints in CNS[177]. In later stages, the strict constraints were loosened and restraint individual B-factors were refined. R and R_{free} were monitored throughout. R_{free} was calculated by selecting 5% of the reflection data in thin slices that were omitted in refinement. The final model has R/R_{free} values of 26.3% and 27.4%, good geometry and no outliers in the Ramachandran plot.

Initial phases for the determination of the structure of GLIC were obtained by molecular replacement with PHASER[178] using a partial structure of ELIC as search model. All side chains of the ELIC pentamer were truncated to alanine and helix $\alpha 2$ and the loop regions in the interface between the two domains were removed. Phases were improved and extended to 3.1 Å by fivefold NCS symmetry averaging in DM[175]. The model was built in O[176] and initially refined maintaining strict fivefold NCS constraints in CNS[177] and PHENIX[179]. In later stages, the strict constraints were loosened and restraint individual B-factors were refined. R and R_{free} were monitored throughout. R_{free} was calculated by selecting 5% of the reflection data in thin slices that were omitted in refinement. The final model has R/R_{free} values of 23.8% and 26.6%, good geometry and no outliers in the Ramachandran plot.

The pore radii of ELIC, GLIC and nAChR were calculated with the program HOLE[56]. The molecular surfaces were calculated with MSMS[180].

4.4. Electrophysiology

4.4.1. Recording in the artificial lipid bilayer

Liposomes containing ELIC were fused to bilayers formed from POPE/POPG lipids (Avanti) and recorded in a horizontal planar lipid bilayer system as previously described[181]. Electrodes were connected to the respective bath solutions through salt bridges. Solutions containing Na^+

ions were prepared with 10 mM Na_2HPO_4 as buffer. NaCl was added to reach the desired Na^+ concentration. Solutions containing K^+ ions were prepared in a similar way but with K_2HPO_4 and KCl instead. Cs^+ solutions were prepared by mixing 10 mM Na_2HPO_4 and 400 mM CsCl. For all solutions, pH was adjusted to 7.0 with HCl. Macroscopic currents were recorded with an Axopatch amplifier 200B (Axon Instruments, Inc.). Currents were measured in sweeps in response to applied voltage pulses ranging between +80 mV to -140 mV followed by a pulse to -140 mV. Macroscopic currents were recorded at pH 7.0. The open probability of the channels was not known. The 'cis' side is connected to the measurement electrode, the 'trans' side to the ground electrode. Data were sampled at 50 μs, filtered at 200 Hz and analyzed with Clampfit (Axon Instruments, Inc.). Currents are normalized to the value at 80 mV, averages between five independent measurements and the standard deviations were used as final data.

4.4.2. Recording in Xenopus oocytes

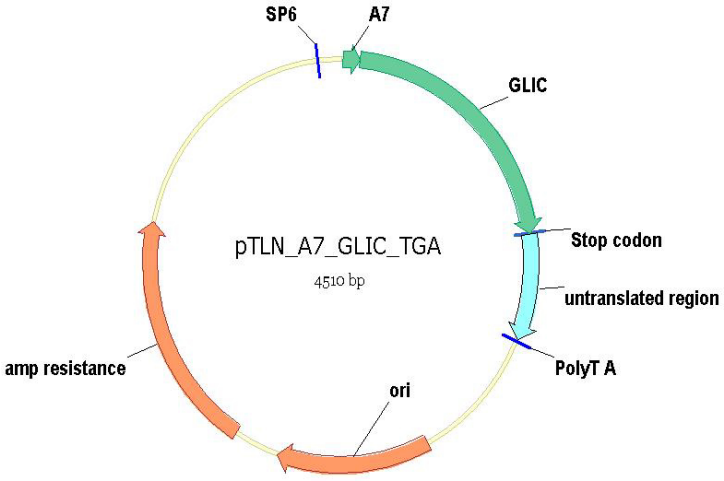

Figure 4.2.: **pLGIC construct in the pTLN vector.** Shown is the construct used for expression of GLIC in *Xenopus* oocytes. Elements shown in green represent the final expressed protein including the α7 signal sequence and GLIC. Orange elements come from the backbone of the pTLN vector and include the origin and the antibiotic resistance. Promoter for the SP6 polymerase, terminator and origin of replication are indicated.

Constructs containing the gene of GLIC and of the mutant E221A preceded by the signal sequence of the human α7-nAChR were cloned into the pTLN vector for expression in *Xenopus laevis* oocytes[182] (see figure 4.2). After linearization of the plasmid DNA by MluI, capped complementary RNA was transcribed with the Message Machine kit (Ambion) using the SP6 RNA polymerase and purified with the RNeasy kit (Qiagen). For expression, 50 nl of 1–50 ng/ μl of RNA was injected into defolliculated oocytes.

Two-electrode voltage-clamp recording

Two-electrode voltage-clamp measurements were performed 2–3 days after injection at 20°C with an OC-725B Oocyte Clamp (Warner Instrument Corp.)). For measuring of wild type currents, injection of 50 nl of 2–3 ng/ μl gave rise to currents below 10 μA, whereas for the E221A mutant 5–7 ng/ μl produced similar currents. Currents were recorded in bath solutions containing 130 mM NaCl, 2 mM KCl, 1.8 mM $CaCl_2$ and 5 mM $MgCl_2$. The respective pH values were stabilized by addition of 10 mM Hepes (pH 7.0) or 10 mM sodium citrate (pH 4.0–5.5). For inhibition studies 5 mM of TBA were added. Low salt solutions contained 30 mM NaCl, 100 mM mannitol, 2 mM KCl, 1.8 mM $CaCl_2$, 1 mM $MgCl_2$ and 10 mM sodium citrate at pH 4.0.

Patch-clamp measurements

Inside-out patch-clamp measurements were recorded with an Axopatch 200B amplifier (Axon Instruments) 3 days after injection of 50 nl of 10–20 ng/ μl RNA. Electrodes had a resistance of 1–3 MΩ. Bath solution contained 150 mM NaCl, 1 mM $CaCl_2$ and 5 mM $MgCl_2$. The respective pH values were stabilized by addition of 10 mM Hepes (pH 7.0) or 10 mM sodium citrate (pH 4.0, pH 5.0). The pipette solutions contained 150 mM NaCl, 1 mM EGTA and 5 mM $MgCl_2$ and 10 mM sodium citrate pH 4.0.

APPENDIX A

ABBREVATIONS

AChBP	acetylcholine binding protein
ELIC	*Erwinia* ligand-gated ion channel
GABA	γ-amino butyric acid
GLIC	*Gloeobacter* ligand-gated ion channel
LBD	ligand-binding domain
LBP	ligand-binding pocket
LFER	linear free energy relationship
MTS	methanethiosulfonates
nAChR	nicotinic acetylcholine receptor
NCS	non-crystallographic symmetry
Ni-NTA	Nickel-nitrilotriaceticacid
pLGIC	pentameric ligand gated ion channel
SCAM	substituted cysteine accessibility method
TM	transmembrane domain
5-HT_3-receptor	5-Hydroxytryptamin-receptor (3^{rd} family), Serotoninreceptor

APPENDIX B

Curriculum vitae

Ricarda J. C. Hilf

Born	6. September 1982
Place of Birth	Heidelberg, Germany
citizenship	german

Education

Oct 2005 – Nov 2009	PhD thesis at the University of Zurich
2005	Diploma thesis at the University of Bayreuth. Title: 'Molecular Details of O_2-Activation in the Non-Heme Iron Enzyme 2-Oxoquinoline 8-Monooxygenase from *Pseudomonas putida* 86'
Oct 2003 – Oct 2005	Study of Biochemistry at the University of Bayreuth
Oct 2001 – Oct 2003	Study of Biochemistry / Molecular Biology at the University of Hamburg
July 2001	Allgemeine Hochschulreife from the Ratsgymnasium Bielefeld

---

Internships

Feb 2004 – Mar 2004	Seven weeks at the EMBL Heidelberg, Germany; 'Radiation Damage on Disulfidebridges during X-Ray Data Collection'
Jul 2002 – Aug 2002	Six weeks at the Max-Planck-Institute for Medical Research in Heidelberg, Germany
Jul 2001 – Sep 2001	Two month at the Department of Biochemistry at the University of Oxford, UK

Conferences and Workshops

August 2009	25th European Crystallographic Meeting, Istanbul, Turkey; Oral presentation: 'Structural Basis for Ion Conduction and Gating in Ligand Gated Ion Channels'
June 2009	Gordon Research Conference: Mechanism of Membrane Transport, Waterville, USA; Oral presentation: 'Ion permeation and gating in prokaryotic pentameric ligand gated ion channels'
June 2009	Three day Workshop on Membrane Protein Production, Crystallisation and Crystallography, Didcot, UK; Oral presentation: 'Case Study: Pentameric Ligand Gated Ion Channels'
January 2009	USGEB meeting: Membranes in Motion, Interlaken, Switzerland; Oral presentation: 'Structural basis for gating in prokaryotic pentameric ligand gated ion channels'
September 2008	Rhine-Knee-Meeting, Freudenstadt, Germany; Oral presentation: 'X-ray structure of a prokaryotic pentameric ligand-gated ion channel'
July 2008	Gordon Research Conference: Ion Channels, Tilton, USA; Poster presentation: 'X-ray structure of a prokaryotic pentameric ligand-gated ion channel'

Publications

1.	Hilf R.J.C. & Dutzler R. A prokaryotic perspective on pentameric ligand-gated ion channel structure. Curr Opin Struct Biol. 2009 Aug;19(4):418-24. Epub 2009 Jul 29.
2.	Hilf R.J.C. & Dutzler R. Structure of a potentially open state of a proton-activated pentameric ligand-gated ion channel. Nature. 2009 Jan 1;457(7225):115-8. Epub 2008 Nov 5.
3.	Hilf R.J.C. & Dutzler R. X-ray structure of a prokaryotic pentameric ligand-gated ion channel. Nature. 2008 Mar 20;452(7185):375-9. Epub 2008 Mar 5.

Awards

2009	Annual award 2009 of the Faculty of Science, University of Zurich
2005	Otto-Warburg Award of the University of Bayreuth, Germany

Zurich, September 2009

BIBLIOGRAPHY

[1] H. Dale, "Chemical transmission of the effects of nerve impulses," *Br Med J*, vol. 1, pp. 835–841, 1934.

[2] H. H. Dale, W. Feldberg, and M. Vogt, "Release of acetylcholine at voluntary motor nerve endings.," *J Physiol*, vol. 86, pp. 353–380, May 1936.

[3] W. Feldberg and A. Fessard, "The cholinergic nature of the nerves to the electric organ of the (*Torpedo marmorata*).," *J Physiol*, vol. 101, pp. 200–216, Aug 1942.

[4] B. Katz and R. Miledi, "Membrane noise produced by acetylcholine.," *Nature*, vol. 226, pp. 962–963, Jun 1970.

[5] E. Neher and B. Sakmann, "Single-channel currents recorded from membrane of denervated frog muscle fibres.," *Nature*, vol. 260, pp. 799–802, Apr 1976.

[6] C. L. Weill, M. G. McNamee, and A. Karlin, "Affinity-labeling of purified acetylcholine receptor from *Torpedo californica*.," *Biochem Biophys Res Commun*, vol. 61, pp. 997–1003, Dec 1974.

[7] M. Noda, H. Takahashi, T. Tanabe, M. Toyosato, Y. Furutani, T. Hirose, M. Asai, S. Inayama, T. Miyata, and S. Numa, "Primary structure of α-subunit precursor of *Torpedo californica* acetylcholine receptor deduced from cDNA sequence.," *Nature*, vol. 299, pp. 793–797, Oct 1982.

[8] M. Noda, H. Takahashi, T. Tanabe, M. Toyosato, S. Kikyotani, Y. Furutani, T. Hirose, H. Takashima, S. Inayama, T. Miyata, and S. Numa, "Structural homology of *Torpedo californica* acetylcholine receptor subunits.," *Nature*, vol. 302, pp. 528–532, Apr 1983.

[9] M. Noda, H. Takahashi, T. Tanabe, M. Toyosato, S. Kikyotani, T. Hirose, M. Asai, H. Takashima, S. Inayama, T. Miyata, and S. Numa, "Primary structures of β- and δ-subunit precursors of *Torpedo californica* acetylcholine receptor deduced from cDNA sequences.," *Nature*, vol. 301, pp. 251–255, Jan 1983.

[10] M. Mishina, T. Kurosaki, T. Tobimatsu, Y. Morimoto, M. Noda, T. Yamamoto, M. Terao, J. Linstrom, T. Takahashi, M. Kuno, and S. Numa, "Expressoin of functional acetylcholine receptor from cloned cDNAs," *Nature*, vol. 307, pp. 604–608, 1984.

[11] J. Kistler, R. M. Stroud, M. W. Klymkowsky, R. A. Lalancette, and R. H. Fairclough, "Structure and function of an acetylcholine receptor.," *Biophys J*, vol. 37, pp. 371–383, Jan 1982.

[12] A. Brisson and P. N. Unwin, "Tubular crystals of acetylcholine receptor.," *J Cell Biol*, vol. 99, pp. 1202–1211, Oct 1984.

[13] N. Unwin, "Refined structure of the nicotinic acetylcholine receptor at 4 Å resolution.," *J Mol Biol*, vol. 346, pp. 967–989, Mar 2005.

[14] M. Mishina, T. Takai, K. Imoto, M. Noda, T. Takahashi, S. Numa, C. Methfessel, and B. Sakmann, "Molecular distinction between fetal and adult forms of muscle acetylcholine receptor.," *Nature*, vol. 321, no. 6068, pp. 406–411, 1986.

[15] R. J. Lukas, J. P. Changeux, N. L. Novère, E. X. Albuquerque, D. J. Balfour, D. K. Berg, D. Bertrand, V. A. Chiappinelli, P. B. Clarke, A. C. Collins, J. A. Dani, S. R. Grady, K. J. Kellar, J. M. Lindstrom, M. J. Marks, M. Quik, P. W. Taylor, and S. Wonnacott, "International Union of Pharmacology. XX. Current status of the nomenclature for nicotinic acetylcholine receptors and their subunits.," *Pharmacol Rev*, vol. 51, pp. 397–401, Jun 1999.

[16] J. L. Eiselé, S. Bertrand, J. L. Galzi, A. Devillers-Thiéry, J. P. Changeux, and D. Bertrand, "Chimaeric nicotinic-serotonergic receptor combines distinct ligand binding and channel specificities.," *Nature*, vol. 366, pp. 479–483, Dec 1993.

[17] K. Imoto, C. Methfessel, B. Sakmann, M. Mishina, Y. Mori, T. Konno, K. Fukuda, M. Kurasaki, H. Bujo, and Y. Fujita, "Location of a δ-subunit region determining ion transport through the acetylcholine receptor channel.," *Nature*, vol. 324, no. 6098, pp. 670–674, 1986.

[18] R. J. Leonard, C. G. Labarca, P. Charnet, N. Davidson, and H. A. Lester, "Evidence that the M2 membrane-spanning region lines the ion channel pore of the nicotinic receptor.," *Science*, vol. 242, pp. 1578–1581, Dec 1988.

[19] M. H. Akabas, D. A. Stauffer, M. Xu, and A. Karlin, "Acetylcholine receptor channel structure probed in cysteine-substitution mutants.," *Science*, vol. 258, pp. 307–310, Oct 1992.

[20] M. Xu and M. H. Akabas, "Amino acids lining the channel of the γ-aminobutyric acid type A receptor identified by cysteine substitution.," *J Biol Chem*, vol. 268, pp. 21505–21508, Oct 1993.

[21] M. H. Akabas, C. Kaufmann, P. Archdeacon, and A. Karlin, "Identification of acetylcholine receptor channel-lining residues in the entire M2 segment of the alpha subunit.," *Neuron*, vol. 13, pp. 919–927, Oct 1994.

[22] M. Xu and M. H. Akabas, "Identification of channel-lining residues in the M2 membrane-spanning segment of the $GABA_a$ receptor α1 subunit.," *J Gen Physiol*, vol. 107, pp. 195–205, Feb 1996.

[23] D. C. Reeves, E. N. Goren, M. H. Akabas, and S. C. Lummis, "Structural and electrostatic properties of the 5-HT3 receptor pore revealed by substituted cysteine accessibility mutagenesis.," *J Biol Chem*, vol. 276, pp. 42035–42042, Nov 2001.

[24] D. Kottwitz, V. Kukhtina, N. Dergousova, T. Alexeev, Y. Utkin, V. Tsetlin, and F. Hucho, "Intracellular domains of the δ-subunits of Torpedo and rat acetylcholine receptors–expression, purification, and characterization.," *Protein Expr Purif*, vol. 38, pp. 237–247, Dec 2004.

[25] L. M. Valor, J. Mulet, F. Sala, S. Sala, J. J. Ballesta, and M. Criado, "Role of the large cytoplasmic loop of the α 7 neuronal nicotinic acetylcholine receptor subunit in receptor expression and function.," *Biochemistry*, vol. 41, pp. 7931–7938, Jun 2002.

[26] X. M. Yu and Z. W. Hall, "A sequence in the main cytoplasmic loop of the α subunit is required for assembly of mouse muscle nicotinic acetylcholine receptor.," *Neuron*, vol. 13, pp. 247–255, Jul 1994.

[27] B. M. Williams, M. K. Temburni, M. S. Levey, S. Bertrand, D. Bertrand, and M. H. Jacob, "The long internal loop of the α3 subunit targets nAChRs to subdomains within individual synapses on neurons in vivo.," *Nat Neurosci*, vol. 1, pp. 557–562, Nov 1998.

[28] M. K. Temburni, R. C. Blitzblau, and M. H. Jacob, "Receptor targeting and heterogeneity at interneuronal nicotinic cholinergic synapses in vivo.," *J Physiol*, vol. 525 Pt 1, pp. 21–29, May 2000.

[29] R. L. Huganir, A. H. Delcour, P. Greengard, and G. P. Hess, "Phosphorylation of the nicotinic acetylcholine receptor regulates its rate of desensitization.," *Nature*, vol. 321, no. 6072, pp. 774–776, 1986.

[30] J. F. Hopfield, D. W. Tank, P. Greengard, and R. L. Huganir, "Functional modulation of the nicotinic acetylcholine receptor by tyrosine phosphorylation.," *Nature*, vol. 336, pp. 677–680, Dec 1988.

[31] M. Jansen, M. Bali, and M. H. Akabas, "Modular design of Cys-loop ligand-gated ion channels: functional 5-HT3 and GABA rho1 receptors lacking the large cytoplasmic M3M4 loop.," *J Gen Physiol*, vol. 131, pp. 137–146, Feb 2008.

[32] P. H. N. Celie, S. E. van Rossum-Fikkert, W. J. van Dijk, K. Brejc, A. B. Smit, and T. K. Sixma, "Nicotine and carbamylcholine binding to nicotinic acetylcholine receptors as studied in AChBP crystal structures.," *Neuron*, vol. 41, pp. 907–914, Mar 2004.

[33] D. L. Beene, G. S. Brandt, W. Zhong, N. M. Zacharias, H. A. Lester, and D. A. Dougherty, "Cation-π interactions in ligand recognition by serotonergic (5-HT3A) and nicotinic acetylcholine receptors: the anomalous binding properties of nicotine.," *Biochemistry*, vol. 41, pp. 10262–10269, Aug 2002.

[34] J. P. Changeux, T. R. Podleski, and L. Wofsy, "Affinity labeling of the acetylcholine-receptor.," *Proc Natl Acad Sci U S A*, vol. 58, pp. 2063–2070, Nov 1967.

[35] C. F. Valenzuela, P. Weign, J. Yguerabide, and D. A. Johnson, "Transverse distance between the membrane and the agonist binding sites on the *Torpedo* acetylcholine receptor: a fluorescence study.," *Biophys J*, vol. 66, pp. 674–682, Mar 1994.

[36] M. Dennis, J. Giraudat, F. Kotzyba-Hibert, M. Goeldner, C. Hirth, J. Y. Chang, C. Lazure, M. Chrétien, and J. P. Changeux, "Amino acids of the Torpedo marmorata acetylcholine receptor α subunit labeled by a photoaffinity ligand for the acetylcholine binding site.," *Biochemistry*, vol. 27, pp. 2346–2357, Apr 1988.

[37] P. N. Kao and A. Karlin, "Acetylcholine receptor binding site contains a disulfide cross-link between adjacent half-cystinyl residues.," *J Biol Chem*, vol. 261, pp. 8085–8088, Jun 1986.

[38] R. E. Middleton and J. B. Cohen, "Mapping of the acetylcholine binding site of the nicotinic acetylcholine receptor: [3H]nicotine as an agonist photoaffinity label.," *Biochemistry*, vol. 30, pp. 6987–6997, Jul 1991.

[39] D. X. Fu and S. M. Sine, "Competitive antagonists bridge the α-γ subunit interface of the acetylcholine receptor through quaternary ammonium-aromatic interactions.," *J Biol Chem*, vol. 269, pp. 26152–26157, Oct 1994.

[40] C. Czajkowski, C. Kaufmann, and A. Karlin, "Negatively charged amino acid residues in the nicotinic receptor δ subunit that contribute to the binding of acetylcholine.," *Proc Natl Acad Sci U S A*, vol. 90, pp. 6285–6289, Jul 1993.

[41] R. J. Prince and S. M. Sine, "Molecular dissection of subunit interfaces in the acetylcholine receptor. Identification of residues that determine agonist selectivity.," *J Biol Chem*, vol. 271, pp. 25770–25777, Oct 1996.

[42] M. W. Nowak, P. C. Kearney, J. R. Sampson, M. E. Saks, C. G. Labarca, S. K. Silverman, W. Zhong, J. Thorson, J. N. Abelson, and N. Davidson, "Nicotinic receptor binding site probed with unnatural amino acid incorporation in intact cells.," *Science*, vol. 268, pp. 439–442, Apr 1995.

[43] D. A. Dougherty, "Cys-loop neuroreceptors: structure to the rescue?," *Chem Rev*, vol. 108, pp. 1642–1653, May 2008.

[44] K. Brejc, W. J. van Dijk, R. V. Klaassen, M. Schuurmans, J. van Der Oost, A. B. Smit, and T. K. Sixma, "Crystal structure of an ACh-binding protein reveals the ligand-binding domain of nicotinic receptors.," *Nature*, vol. 411, pp. 269–276, May 2001.

[45] D. Colquhoun and B. Sakmann, "Fluctuations in the microsecond time range of the current through single acetylcholine receptor ion channels.," *Nature*, vol. 294, pp. 464–466, Dec 1981.

[46] C. Grosman, M. Zhou, and A. Auerbach, "Mapping the conformational wave of acetylcholine receptor channel gating," *Nature*, vol. 403, pp. 773 – 776, 2000.

[47] A. Mitra, G. D. Cymes, and A. Auerbach, "Dynamics of the acetylcholine receptor pore at the gating transition state.," *Proc Natl Acad Sci U S A*, vol. 102, pp. 15069–15074, Oct 2005.

[48] Y. Zhou, J. E. Pearson, and A. Auerbach, "Phi-value analysis of a linear, sequential reaction mechanism: theory and application to ion channel gating.," *Biophys J*, vol. 89, pp. 3680–3685, Dec 2005.

[49] P. Purohit, A. Mitra, and A. Auerbach, "A stepwise mechanism for acetylcholine receptor channel gating.," *Nature*, vol. 446, pp. 930–933, Apr 2007.

[50] A. Auerbach, "How to turn the reaction coordinate into time.," *J Gen Physiol*, vol. 130, pp. 543–546, Dec 2007.

[51] W. Y. Lee and S. M. Sine, "Principal pathway coupling agonist binding to channel gating in nicotinic receptors.," *Nature*, vol. 438, pp. 243–247, Nov 2005.

[52] C. Bouzat, F. Gumilar, G. Spitzmaul, H.-L. Wang, D. Rayes, S. B. Hansen, P. Taylor, and S. M. Sine, "Coupling of agonist binding to channel gating in an ACh-binding protein linked to an ion channel.," *Nature*, vol. 430, pp. 896–900, Aug 2004.

[53] X. Xiu, A. P. Hanek, J. Wang, H. A. Lester, and D. A. Dougherty, "A unified view of the role of electrostatic interactions in modulating the gating of Cys loop receptors.," *J Biol Chem*, vol. 280, pp. 41655–41666, Dec 2005.

[54] T. L. Kash, A. Jenkins, J. C. Kelley, J. R. Trudell, and N. L. Harrison, "Coupling of agonist binding to channel gating in the $GABA_A$ receptor.," *Nature*, vol. 421, pp. 272–275, Jan 2003.

[55] S. C. R. Lummis, D. L. Beene, L. W. Lee, H. A. Lester, R. W. Broadhurst, and D. A. Dougherty, "Cis-trans isomerization at a proline opens the pore of a neurotransmitter-gated ion channel.," *Nature*, vol. 438, pp. 248–252, Nov 2005.

[56] O. S. Smart, J. G. Neduvelil, X. Wang, B. A. Wallace, and M. S. Sansom, "HOLE: a program for the analysis of the pore dimensions of ion channel structural models.," *J Mol Graph*, vol. 14, pp. 354–60, 376, Dec 1996.

[57] W. Humphrey, A. Dalke, and K. Schulten, "VMD: visual molecular dynamics.," *J Mol Graph*, vol. 14, pp. 33–8, 27–8, Feb 1996.

[58] E. A. Merritt and D. J. Bacon, "Raster3D: photorealistic molecular graphics.," *Methods Enzymol*, vol. 277, pp. 505–524, 1997.

[59] O. Beckstein and M. S. P. Sansom, "A hydrophobic gate in an ion channel: the closed state of the nicotinic acetylcholine receptor.," *Phys Biol*, vol. 3, pp. 147–159, Jun 2006.

[60] C. Miller, "Genetic manipulation of ion channels: a new approach to structure and mechanism.," *Neuron*, vol. 2, pp. 1195–1205, Mar 1989.

[61] B. Corry, "Theoretical conformation of the closed and open states of the acetylcholine receptor channel.," *Biochim Biophys Acta*, vol. 1663, pp. 2–5, May 2004.

[62] B. Corry, "An energy-efficient gating mechanism in the acetylcholine receptor channel suggested by molecular and brownian dynamics.," *Biophys J*, vol. 90, pp. 799–810, Feb 2006.

[63] O. Beckstein, P. C. Biggin, and M. S. P. Sansom, "A hydrophobic gating mechanism for nanopores," *J. Phys. Chem. B*, vol. 105, no. 51, pp. 12902–12905, 2001.

[64] B. H. White and J. B. Cohen, "Agonist-induced changes in the structure of the acetylcholine receptor M2 regions revealed by photoincorporation of an uncharged nicotinic noncompetitive antagonist.," *J Biol Chem*, vol. 267, pp. 15770–15783, Aug 1992.

[65] E. Arevalo, D. C. Chiara, S. A. Forman, J. B. Cohen, and K. W. Miller, "Gating-enhanced accessibility of hydrophobic sites within the transmembrane region of the nicotinic acetylcholine receptor's δ-subunit. A time-resolved photolabeling study.," *J Biol Chem*, vol. 280, pp. 13631–13640, Apr 2005.

[66] G. Wilson and A. Karlin, "Acetylcholine receptor channel structure in the resting, open, and desensitized states probed with the substituted-cysteine-accessibility method.," *Proc Natl Acad Sci U S A*, vol. 98, pp. 1241–1248, Jan 2001.

[67] G. G. Wilson and A. Karlin, "The location of the gate in the acetylcholine receptor channel.," *Neuron*, vol. 20, pp. 1269–1281, Jun 1998.

[68] Y. Paas, G. Gibor, R. Grailhe, N. Savatier-Duclert, V. Dufresne, M. Sunesen, L. P. de Carvalho, J.-P. Changeux, and B. Attali, "Pore conformations and gating mechanism of a Cys-loop receptor.," *Proc Natl Acad Sci U S A*, vol. 102, pp. 15877–15882, Nov 2005.

[69] J. A. Dani, "Open channel structure and ion binding sites of the nicotinic acetylcholine receptor channel.," *J Neurosci*, vol. 9, pp. 884–892, Mar 1989.

[70] A. Taly, "Opened by a twist: a gating mechanism for the nicotinic acetylcholine receptor.," *Eur Biophys J*, vol. 36, pp. 911–918, Nov 2007.

[71] A. Miyazawa, Y. Fujiyoshi, and N. Unwin, "Structure and gating mechanism of the acetylcholine receptor pore.," *Nature*, vol. 423, pp. 949–955, Jun 2003.

[72] N. Unwin, "Acetylcholine receptor channel imaged in the open state.," *Nature*, vol. 373, pp. 37–43, Jan 1995.

[73] N. Unwin, "Projection structure of the nicotinic acetylcholine receptor: distinct conformations of the α subunits.," *J Mol Biol*, vol. 257, pp. 586–596, Apr 1996.

[74] N. Unwin, C. Toyoshima, and E. Kubalek, "Arrangement of the acetylcholine receptor subunits in the resting and desensitized states, determined by cryoelectron microscopy of crystallized *Torpedo* postsynaptic membranes.," *J Cell Biol*, vol. 107, pp. 1123–1138, Sep 1988.

[75] N. Unwin, A. Miyazawa, J. Li, and Y. Fujiyoshi, "Activation of the nicotinic acetylcholine receptor involves a switch in conformation of the α subunits.," *J Mol Biol*, vol. 319, pp. 1165–1176, Jun 2002.

[76] C. Labarca, M. W. Nowak, H. Zhang, L. Tang, P. Deshpande, and H. A. Lester, "Channel gating governed symmetrically by conserved leucine residues in the M2 domain of nicotinic receptors.," *Nature*, vol. 376, pp. 514–516, Aug 1995.

[77] A. Taly, M. Delarue, T. Grutter, M. Nilges, N. L. Novère, P.-J. Corringer, and J.-P. Changeux, "Normal mode analysis suggests a quaternary twist model for the nicotinic receptor gating mechanism.," *Biophys J*, vol. 88, pp. 3954–3965, Jun 2005.

[78] A. Taly, P.-J. Corringer, T. Grutter, L. P. de Carvalho, M. Karplus, and J.-P. Changeux, "Implications of the quaternary twist allosteric model for the physiology and pathology of nicotinic acetylcholine receptors.," *Proc Natl Acad Sci U S A*, vol. 103, pp. 16965–16970, Nov 2006.

[79] X. Cheng, B. Lu, B. Grant, R. J. Law, and J. A. McCammon, "Channel opening motion of α7 nicotinic acetylcholine receptor as suggested by normal mode analysis.," *J Mol Biol*, vol. 355, pp. 310–324, Jan 2006.

[80] P. J. Corringer, N. L. Novère, and J. P. Changeux, "Nicotinic receptors at the amino acid level.," *Annu Rev Pharmacol Toxicol*, vol. 40, pp. 431–458, 2000.

[81] H. Zhang and A. Karlin, "Identification of acetylcholine receptor channel-lining residues in the M1 segment of the β-subunit.," *Biochemistry*, vol. 36, pp. 15856–15864, Dec 1997.

[82] G. D. Cymes, Y. Ni, and C. Grosman, "Probing ion-channel pores one proton at a time.," *Nature*, vol. 438, pp. 975–980, Dec 2005.

[83] Y. Zhou, J. H. Morais-Cabral, A. Kaufman, and R. MacKinnon, "Chemistry of ion coordination and hydration revealed by a K^+ channel-Fab complex at 2.0 Å resolution.," *Nature*, vol. 414, pp. 43–48, Nov 2001.

[84] R. Dutzler, E. B. Campbell, M. Cadene, B. T. Chait, and R. MacKinnon, "X-ray structure of a ClC chloride channel at 3.0 Å reveals the molecular basis of anion selectivity.," *Nature*, vol. 415, pp. 287–294, Jan 2002.

[85] Y. Zhou and R. MacKinnon, "The occupancy of ions in the K^+ selectivity filter: charge balance and coupling of ion binding to a protein conformational change underlie high conduction rates.," *J Mol Biol*, vol. 333, pp. 965–975, Nov 2003.

[86] R. Dutzler, E. B. Campbell, and R. MacKinnon, "Gating the selectivity filter in ClC chloride channels.," *Science*, vol. 300, pp. 108–112, Apr 2003.

[87] L. Y. Huang, W. A. Catterall, and G. Ehrenstein, "Selectivity of cations and nonelectrolytes for acetylcholine-activated channels in cultured muscle cells.," *J Gen Physiol*, vol. 71, pp. 397–410, Apr 1978.

[88] T. M. Dwyer, D. J. Adams, and B. Hille, "The permeability of the endplate channel to organic cations in frog muscle.," *J Gen Physiol*, vol. 75, pp. 469–492, May 1980.

[89] J. L. Yakel, X. M. Shao, and M. B. Jackson, "The selectivity of the channel coupled to the 5-HT3 receptor.," *Brain Res*, vol. 533, pp. 46–52, Nov 1990.

[90] J. Yang, "Ion permeation through 5-hydroxytryptamine-gated channels in neuroblastoma N18 cells.," *J Gen Physiol*, vol. 96, pp. 1177–1198, Dec 1990.

[91] B. N. Cohen, C. Labarca, N. Davidson, and H. A. Lester, "Mutations in M2 alter the selectivity of the mouse nicotinic acetylcholine receptor for organic and alkali metal cations.," *J Gen Physiol*, vol. 100, pp. 373–400, Sep 1992.

[92] D. Bertrand, J. L. Galzi, A. Devillers-Thiéry, S. Bertrand, and J. P. Changeux, "Mutations at two distinct sites within the channel domain M2 alter calcium permeability of neuronal α 7 nicotinic receptor.," *Proc Natl Acad Sci U S A*, vol. 90, pp. 6971–6975, Aug 1993.

[93] F. Wang and K. Imoto, "Pore size and negative charge as structural determinants of permeability in the *Torpedo* nicotinic acetylcholine receptor channel.," *Proc Biol Sci*, vol. 250, pp. 11–17, Oct 1992.

[94] J. Bormann, O. P. Hamill, and B. Sakmann, "Mechanism of anion permeation through channels gated by glycine and γ-aminobutyric acid in mouse cultured spinal neurones.," *J Physiol*, vol. 385, pp. 243–286, Apr 1987.

[95] K. Fatima-Shad and P. H. Barry, "Anion permeation in GABA- and glycine-gated channels of mammalian cultured hippocampal neurons.," *Proc Biol Sci*, vol. 253, pp. 69–75, Jul 1993.

[96] K. Imoto, C. Busch, B. Sakmann, M. Mishina, T. Konno, J. Nakai, H. Bujo, Y. Mori, K. Fukuda, and S. Numa, "Rings of negatively charged amino acids determine the acetylcholine receptor channel conductance.," *Nature*, vol. 335, pp. 645–648, Oct 1988.

[97] T. Konno, C. Busch, E. V. Kitzing, K. Imoto, F. Wang, J. Nakai, M. Mishina, S. Numa, and B. Sakmann, "Rings of anionic amino acids as structural determinants of ion selectivity in the acetylcholine receptor channel.," *Proc Biol Sci*, vol. 244, pp. 69–79, May 1991.

[98] M. L. Jensen, A. Schousboe, and P. K. Ahring, "Charge selectivity of the Cys-loop family of ligand-gated ion channels.," *J Neurochem*, vol. 92, pp. 217–225, Jan 2005.

[99] K. Imoto, T. Konno, J. Nakai, F. Wang, M. Mishina, and S. Numa, "A ring of uncharged polar amino acids as a component of channel constriction in the nicotinic acetylcholine receptor.," *FEBS Lett*, vol. 289, pp. 193–200, Sep 1991.

[100] A. Villarroel, S. Herlitze, M. Koenen, and B. Sakmann, "Location of a threonine residue in the α-subunit M2 transmembrane segment that determines the ion flow through the acetylcholine receptor channel.," *Proc Biol Sci*, vol. 243, pp. 69–74, Jan 1991.

[101] K. Imoto, "Ion channels: molecular basis of ion selectivity.," *FEBS Lett*, vol. 325, pp. 100–103, Jun 1993.

[102] A. Villarroel and B. Sakmann, "Threonine in the selectivity filter of the acetylcholine receptor channel.," *Biophys J*, vol. 62, pp. 196–205; discussion 205–8, Apr 1992.

[103] J. A. Dani, "Structure, diversity, and ionic permeability of neuronal and muscle acetylcholine receptors.," *EXS*, vol. 66, pp. 47–59, 1993.

[104] J. L. Galzi, A. Devillers-Thiéry, N. Hussy, S. Bertrand, J. P. Changeux, and D. Bertrand, "Mutations in the channel domain of a neuronal nicotinic receptor convert ion selectivity from cationic to anionic.," *Nature*, vol. 359, pp. 500–505, Oct 1992.

[105] P. J. Corringer, S. Bertrand, J. L. Galzi, A. Devillers-Thiéry, J. P. Changeux, and D. Bertrand, "Mutational analysis of the charge selectivity filter of the $\alpha 7$ nicotinic acetylcholine receptor.," *Neuron*, vol. 22, pp. 831–843, Apr 1999.

[106] A. Keramidas, A. J. Moorhouse, K. D. Pierce, P. R. Schofield, and P. H. Barry, "Cation-selective mutations in the M2 domain of the inhibitory glycine receptor channel reveal determinants of ion-charge selectivity.," *J Gen Physiol*, vol. 119, pp. 393–410, May 2002.

[107] M. L. Jensen, D. B. Timmermann, T. H. Johansen, A. Schousboe, T. Varming, and P. K. Ahring, "The β subunit determines the ion selectivity of the $GABA_A$ receptor.," *J Biol Chem*, vol. 277, pp. 41438–41447, Nov 2002.

[108] S. B. Hansen, H.-L. Wang, P. Taylor, and S. M. Sine, "An ion selectivity filter in the extracellular domain of cys-loop receptors reveals determinants for ion conductance.," *J Biol Chem*, vol. 283, pp. 36066–36070, Dec 2008.

[109] B. Sakmann, J. Patlak, and E. Neher, "Single acetylcholine-activated channels show burst-kinetics in presence of desensitizing concentrations of agonist.," *Nature*, vol. 286, pp. 71–73, Jul 1980.

[110] D. Colquhoun and D. C. Ogden, "Activation of ion channels in the frog end-plate by high concentrations of acetylcholine.," *J Physiol*, vol. 395, pp. 131–159, Jan 1988.

[111] E. L. Ochoa, A. Chattopadhyay, and M. G. McNamee, "Desensitization of the nicotinic acetylcholine receptor: molecular mechanisms and effect of modulators.," *Cell Mol Neurobiol*, vol. 9, pp. 141–178, Jun 1989.

[112] B. Katz and S. Thesleff, "A study of the desensitization produced by acetylcholine at the motor end-plate.," *J Physiol*, vol. 138, pp. 63–80, Aug 1957.

[113] P. J. Corringer, S. Bertrand, S. Bohler, S. J. Edelstein, J. P. Changeux, and D. Bertrand, "Critical elements determining diversity in agonist binding and desensitization of neuronal nicotinic acetylcholine receptors.," *J Neurosci*, vol. 18, pp. 648–657, Jan 1998.

[114] P. M. Lippiello, S. B. Sears, and K. G. Fernandes, "Kinetics and mechanism of L-[3H]nicotine binding to putative high affinity receptor sites in rat brain.," *Mol Pharmacol*, vol. 31, pp. 392–400, Apr 1987.

[115] J. D. Clements, "Transmitter timecourse in the synaptic cleft: its role in central synaptic function.," *Trends Neurosci*, vol. 19, pp. 163–171, May 1996.

[116] R. Giniatullin, A. Nistri, and J. L. Yakel, "Desensitization of nicotinic ACh receptors: shaping cholinergic signaling.," *Trends Neurosci*, vol. 28, pp. 371–378, Jul 2005.

[117] A. B. Smit, N. I. Syed, D. Schaap, J. van Minnen, J. Klumperman, K. S. Kits, H. Lodder, R. C. van der Schors, R. van Elk, B. Sorgedrager, K. Brejc, T. K. Sixma, and W. P. Geraerts, "A glia-derived acetylcholine-binding protein that modulates synaptic transmission.," *Nature*, vol. 411, pp. 261–268, May 2001.

[118] J. P. Gallivan and D. A. Dougherty, "Cation–π interactions in structural biology.," *Proc Natl Acad Sci U S A*, vol. 96, pp. 9459–9464, Aug 1999.

[119] S. B. Hansen, G. Sulzenbacher, T. Huxford, P. Marchot, P. Taylor, and Y. Bourne, "Structures of Aplysia AChBP complexes with nicotinic agonists and antagonists reveal distinctive binding interfaces and conformations.," *EMBO J*, vol. 24, pp. 3635–3646, Oct 2005.

[120] P. H. N. Celie, I. E. Kasheverov, D. Y. Mordvintsev, R. C. Hogg, P. van Nierop, R. van Elk, S. E. van Rossum-Fikkert, M. N. Zhmak, D. Bertrand, V. Tsetlin, T. K. Sixma, and A. B. Smit, "Crystal structure of nicotinic acetylcholine receptor homolog AChBP in complex with an α-conotoxin PnIA variant.," *Nat Struct Mol Biol*, vol. 12, pp. 582–588, Jul 2005.

[121] P. H. N. Celie, R. V. Klaassen, S. E. van Rossum-Fikkert, R. van Elk, P. van Nierop, A. B. Smit, and T. K. Sixma, "Crystal structure of acetylcholine-binding protein from *Bulinus truncatus* reveals the conserved structural scaffold and sites of variation in nicotinic acetylcholine receptors.," *J Biol Chem*, vol. 280, pp. 26457–26466, Jul 2005.

[122] C. D. Dellisanti, Y. Yao, J. C. Stroud, Z.-Z. Wang, and L. Chen, "Crystal structure of the extracellular domain of nAChR α1 bound to α-bungarotoxin at 1.94 Å resolution.," *Nat Neurosci*, vol. 10, pp. 953–962, Aug 2007.

[123] N. Unwin, "The nicotinic acetylcholine receptor of the *Torpedo* electric ray.," *J Struct Biol*, vol. 121, no. 2, pp. 181–190, 1998.

[124] C. Miller, "Open-state substructure of single chloride channels from *Torpedo* electroplax.," *Philos Trans R Soc Lond B Biol Sci*, vol. 299, pp. 401–411, Dec 1982.

[125] A. Brisson and P. N. Unwin, "Quaternary structure of the acetylcholine receptor.," *Nature*, vol. 315, no. 6019, pp. 474–477, 1985.

[126] C. Toyoshima and N. Unwin, "Ion channel of acetylcholine receptor reconstructed from images of postsynaptic membranes.," *Nature*, vol. 336, pp. 247–250, Nov 1988.

[127] C. Toyoshima and N. Unwin, "Three-dimensional structure of the acetylcholine receptor by cryoelectron microscopy and helical image reconstruction.," *J Cell Biol*, vol. 111, pp. 2623–2635, Dec 1990.

[128] N. Unwin, "Nicotinic acetylcholine receptor at 9 Å resolution.," *J Mol Biol*, vol. 229, pp. 1101–1124, Feb 1993.

[129] J. Berriman and N. Unwinw, "Analysis of transient structures by cryo-microscopy combined with rapid mixing of spray droplets.," *Ultramicroscopy*, vol. 56, pp. 241–252, Dec 1994.

[130] R. Beroukhim and N. Unwin, "Three-dimensional location of the main immunogenic region of the acetylcholine receptor.," *Neuron*, vol. 15, pp. 323–331, Aug 1995.

[131] A. Miyazawa, Y. Fujiyoshi, M. Stowell, and N. Unwin, "Nicotinic acetylcholine receptor at 4.6 Å resolution: transverse tunnels in the channel wall.," *J Mol Biol*, vol. 288, pp. 765–786, May 1999.

[132] E. Kubalek, S. Ralston, J. Lindstrom, and N. Unwin, "Location of subunits within the acetylcholine receptor by electron image analysis of tubular crystals from *Torpedo marmorata*.," *J Cell Biol*, vol. 105, pp. 9–18, Jul 1987.

[133] C. Miller, "Ion channel surprises: prokaryotes do it again!," *Neuron*, vol. 25, pp. 7–9, Jan 2000.

[134] R. Milkman, "An *Escherichia coli* homologue of eukaryotic potassium channel proteins.," *Proc Natl Acad Sci U S A*, vol. 91, pp. 3510–3514, Apr 1994.

[135] D. A. Doyle, J. M. Cabral, R. A. Pfuetzner, A. Kuo, J. M. Gulbis, S. L. Cohen, B. T. Chait, and R. MacKinnon, "The structure of the potassium channel: molecular basis of K^+ conduction and selectivity.," *Science*, vol. 280, pp. 69–77, Apr 1998.

[136] A. Tasneem, L. M. Iyer, E. Jakobsson, and L. Aravind, "Identification of the prokaryotic ligand-gated ion channels and their implications for the mechanisms and origins of animal Cys-loop ion channels.," *Genome Biol*, vol. 6, no. 1, p. R4, 2005.

[137] N. Bocquet, L. P. de Carvalho, J. Cartaud, J. Neyton, C. L. Poupon, A. Taly, T. Grutter, J.-P. Changeux, and P.-J. Corringer, "A prokaryotic proton-gated ion channel from the nicotinic acetylcholine receptor family.," *Nature*, vol. 445, pp. 116–119, Jan 2007.

[138] H. Nielsen, J. Engelbrecht, S. Brunak, and G. von Heijne, "Identification of prokaryotic and eukaryotic signal peptides and prediction of their cleavage sites.," *Protein Eng*, vol. 10, pp. 1–6, Jan 1997.

[139] M. Larkin, G. Blackshields, N. Brown, R. Chenna, P. McGettigan, H. McWilliam, F. Valentin, I. Wallace, A. Wilm, R. Lopez, J. Thompson, T. Gibson, and D. Higgins, "Clustal W and Clustal X version 2.0," *Bioinformatics*, vol. 23, no. 21, pp. 2947–2948, 2007.

[140] P. Gouet, E. Courcelle, D. I. Stuart, and F. Métoz, "ESPript: analysis of multiple sequence alignments in PostScript.," *Bioinformatics*, vol. 15, pp. 305–308, Apr 1999.

[141] P. Gouet, X. Robert, and E. Courcelle, "ESPript/ENDscript: Extracting and rendering sequence and 3D information from atomic structures of proteins.," *Nucleic Acids Res*, vol. 31, pp. 3320–3323, Jul 2003.

[142] W. A. Hendrickson and M. M. Teeter, "Structure of the hydrophobic protein crambin determined directly from the anomalous scattering of sulphur," *Nature*, vol. 290, pp. 107–113, 1981.

[143] Z. Dauter and D. A. Adamiak, "Anomalous signal of phosphorus used for phasing dna oligomer: importance of data redundancy.," *Acta Crystallogr D Biol Crystallogr*, vol. 57, pp. 990–995, Jul 2001.

[144] Z. Dauter, M. Dauter, and E. Dodson, "Jolly sad.," *Acta Crystallogr D Biol Crystallogr*, vol. 58, pp. 494–506, Mar 2002.

[145] T. R. Schneider and G. M. Sheldrick, "Substructure solution with SHELXD.," *Acta Crystallogr D Biol Crystallogr*, vol. 58, pp. 1772–1779, Oct 2002.

[146] M. Weiss, "Global indicators of X-ray data quality," *J. Appl. Cryst.*, vol. 34, pp. 130–135, 2001.

[147] C. Mueller-Dieckmann, S. Panjikar, P. Tucker, and M. Weiss, "On the routine use of soft X-rays in macromolecular crystallography. Part III. The optimal data-collection wavelength.," *Acta Crystallogr*, vol. D61, pp. 1263–1272, 2005.

[148] Z. Dauter, "Estimation of anomalous signal in diffraction data.," *Acta Crystallogr D Biol Crystallogr*, vol. 62, pp. 867–876, Aug 2006.

[149] M. Weiss and R. Hilgenfeld, "On the use of the merging R factor as a quality indicator for X-ray data," *J Appl Cryst*, vol. 30, pp. 203–205, 1997.

[150] K. Diederichs and P. A. Karplus, "Improved R-factors for diffraction data analysis in macromolecular crystallography.," *Nat Struct Biol*, vol. 4, pp. 269–275, Apr 1997.

[151] T. Blundell and L. Johnson, *Protein Crystallography*. New York: Academic Press., 1976.

[152] D. Gewirth, *The HKL Manual, a Description of the Programs DENZO, XDISPLAYF and SCALEPACK*, vol. 4th ed. New Haven, CT: Yale University, 1995.

[153] S. J. Harrop, J. R. Helliwell, T. C. Wan, A. J. Kalb, L. Tong, and J. Yariv, "Structure solution of a cubic crystal of concanavalin a complexed with methyl alpha-d-glucopyranoside.," *Acta Crystallogr D Biol Crystallogr*, vol. 52, pp. 143–155, Jan 1996.

[154] M. Weiss, "Global indicators of X-ray data quality," *J. Appl. Cryst.*, vol. 34, pp. 130–135, 2000.

[155] CCP4. Collaborative Computational Project Nr. 4., "The CCP4 Suite: Programs for X-ray crystallography.," *Acta Crystallogr*, vol. D50, pp. 760–763, 1994.

[156] R. J. C. Hilf and R. Dutzler, "X-ray structure of a prokaryotic pentameric ligand-gated ion channel.," *Nature*, vol. 452, pp. 375–379, Mar 2008.

[157] T. Yamakura and R. A. Harris, "Effects of gaseous anesthetics nitrous oxide and xenon on ligand-gated ion channels. comparison with isoflurane and ethanol.," *Anesthesiology*, vol. 93, pp. 1095–1101, Oct 2000.

[158] T. Yamakura, C. Borghese, and R. A. Harris, "A transmembrane site determines sensitivity of neuronal nicotinic acetylcholine receptors to general anesthetics," *J Biol Chem*, vol. 275, pp. 40879–40886, 2000.

[159] P. Kolb and A. Caflisch, "Automatic and efficient decomposition of two-dimensional structures of small molecules for fragment-based high-throughput docking.," *J Med Chem*, vol. 49, pp. 7384–7392, Dec 2006.

[160] R. J. C. Hilf and R. Dutzler, "Structure of a potentially open state of a proton-activated pentameric ligand-gated ion channel.," *Nature*, vol. 457, pp. 115–118, Jan 2009.

[161] R. J. C. Hilf and R. Dutzler, "A prokaryotic perspective on pentameric ligand-gated ion channel structure.," *Curr Opin Struct Biol*, Jul 2009.

[162] N. Bocquet, H. Nury, M. Baaden, C. L. Poupon, J.-P. Changeux, M. Delarue, and P.-J. Corringer, "X-ray structure of a pentameric ligand-gated ion channel in an apparently open conformation.," *Nature*, vol. 457, pp. 111–114, Jan 2009.

[163] H.-L. Wang, R. Toghraee, D. Papke, X.-L. Cheng, J. A. McCammon, U. Ravaioli, and S. M. Sine, "Single-channel current through nicotinic receptor produced by closure of binding site C-loop.," *Biophys J*, vol. 96, pp. 3582–3590, May 2009.

[164] M. Yi, H. Tjong, and H.-X. Zhou, "Spontaneous conformational change and toxin binding in α7 acetylcholine receptor: insight into channel activation and inhibition.," *Proc Natl Acad Sci U S A*, vol. 105, pp. 8280–8285, Jun 2008.

[165] X. Cheng, I. Ivanov, H. Wang, S. M. Sine, and J. A. McCammon, "Molecular-dynamics simulations of ELIC–a prokaryotic homologue of the nicotinic acetylcholine receptor.," *Biophys J*, vol. 96, pp. 4502–4513, Jun 2009.

[166] N. L. Absalom, P. R. Schofield, and T. M. Lewis, "Pore structure of the cys-loop ligand-gated ion channels.," *Neurochem Res*, vol. 34, pp. 1805–1815, Oct 2009.

[167] C. M. Nimigean, "A radioactive uptake assay to measure ion transport across ion channel-containing liposomes.," *Nat Protoc*, vol. 1, no. 3, pp. 1207–1212, 2006.

[168] L. C. Johansson, A. B. Wöhri, G. Katona, S. Engström, and R. Neutze, "Membrane protein crystallization from lipidic phases.," *Curr Opin Struct Biol*, Jul 2009.

[169] G. Sennhauser, P. Amstutz, C. Briand, O. Storchenegger, and M. G. Grütter, "Drug export pathway of multidrug exporter AcrB revealed by DARPin inhibitors.," *PLoS Biol*, vol. 5, p. e7, Jan 2007.

[170] S. F. Altschul, T. L. Madden, A. A. Schäffer, J. Zhang, Z. Zhang, W. Miller, and D. J. Lipman, "Gapped BLAST and PSI-BLAST: a new generation of protein database search programs.," *Nucleic Acids Res*, vol. 25, pp. 3389–3402, Sep 1997.

[171] A. Accardi, L. Kolmakova-Partensky, C. Williams, and C. Miller, "Ionic currents mediated by a prokaryotic homologue of CLC Cl^- channels.," *J Gen Physiol*, vol. 123, pp. 109–119, Feb 2004.

[172] W. Kabsch, "Automatic processing of rotation diffraction data from crystals of initially unknown symmetry and cell constants," *J. Appl. Cryst.*, vol. 26, pp. 795–800, 1993.

[173] T. Pape and T. Schneider, "HKL2MAP: a graphical user interface for phasing with SHELX programs," *J. Appl. Cryst.*, vol. D58, pp. 1772–1779, 2004.

[174] E. de La Fortelle and G. Bricogne, *Methods in Enzymology*, pp. 492–494. Academic, New York, 1997. editor: CW Carter and RM Sweet.

[175] K. Cowtan, "An automated procedure for phase improvement by density modification," *Joint CCP4 ESF-EACBM Newslett. Protein Crystallogr.*, vol. 31, pp. 34–38, 1994.

[176] T. A. Jones, J. Y. Zou, S. W. Cowan, and M. Kjeldgaard, "Improved methods for building protein models in electron density maps and the location of errors in these models.," *Acta Crystallogr A*, vol. 47 (Pt 2), pp. 110–119, Mar 1991.

[177] A. T. Brünger, P. D. Adams, G. M. Clore, W. L. DeLano, P. Gros, R. W. Grosse-Kunstleve, J. S. Jiang, J. Kuszewski, M. Nilges, N. S. Pannu, R. J. Read, L. M. Rice, T. Simonson, and G. L. Warren, "Crystallography & NMR system: A new software suite for macromolecular structure determination.," *Acta Crystallogr D Biol Crystallogr*, vol. 54, pp. 905–921, Sep 1998.

[178] A. J. McCoy, R. W. Grosse-Kunstleve, P. D. Adams, M. D. Winn, L. C. Storoni, and R. J. Read, "Phaser crystallographic software.," *J Appl Crystallogr*, vol. 40, pp. 658–674, Aug 2007.

[179] P. D. Adams, R. W. Grosse-Kunstleve, L. W. Hung, T. R. Ioerger, A. J. McCoy, N. W. Moriarty, R. J. Read, J. C. Sacchettini, N. K. Sauter, and T. C. Terwilliger, "PHENIX: building new software for automated crystallographic structure determination.," *Acta Crystallogr D Biol Crystallogr*, vol. 58, pp. 1948–1954, Nov 2002.

[180] M. F. Sanner, A. J. Olson, and J. C. Spehner, "Reduced surface: an efficient way to compute molecular surfaces.," *Biopolymers*, vol. 38, pp. 305–320, Mar 1996.

[181] C. M. Nimigean and C. Miller, "Na^+ block and permeation in a K^+ channel of known structure.," *J Gen Physiol*, vol. 120, pp. 323–335, Sep 2002.

[182] C. Lorenz, M. Pusch, and T. J. Jentsch, "Heteromultimeric ClC chloride channels with novel properties.," *Proc Natl Acad Sci U S A*, vol. 93, pp. 13362–13366, Nov 1996.